Technical Report GL-93-6
May 1993

US Army Corps
of Engineers
Waterways Experiment
Station

Geogrid Reinforced Base Courses for Flexible Pavements for Light Aircraft: Test Section Construction, Behavior Under Traffic, Laboratory Tests, and Design Criteria

by Steve L. Webster
Geotechnical Laboratory

Approved For Public Release; Distribution Is Unlimited

Prepared for Federal Aviation Administration

Technical Report GL-93-6
May 1993

Geogrid Reinforced Base Courses for Flexible Pavements for Light Aircraft: Test Section Construction, Behavior Under Traffic, Laboratory Tests, and Design Criteria

by Steve L. Webster
Geotechnical Laboratory

U.S. Army Corps of Engineers
Waterways Experiment Station
3909 Halls Ferry Road
Vicksburg, MS 39180-6199

Final report

Approved for public release; distribution is unlimited

Prepared for U.S. Department of Transportation
Federal Aviation Administration
Washington, DC 20591-0001

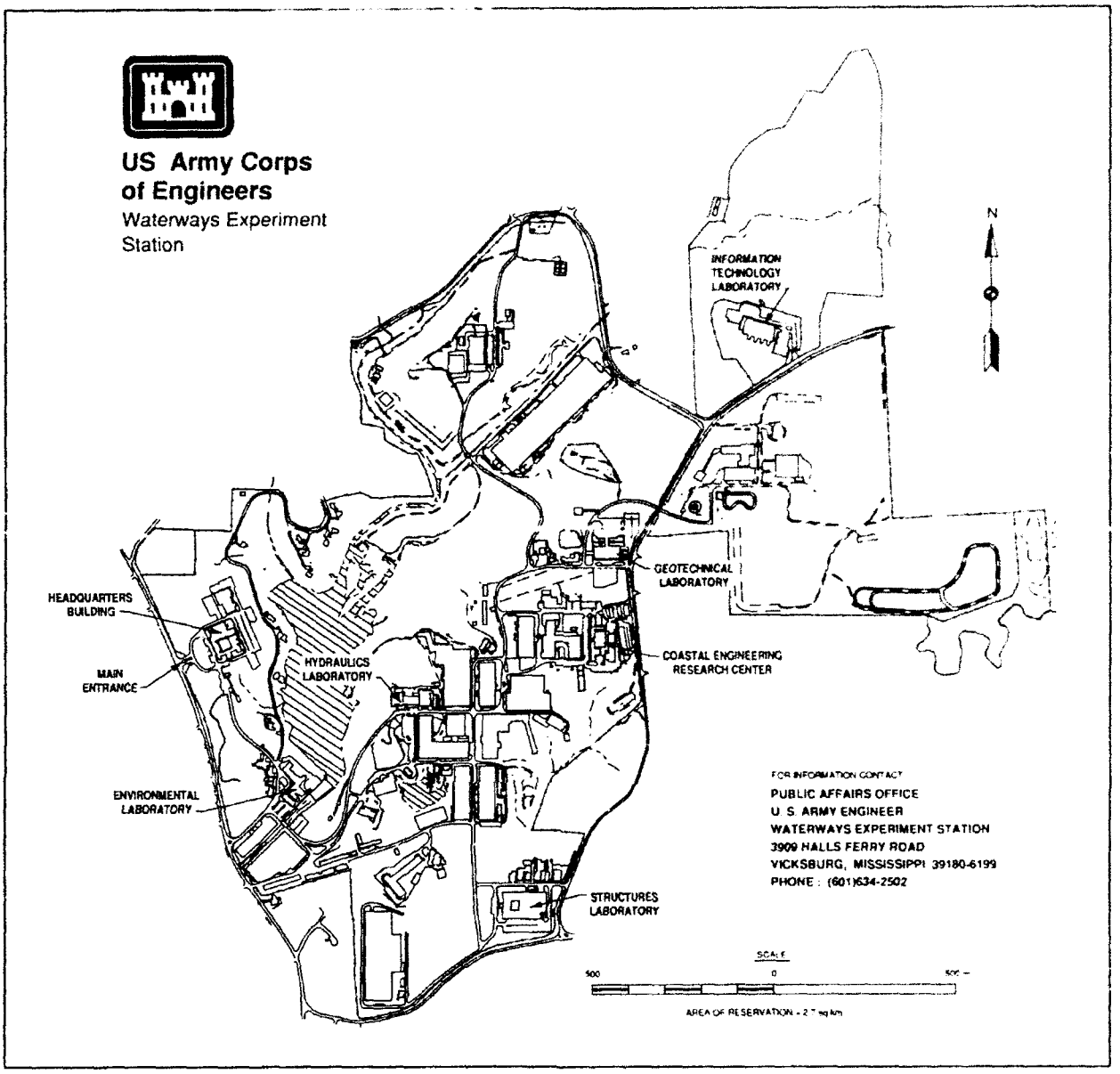

Waterways Experiment Station Cataloging-in-Publication Data

Webster, Steve L.

Geogrid reinforced base courses for flexible pavements for light aircraft: test section construction, behavior under traffic, laboratory tests, and design criteria/by Steve L. Webster; prepared for U.S. Department of Transportation, Federal Aviation Administration.

100 p.: ill.; 28 cm. -- (Technical report; GL-93-6)

Includes bibliographical references.

1. Runways (Aeronautics) -- Testing. 2. Pavements, Flexible -- Design and construction. 3. Geogrids. 4. Pavements -- Subgrades. I. United States. Federal Aviation Administration. II. U.S. Army Engineer Waterways Experiment Station. III. United States. Dept. of Transportation. IV. Title. V. Series: Technical report (U.S. Army Engineer Waterways Experiment Station) ; GL-93-6.

PREFACE

The information reported herein was sponsored by the US Department of Transportation, Federal Aviation Administration (FAA), under Interagency Agreement No. DTFAA01-89-Z-02029, "Grid Reinforced Aggregate Base Courses for General Aviation Airports." This report is the final project report covering results of field test section construction, behavior under traffic, laboratory tests, and design criteria. Interim report DOT/FAA/RD-90/28 covered a literature review and field test section design on geogrid reinforced base courses for flexible pavements for light aircraft. Technical Monitor for this study was Mr. Hisao Tomita.

This study was conducted during the period October 1990 thru July 1992 under the general supervision of Dr. W. F. Marcuson III, Director, Geotechnical Laboratory (GL), US Army Engineer Waterways Experiment Station (WES). Direct supervision was provided by Mr. H. H. Ulery, Jr., former Chief, and Dr. G. M. Hammitt II, Chief, Pavement Systems Division (PSD), and Dr. A. J. Bush, Jr., Chief, Criteria Development and Applications Branch (CD&AB), PSD. Mr. T. P. Williams, CD&AD, PSD, was engineering technician in charge of construction, traffic testing, and data collection. This report was prepared by Mr. Steve L. Webster, CD&AD, PSD.

At the time of publication of this report, Director of WES was Dr. Robert W. Whalin. Commander was COL Leonard G. Hassell, EN.

TABLE OF CONTENTS

LIST OF FIGURES

METRIC CONVERSION FACTORS

APPROXIMATE CONVERSIONS TO METRIC MEASURES

SYMBOL	WHEN YOU KNOW	MULTIPLY BY	TO FIND	SYMBOL
		LENGTH		
in.	inches	2.54	centimeters	cm
ft	feet	30	centimeters	cm
yd	yards	0.9	meters	m
mi	miles	1.6	kilometers	km
		AREA		
in^2	square inches	6.5	square centimeters	cm^2
ft^2	square feet	0.09	square meters	m^2
yd^2	square yards	0.8	square meters	m^2
mi^2	square miles	2.6	square kilometers	km^2
	acres	0.4	hectares	ha
		MASS (weight)		
oz	ounces	28	grams	g
lb	pounds	0.45	kilograms	kg
	short tons (2000 lb)	0.9	tonnes	t
		VOLUME		
tsp	teaspoons	5	milliliters	ml
Tbsp	tablespoons	15	milliliters	ml
fl oz	fluid ounces	30	milliliters	ml
c	cups	0.24	liters	l
pt	pints	0.47	liters	l
qt	quarts	0.95	liters	l
gal	gallons	3.8	liters	l
ft^3	cubic feet	0.03	cubic meters	m^3
yd^3	cubic yards	0.76	cubic meters	m^3
		TEMPERATURE (exact)		
°F	Fahrenheit temperature	5/9(after subtracting 32) C=5/9(F-32)	Celsius temperature	°C

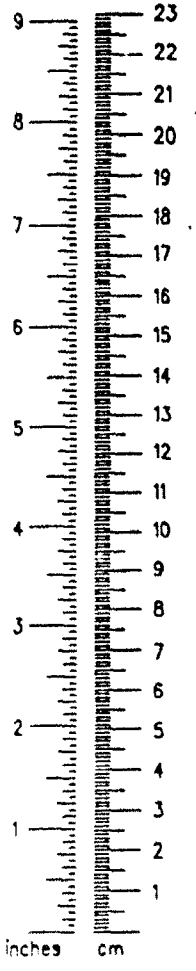

APPROXIMATE CONVERSIONS TO ENGLISH MEASURES

SYMBOL	WHEN YOU KNOW	MULTIPLY BY	TO FIND	SYMBOL
		LENGTH		
mm	millimeters	0.04	inches	in.
cm	centimeters	0.4	inches	in.
m	meters	3.3	feet	ft
m	meters	1.1	yards	yd
km	kilometers	0.6	miles	mi
		AREA		
cm^2	square centimeters	0.16	square inches	in^2
m^2	square meters	1.2	square yards	yd^2
km^2	square kilometers	0.4	square miles	mi^2
ha	hectares (10,000 m^2)	2.5	acres	
		MASS (weight)		
g	grams	0.036	ounces	oz
kg	kilograms	2.2	pounds	lb
t	tonnes (1000 kg)	1.1	short tons	
		VOLUME		
ml	milliliters	0.03	fluid ounces	fl oz
l	liters	2.1	pints	pt
l	liters	1.06	quarts	qt
l	liters	0.26	gallons	gal
m^3	cubic meters	35	cubic feet	ft^3
m^3	cubic meters	1.3	cubic yards	yd^3
		TEMPERATURE (exact)		
°C	Celsius temperature	9/5(then add 32) F=9/5C+32	Fahrenheit temperature	°F

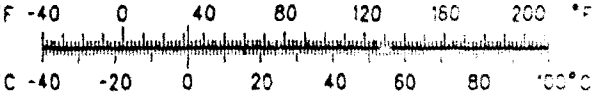

INTRODUCTION

BACKGROUND

A previous interim report[1] presented the results of a literature review investigating geogrid-reinforced base courses for flexible pavements for light aircraft and the design of a geogrid test section for field testing the validity of potential geogrid reinforcement results. Geogrids are deformed or nondeformed grid-like polymeric materials formed by intersecting ribs joined at the junctions. Geogrids are used for reinforcement with foundations, soil, rock, earth, or any other geotechnical engineering-related material as an integral part of a human-made project, structure, or system.

The literature review included related areas such as geogrid ballast reinforcement for railroad track bed, reinforcement for aggregate surfaced pavements, and reinforcement for flexible pavements.

Based on the literature review, geogrids were found to have application in ballast reinforcement for railroad track bed and in reinforcement for aggregate surfaced pavements. Full-scale field tests have verified that for subgrade CBR strengths of 1.5 to 5.0, geogrid reinforced aggregate surfaced pavements can carry about 3.5 times more traffic repetitions than equivalent nonreinforced pavements before a 1.5-in. rut depth was reached.

The improvement mechanisms for geogrid reinforced aggregate layers are known, and both laboratory and analytical studies indicated that geogrid reinforcement of aggregate bases can improve flexible pavement performance.

Geogrids perform better than geotextiles in base layer reinforcement mainly because of grid interlock with aggregate particles[1]. Poor friction properties of geotextiles do not allow good interlock with aggregate particles.

A test section design was presented for validating, through full-scale traffic tests, the geogrid base reinforcement potential for flexible pavements for light aircraft.

PURPOSE

The purposes of this report are to (1) describe the construction of the field test section, (2) describe the behavior of the test section under traffic, (3) present the results of laboratory tests conducted on the geogrid products tested, and (4) offer design criteria for geogrid base reinforcement for flexible pavements for light aircraft (gross aircraft weight not exceeding 30,000 lb).

SCOPE

This report describes the construction of the field test section, the behavior of the test section under traffic testing using a 30,000-lb single tire load, the data collected, laboratory tests that were conducted on the various geogrid products used in the field test section, and development of design criteria for geogrid base reinforcement for flexible pavements for

light aircraft. Results of an analytical study on the performance of the reinforced pavement sections will be reported in a separate report.

TEST SECTION DESIGN

LAYOUT

A layout of the test section is shown in figure 1. The test section contained 4 traffic lanes. Each traffic lane contained 4 test items. Traffic lanes 1 and 2 utilized distributed type traffic (see figure 2) over a width of 5 wheel widths. A three-factor experimental design model for traffic lanes 1 and 2 is shown in figure 3. Test items within these lanes were designed to measure the base reinforcement potential of geogrids. Traffic lanes 3 and 4 utilized channelized traffic and were designed to determine the comparative performance of the various types of geogird products available on the market. All test items were surfaced with a 2-in. asphaltic concrete surface meeting FAA Item P-401[2] requirements for pavements designed for aircraft gross weights less than 60,000 lbs or tire pressure less than 100 psi.

a. Traffic Lane 1. Figure 4 shows a profile section of traffic lane 1. This lane contained two base course thicknesses, each with and without SS-2 geogrid reinforcement placed at the bottom of the base. The conventional unreinforced test item 4 was designed to fail (1-in. rut) at a low traffic coverage level (approximately 100 coverages). Item 1 was designed to fail at approximately 500 coverages of test traffic. Items 2 and 3 were designed to measure direct performance improvement using geogrid reinforcement at the base of the base course.

b. Traffic Lane 2. Figure 5 shows the profile of lane 2. The base layer thicknesses of this lane were designed to fail at approximately the same coverage levels as those in lane 1. Based on full-scale traffic tests on geogrid reinforced aggregate layers over weak clay subgrades[1], the 3 CBR subgrade in traffic lane 2 should allow good reinforcement potential for geogrids in flexible pavements. The 3 CBR subgrade required thicker base layers which allowed testing the geogrid performance at a relatively deep (20-in. depth) location in the pavement.

c. Traffic Lanes 3 and 4. Figure 6 and 7 show the profiles of lane 3 and 4, respectively. These two traffic lanes were designed to accomplish the following.

(1) Lane 3 (Items 2 and 3). These items tested the most effective location for the geogrid. On relatively thick pavements, laboratory tests[1] have shown better performance with the geogrid placed in the middle of the base layer.

(2) Lane 3 (Items 3 and 4). These items tested the importance of the geogrid secant modulus for the same type material (SS-2 versus SS-1).

(3) Lane 3 (Items 1 and 2) and Lane 4 (Items 1-3). These items tested the comparative performance of the various types of geogrid products available on the market. The performance variables of these products include structure, polymer composition, junction method, mass per unit area, aperture size, thickness, and tensile strengths. No known laboratory test program could be substituted and accomplish what these tests items provided.

(4) Lane 4 (Item 4). This item was a control item to compare with the reinforcement items in the channelized traffic lanes 3 and 4.

MATERIALS

a. Heavy Clay Subgrade. The subgrade under all test items consisted of a heavy clay (CH) material, the properties of which are shown in figure 8. This material had a liquid limit (LL) of 67 and a plasticity index (PI) of 45 and was classified as a clay (CH) according to the Unified Soil Classification System. The clay, locally known as buckshot, was obtained from a backswamp deposit along the Mississippi River near Vicksburg, MS. Laboratory compaction and CBR data for the as-molded condition are shown in figure 9. This soil was selected because it could be processed to selected moisture contents and compacted in layers to design CBR strengths that would not change significantly throughout traffic testing. A 3 CBR subgrade represented a low strength subgrade which should show good base reinforcement potential without the necessity of a geotextile separator. An 8 CBR subgrade represented a firmer subgrade which would determine if geogrid reinforcement benefits diminish as subgrade strength increases.

b. Base Course. A marginal-graded crushed limestone was used as base course material. This material, classification data shown in figure 10, marginally met the FAA Item P-208[2] for Aggregate Base Course. The material was marginal because the amount of the fraction of material passing the No. 200 mesh (12.3 percent) exceeded the limit of one-half the fraction passing the No. 40 mesh (22.0 percent). Results from the literature review indicated that lower quality bases offered the highest improvement level for geogrid base reinforcement. Laboratory compaction data are shown in figure 11.

c. Asphaltic Concrete. A 2-in.-thick asphaltic concrete (AC) surfacing layer was specified for all test items of the test section. The AC surfacing was not a test variable. The AC surfacing was installed by a local paving contractor and met FAA Item P-401[2] requirements for pavements designed for aircraft gross weights less than 60,000 lbs or tire pressure less than 100 psi. The maximum aggregate size was 1/2 in. and the minimum Marshall Stability was 1500 lbs.

d. Geogrids. Table 1 lists the geogrid products used in the field test section. Two general types of geogrids were tested. Three products had a sheet type structure with a polypropylene polymer composition. The remaining three products were coated polyester with a woven structure. The mass per unit area varied form 5.9 to 9.0 oz/sq yd. The aperture size ranged from 0.69 to 1.8 in. Based on the wide-width tensile test (ASTM Test Method D 4595-86[3]), the 5 percent secant modulus (tensile load per inch of width at 5 percent strain divided by 0.05) ranged from 710 to 2000 lb/in. Figure 12 shows the geogrids that were tested.

Table 1

Geogrid Products Used in the Field Test Section*

Product Name	Structure	Polymer Composition	Junction Method	1990 Cost $/sq yd	Dimensional Properties		5 percent Secant Modulus***	
					Mass/Unit Area** oz/sq yd	Aperture Size in.	MD lb/in.	XMD lb/in.
SS-1	Punched Sheet-Drawn	Polypropylene	Planar	1.69	6.4	1.0 × 1.3	950	1,470
SS-2	Punched Sheet-Drawn	Polypropylene	Planar	2.95	9.0	1.0 × 1.3	1,170	2,000
Geogrid X	Bi-oriented	Polypropylene	Extruded	1.50	5.9	1.8 × 1.7	920	1,250
FX-3000/ Fortrac35/20-20	Woven	Polyester/ PVC Coating	Interwoven	3.00	9.0	0.9 × 0.9	1,840	840
GB-3022	Woven	Polyester/ PVC Coating	Interwoven	3.40	5.7	0.69 × 0.75	1,250	920
Miragrid 5T	Woven	Polyester	Knitted/ Coated	5.15	8.0	1.2 × 1.3	1,300	710

* Data based on available literature
(Cost based on purchase of test materials)
** ASTM D3776-84
*** ASTM D4595-86
MD = machine direction
XMD = cross-machine direction

CONSTRUCTION

GENERAL

The test section was constructed during the period October-December 1990. All work was accomplished by WES personnel except for the AC wearing surface, which was placed under contract by APAC Inc., Vicksburg, MS.

EXCAVATION

The test section was located at the U.S. Army Engineer Waterways Experiment Station (WES), Vicksburg, MS, in a sheltered area under WES Hangar No. 4. The existing soil floor was excavated to a depth of 40 in. and the lean clay soil in the bottom of the trench was compacted to a CBR strength greater than 10. The bottom and sides of the trench were lined with 6 mil sheet polyethylene in order to minimize drying of the heavy clay subgrade during traffic tests.

HEAVY CLAY SUBGRADE

The heavy clay subgrade was preprocessed to a water content that was desired for compaction. It was then hauled in dump trucks to the test area and spread with a bulldozer. Compaction was accomplished using a rubber-tired roller to obtain maximum density in the wet clay subgrade. The subgrade was placed and compacted in 6-in. lifts. A smooth steel drum vibratory compactor was used to produce a smooth final subgrade surface. Figure 13 shows the final subgrade surface condition prior to geogrid installation.

GEOGRIDS

The geogrids were installed on the subgrade surface in all geogrid items except item 2 of lane 3. In this item the geogrid was placed in the middle of the base course layer. The strength of the geogrids varied in the machine direction (the direction in the plane of the geogrid parallel to the direction of manufacture) and cross-machine direction (the direction in the plane of the geogrid perpendicular to the direction of manufacture). In all cases the geogrids were installed with the high strength direction perpendicular to the direction of traffic. This oriented the higher strength direction of the geogrid to resist lateral movement of the aggregate base material. The sheet-type polypropylene geogrids were unrolled in the direction of traffic. The woven-type polyester geogrids were unrolled perpendicular to the direction of traffic. Overlap joints under the traffic lanes were required for all test items containing the woven type polyester geogrids. Overlap joints between geogrid sections in these items were 1 ft. No overlap joints were required in items containing the sheet-type polypropylene geogrids. Figures 14 and 15 show geogrid installation on the subgrade. No problems were encountered during geogrid installation and all geogrids remained flat on the subgrade during base course placement.

BASE COURSE

The crushed limestone base course for all items was back dumped (figure 16), spread with a bulldozer, and compacted in maximum 6-in.-thick

lifts using the smooth drum vibratory compactor (figure 17). The top lift of the base course was also compacted with a self-propelled 36,000-lb rubber-tired roller in order to achieve as high as possible density in the base layer. Figure 18 shows the top lift of the base layer prior to installing the AC surfacing.

ASPHALTIC CONCRETE

The 2-in.-thick AC surfacing layer was installed by a local paving contractor. The AC surfacing covered an area 50 ft wide by 224 ft long. The AC surfacing covered all test items and also extended 40 ft past each end of the test section in order to allow the load test cart to completely clear the test items after each traffic pass. Since the AC surfacing was not a test variable, no laboratory or field compaction data was obtained. Twelve core samples were taken from the AC surfacing for thickness measurements. The AC thickness ranged from approximately 2.2 in. to 2.6 in. and averaged 2.4 in.

PROPERTIES OF AS-CONSTRUCTED BASE AND SUBGRADE

Cross section level readings taken during construction indicated that the base layer thicknesses of all test items were constructed to within one inch of design thickness.

Table 2 shows a summary of the average as-constructed CBR, water content, and density data as measured during construction. The subgrade data were measured at various locations on the soil surface after each construction lift of soil was installed. Since past experience with test section construction indicated that subgrade soils tend to gain some strength with time, it was desired to construct the subgrade soils to CBR strength values slightly less than design value. Test lane 1 had an average subgrade strength of CBR 7.1 (design CBR 8). Test lanes 2-4 averaged CBR 2.5 (design CBR 3). The subgrade water content, density, and CBR strengths for all four test lanes were carefully controlled during construction and did not vary significantly for any test item. The crushed stone base course was compacted to an average 95 percent of ASTM D 1557 maximum density at optimum water content. Compaction of the base to 100 percent of ASTM D 1557 was not attempted for fear of rutting the subgrade.

Table 2

As-Constructed CBR, Water Content, and Density Data

Test Lane	Item	Material	Depth in.	CBR	Water Content Percent	Dry Density pcf	Percent Density *
1	1-4	Cr stone base	2		4.1	136.1	95
		Subgrade (CH)	8-12	7.1	26.3	92.8	102
		Subgrade (CH)	16	6.9	26.2	92.3	101
		Subgrade (CH)	22	7.3	25.9	93.5	103
2-4	1-4	Cr stone base	2		4.3	136.4	95
		Subgrade (CH)	16	2.5	31.4	86.6	98
		Subgrade (CH)	22	2.7	30.5	86.9	98
		Subgrade (CH)	28	2.3	31.9	86.0	98

* Cr stone based on ASTM D 1557 maximum density at optimum water content. CH subgrade based on ASTM D 698 maximum density at field in-place water content.

INSTRUMENTATION

Instrumentation of the test section consisted of four sets of Multi-Depth Deflectometer (MDD) modules installed in test items 1 and 2 of traffic lanes 1 and 2. Figure 19 shows a layout of the MDD test locations. The MDD is an LVDT deflection measuring device which is retrofitted into the pavement layers. Up to six MDD modules can be installed in a single 1.5-in. diameter hole that has been augured through the pavement system. The modules are clamped against the sides of the hole at selected depths and the center core is attached to an anchor located approximately 8 ft below the pavement surface. The MDD can measure either the relative elastic deformation or the total permanent deformation at each test location in the pavement system. Figure 20 shows a profile of the MDD module locations in traffic lane 1, items 1 and 2. The top MDD modules were located at a 2-in. depth just under the AC surface layer. Additional modules were located just under the base layer or geogrid reinforcement and at 1-ft depths in the subgrade. Figure 21 shows the MDD module test locations for traffic lane 2. Since the base course layer was 18 in. thick, an additional set of MDD modules were installed in the middle of the base layer. The MDD instrumentation was installed under contract by the Texas Transportation Institute, Texas A&M University under the direction of Dr. Tom Scullion. Figure 22 shows the components of an MDD module and figure 23 shows a typical cross section of MDD after installation.

BEHAVIOR OF TEST SECTION UNDER TRAFFIC

APPLICATION OF TRAFFIC

Test traffic was applied from January through June 1991 using a 30-kip single-wheel-assembly test cart shown in figure 24. The cart was equipped with an outrigger wheel to prevent overturning and was powered by the front half of a four-wheel-drive truck. The test wheel and tire were for a C-130 aircraft and the 20.00 x 20, 26 ply tire was inflated to provide a contact pressure of 68 psi. The tire load was 30,000 lb with a contact area of 442 sq in. The measured tire contact width was 17.25 in. Test traffic was applied by driving the test cart forward and then in reverse over the entire length of the test section. The lateral traffic distribution pattern shown in figure 2 was used for lanes 1 and 2. A wheel path width of 17.5 in. was estimated from previous field tests and used for marking the traffic patterns on the pavement for test lanes 1 and 2 during construction. The actual loaded tire contact width measured during traffic tests was slightly less at 17.25 in. In lanes 3 and 4, the test tire was channelized in a 2-ft-wide tracking zone.

FAILURE CRITERIA

Failure of a test item was defined as 1 in. of rutting. Traffic was usually continued on a test item until 3 in. of rutting occurred or until each item in the traffic lane reached 1 in. of rutting. Traffic pass the 1-in. failure was done in order to see if the geogrid reinforcement benefit would increase at higher rut depths. Gravel surfaced pavements can usually stand 3 in. of rutting compared to the 1 in. for flexible pavements. For economic reasons, traffic on lane 1 was stopped after 10,000 passes even though all items had not failed.

RUT DEPTH MEASUREMENTS

Rut depth measurements were recorded at intervals throughout the traffic test period. Rut depth measurements were made by placing a metal straight edge across the traffic lane at three locations in each item (item quarter points) and measuring the maximum rut depth using a ruler. The rut depth included both the permanent deformation and upheaval within the traffic lane. The average of the three readings was recorded as the average rut depth for a given traffic pass level.

a. Lane 1. Rut depth measurements for lane 1 (8 CBR subgrade) are shown in figure 25. Lane 1, item 4 (L1I4) the control item with a 6-in. base rutted 1 in. after 670 traffic passes. The remaining test items had rut depths of less than 1 in. after traffic was concluded at 10,000 passes. Extrapolated traffic passes for a 1-in. rut were 15,000 for L1I1 (10-in. base, control) and L1I3 (6-in. base, SS-2). L1I2 (10-in. base, SS-2) would have required approximately 100,000 traffic passes to produce a 1-in. rut. The significant result of this data was that the 6-in. base with SS-2 (L1I3) performed the same as the control 10-in. base (L1I1). This showed that the SS-2 reinforcement was equal to 4-in. of base material.

b. Lane 2. Rut depth measurements for lane 2 (3 CBR subgrade) are shown in figure 26. L2I4 (12-in. base, control) rutted 1-in. at 90 traffic passes while L2I3 (12-in. base, SS-2) required 282 passes. L2I1 (18-in. base, control) rutted 1-in. at 1131 passes compared with L2I3 (18-in. base, SS-2) at 1432 passes. Both the lane 1 and lane 2 rut depth data showed that the traffic improvement benefit of geogrid reinforcement was high (22.6 times more traffic passes) for the thin 6-in. base layer and dropped off to very little (1.3 times more traffic passes) under the 18-in. base. This showed that geogrid reinforcement benefit is dependent on depth of placement.

c. Lanes 3 and 4. Rut depth measurements for the control item and various geogrid products tested in lanes 3 and 4 (3 CBR subgrade, 14-in. base) are shown in figure 27. Traffic performance for a 1-in. rut in ascending order were L4I2 (Miragird 5T) at 97 passes, L4I1 (Geogrid X) at 100 passes, L4I4 (control) at 106 passes, L4I3 (Fortrac 35/20-20) at 117 passes, L3I1 (GB-3022) at 170 passes, L3I4 (SS-1) at 285 passes, and L3I3 (SS-2) at 500 passes. An important finding from the rut depth data was the wide range of performance of the various geogrid products. Two of the woven polyester geogrids and one sheet-type polypropylene geogrid did not offer any significant reinforcement benefit while the best performing geogrid had an almost 5 times improvement in traffic passes.

Lane 4 rut depth measurements comparing L4I2 (geogrid placed in the middle of the base), L4I3 (bottom of the base), and L3I4 (control) are shown in figure 28. Results showed that geogrid reinforcement at the bottom of the base was more effective than in the middle of the base for these 14-in.-thick base layers on a 3 CBR subgrade and surfaced with 2 in. of AC.

CROSS SECTION LEVEL MEASUREMENTS

Surface cross section elevation measurements were recorded at intervals throughout the test traffic period. The cross section measurements were made across the traffic lanes at the same item quarter point locations where the rut depth measurements were made. Cross section measurements were also made on the top of the base and geogrid or geogrid/subgrade interface in a test pit dug across each item after traffic. The cross section measurements were made at 6-in. increments across the traffic lane. One measure of traffic performance obtained from the cross section data was the average maximum permanent surface depression (ignoring any upheaval). Typical cross section plots were also useful for describing test item layer conditions at various traffic pass levels.

a. Permanent surface depression. Figures 29-32 show a record of the maximum permanent surface depression for traffic lanes 1-4. Each point plotted represents the average maximum surface depression based on the three cross section locations for each test item. In general, the permanent surface depression plots follow the same pattern as the rut depth plots. One exception was L1I3 (6-in. base, SS-2) whose permanent surface depression followed that of L1I2 (10-in. base, SS-2) instead of L1I1 (10-in. base, control). Extrapolating traffic to a 1-in. permanent surface depression for L1I3 (6-in. base, SS-2) and L1I3 (10-in. base, SS-2) in figure 29 would yield traffic passes of 18,930 and 14,775, respectively. One explanation for the better performance of the reinforced 6-in. base versus the reinforced 10-in.

base, based on permanent surface depression, could be the depth-of-placement factor of the geogrid. Another explanation could be that the 10-in. base consolidated more than the 6-in. base.

b. Typical cross sections. Figures 33-48 show typical cross sections of the various test items at the location where a trench was dug across each item. It should be noted that in the control items the subgrade interface was hard to locate accurately, and the subgrade elevations could be off up to about 1 in. Also, in the reinforced items the solid line for the subgrade elevations represents level readings taken on top of the geogrid reinforcement. The dashed line below the subgrade just signifies that a geogrid reinforcement was used. Visual observations made while digging the trenches indicated some subgrade material could be found slightly above the geogrid reinforcement layer intermixed with base material. The amount of subgrade penetration above the geogrid could not be measured but was considered to be small.

AFTER TRAFFIC CBR, WATER CONTENT, AND DENSITY DATA

Table 3 shows the after-traffic CBR, water content, and density of the base and subgrade materials. The data show that the base material dried out slightly (0.7-1.7 percent) and increased in dry density approximately 7.6 pcf (5.5 percent). The subgrade strengths, water contents, and dry densities did not change significantly from the as-constructed values.

a. Lane 1. The top 6 in. of base had increased from its 95 percent maximum ASTM D 1557 density to approximately 100 percent. The CBR of the base surface was 100 plus for items 1-3. The base in item 4 had been severely displaced by traffic and was not tested for CBR strength. The average water content of the base after traffic was 2.5 percent. The after-traffic average subgrade CBR's were 7.4, 7.1, 7.3, and 7.9 for items 1-4, respectively. The overall after-traffic average subgrade CBR for lane 1 was 7.4. Averaging the as-constructed CBR of 7.1 with the after-traffic CBR of 7.4 yielded a rated CBR of 7.3 for lane 1. The subgrade water content dried only slightly from 26.0 percent before traffic to 25.2 percent after traffic. The average dry density of the subgrade after traffic was 93.5 pcf.

b. Lane 2. The top 6-in. of base had increased to 101 percent of maximum density. The base CBR of items 1 and 2 (18-in. base) was 100 plus at the surface and in the 70's at a depth of 8-10 in. in the base. The base CBR's of items 3 and 4 (12-in. base) were less, with item 3 (reinforced) being higher than item 4 (control). The thinner base layers were apparently too unstable over the weak subgrade to be strengthened significantly by traffic. However, item 3 had a higher CBR strength than item 4, indicating that the reinforcement may have helped stabilize the base in item 3. The average water content of the base for lane 2 was 3.1 percent. The after-traffic average subgrade CBR's were 3.1, 3.0, 3.0, and 2.9 for items 1-4, respectively. The overall after-traffic average subgrade CBR for lane 2 was 3.0. Averaging the as-constructed CBR of 2.5 with the after-traffic CBR of 3.0 yielded a rated CBR of 2.8 for lane 2. The subgrade water content averaged 31.3 percent, the same as during construction. The average dry density of the subgrade after traffic was 87.4 pcf.

Table 3

After-Traffic CBR, Water Content, and Density Data

Test Lane	Item	Material	Depth in.	CBR	Water Content Percent	Dry Density pcf	Percent Density *
1	1	Cr stone base	2	142.3	2.3	143.7	100
		Subgrade (CH)	14	6.2	23.9	94.8	104
		Subgrade (CH)	20	8.3	26.0	92.5	102
		Subgrade (CH	24	7.6	26.3	92.5	102
1	2	Cr stone base	2	114.0	2.8	145.7	101
		Subgrade (CH)	13	6.3	27.6	91.3	101
		Subgrade (CH)	18	7.2	23.0	95.4	104
		Subgrade (CH)	24	7.8	21.8	95.8	105
1	3	Cr stone base	2	104.0	2.3	137.3	95
		Subgrade (CH)	9	5.0	27.7	91.9	102
		Subgrade (CH)	14	8.6	26.3	92.7	102
		Subgrade (CH)	20	8.4	22.8	95.0	104
1	4	Subgrade (CH)	9	7.9	26.5	93.4	103
2	1	Cr stone base	2	105.3	2.9	14[illegible].6	100
		Cr stone base	8	82.3			
		Subgrade (CH)	22	3.3	30.6	88.2	100
		Subgrade (CH)	26	3.3	31.0	87.0	98
		Subgrade (CH)	32	2.8	31.8	86.7	9

(Continued)

Table 3 (Continued)

Test Lane	Item	Material	Depth in.	CBR	Water Content Percent	Dry Density pcf	Percent Density *
2	2	Cr stone base	2	113.3	2.9	145.5	101
		Cr stone base	12	74.0	3.3		
		Subgrade (CH)	20	3.2	31.2	88.2	100
		Subgrade (CH)	26	3.0	31.6	87.1	100
		Subgrade (CH)	32	2.9	30.8	87.2	99
2	3	Cr stone base	2	87	3.0	149.3	104
		Cr stone base	8	53.0	3.2		
		Subgrade (CH)	14	2.6	31.5	87.6	100
		Subgrade (CH)	18	3.6	30.7	88.1	100
		Subgrade (CH)	24	2.7	31.8	86.6	99
2	4	Cr stone base	2	77	3.3	143.6	100
		Cr stone base	8	30.0	3.2		
		Subgrade (CH)	12	2.3	31.6	87.2	99
		Subgrade (CH)	18	3.2	31.3	87.8	99
		Subgrade (CH)	24	3.1	31.8	86.5	99
3	1	Cr stone base	2	85.7	3.3		
		Subgrade (CH)	16	2.9	30.1	88.4	99
3	2	Cr stone base	2	103.7	3.0		
		Subgrade (CH)	16	2.9	30.1	87.9	99

(Continued)

Table 3 (Concluded)

Test Lane	Item	Material	Depth in.	CBR	Water Content Percent	Dry Density pcf	Percent Density *
3	3	Cr stone base	2	92.7	3.3		
		Subgrade (CH)	16	2.3	32.9	86.9	100
3	4	Cr stone base	2				
		Subgrade (CH)	16	3.1	31.2	87.2	99
4	1	Cr stone base	2	87.5	3.8		
		Subgrade (CH)	16	3.4	29.5	89.2	100
	2	Cr stone base	2	104.0	3.3		
		Subgrade (CH)	16	3.3	30.1	88.2	99
	3	Cr stone base	2	99.3	3.5		
		Subgrade (CH)	16	2.3	32.0	87.1	99
	4	Cr stone base	2				
		Subgrade (CH)	16	2.9	31.0	87.5	99

* Cr stone based on ASTM D 1557 maximum density at optimum water content. CH subgrade based on ASTM D 698 maximum density at field in-place water content.

c. Lane 3. The surface CBR's of the base were 80 plus and the average water content was 3.1 percent. After-traffic CBR's on the subgrade surface averaged 2.9, 2.9, 2.3, and 3.1 for items 1-4, respectively. The overall after-traffic average subgrade CBR for lane 3 was 2.8. Averaging the as-constructed CBR of 2.5 with the after-traffic CBR of 2.8 yielded a rated CBR of 2.7 for lane 3. The subgrade water content averaged 31.1 percent, essentially the same as during construction. The average dry density of the subgrade after traffic was 87.6 pcf.

d. Lane 4. The surface CBR's of the base were 80 plus and the average water content was 3.5 percent. After-traffic CBR's on the subgrade surface averaged 3.4, 3.3, 2.3, and 2.9 for items 1-4, respectively. The overall after-traffic average subgrade CBR for lane 4 was 3.0. Averaging the as-constructed CBR of 2.5 with the after-traffic CBR of 3.0 yielded a rated CBR of 2.8 for lane 4. The subgrade water content averaged 30.7 percent, just slightly less than during construction. The average dry density of the subgrade after traffic was 88.0 pcf.

AFTER-TRAFFIC PHOTOS

In general, test items did not show any signs of cracking until 1 in. of rutting occurred. At approximately 1 in. of rutting, longitudinal hairline cracks would become visible along the outer edges of wheel paths. The cracks would lengthen and widen with additional traffic.

a. Lane 1. Test items 1 and 2 showed no visible damage and had less than 1 in. of rutting at the conclusion of traffic tests. Figure 49 shows items 3 (6-in. base, SS-2) and 4 (6-in. base, control) after 2016 passes of traffic. The traffic lane is outlined by the two wide painted lines in the photo. The perpendicular line across the traffic lane marks the change from item 3 (bottom of photo) and item 4 (top of photo). Item 3 had an average rut depth of 0.5 in. while item 4 averaged just over 3 in. The longitudinal cracks and severe rutting in item 4 virtually stopped at the line separating the two items. Figure 50 (looking in opposite direction from figure 49) shows the rutting in item 4 and a portion of the AC surface removed. Two clay subgrade ridges were visible just beneath the AC layer (dark areas at C/L and 8-in. left of C/L on the pin board). Aggregate skid marks were visible on the surface of what was left of the base layer. The skid marks indicated that the base material had moved laterally toward the outside edges of the traffic lane. Figure 51 shows the trench after the remaining base material was removed. The two subgrade ridges can be seen protruding up to the bottom of the AC surfacing. The base thickness was approximately 7.5 in. thick just outside the right side (East) lane line. Figure 36 shows the cross-section elevations for the trench (East is on the left side of figure 36). The mode of failure was lateral movement of the base material originating at the base/subgrade interface. The geogrid reinforcement prevented this from occurring in item 3. Figure 52 shows the trench after some of the subgrade material was removed. The vertical face on the side of the trench shows the material layer interfaces at this failure location.

b. Lane 2. Failures in lane 2 followed the typical pattern of longitudinal cracking starting after 1 in. of rutting. The cracks became more visible as traffic and rutting progressed.

c. Lane 3 and 4. Figure 53 shows L4I1 (Geogrid X) on the left and L3I1 (GB-3022) on the right after 1500 passes. Figure 54 shows L4I2 (Miragrid 5T) on the left and L3I2 (SS-2 at mid-base location) after 1500 passes. Figure 55 shows L4I3 (Fortrac 35/20-20) on the left after 1500 passes and L3I3 (SS-2) on the right after 2000 passes. Figure 56 shows L4I4 (control) on the left after 1500 passes and L3I4 (SS-1) on the right after 2000 passes. Traffic on these items was channelized as the load cart tire wandered only about 6 in. in the single-wheel-width traffic lanes. Channelized traffic is usually more severe on pavement performance than the distributed type traffic used on lanes 1 and 2. The traffic tests on lanes 3 and 4 were designed for obtaining performance data versus different geogrid properties, and not for obtaining thickness design criteria.

MDD DEFORMATION MEASUREMENTS

The installations of MDD were described under the instrumentation section of this report, and test locations and MDD module depths are shown in figures 19-21.

a. Relative elastic deformations.

(1) Lane 1, 10-in.-thick base. Figures 57-59 show the initial elastic deformations for L1I1 (unreinforced) and L1I2 (reinforced) for the first few traffic passes of the 30,000-lb tire load. The MDD test number, for example "L10005C" for L1I1 in figure 59, is explained as follows. "L1" stands for lane 1, "0005" is traffic pass number 5, and "C" is wheel path C (see figure 2). All MDD module locations were in the center of wheel path C. As shown by figure 59, there was no significant difference in the magnitudes of displacements for the 2-in., 12-in., and 24-in. MDD depth locations for the unreinforced and reinforced items. It should be noted that the time scales are different in the plots so the length of the displacements do not match. Also, the MDD displacements were reset to a zero reading before each recorded traffic pass.

Figures 60-62 show the elastic deformations at the MDD locations in wheel path C for L1I1 (unreinforced) and L1I2 (reinforced) caused by traffic in wheel paths A, B, and C after 1531, 1533, and 1535 passes, respectively. For example, as the test tire moved along in wheel path A, figure 60 shows elastic displacements at the MDD 2-in. depth in wheel path C increase to a maximum of about 25-30 mils as the test tire approached the MDD location and then drop off to a residual displacement of about 10 mils as the test tire moved away from the MDD location. Traffic in wheel path B (figure 61) caused minor elastic displacement at the MDD 2-in. depth followed by residual upheaval of approximately 60 mils in the unreinforced item and 40 mils in the reinforced item. Traffic in wheel path C (figure 62) then caused displacements up to 235 mils for the MDD 2-in. depth in the unreinforced item and up to 215 mils for the MDD 2-in. depth in the reinforced item. The residual displacement was 70 mils for the unreinforced item and 50 mils for the reinforced item for the MDD 2-in. depth.

The MDD deflection results for lane 1 showed that initial elastic deflections were not different for the reinforced and unreinforced items.

However, as traffic progressed, the deflections in the unreinforced item were higher than in the reinforced item.

(2) Lane 2, 18-in.-thick base. Figures 63-67 show the elastic deformations for L2I1 (unreinforced) and L2I2 (reinforced) for 5, 41, 167, 221, and 329 passes. As with the 10-in.-thick base items in lane 1, the initial displacements were about the same for the unreinforced and reinforced items. As traffic progressed, the displacements in the unreinforced item became higher than those in the reinforced item. This was true for the 2-in., 11-in., 20-in., and 32-in. depth MDD modules. The flat lines for the 2-in. depth MDD modules in figures 66 and 67 resulted because the MDD modules were out of range at these high displacements. At 329 passes (figure 67) the residual displacement at the 2-in. depth was 90 mils for the unreinforced item and only 55 mils for the reinforced item.

b. Permanent deformations. A record of the permanent displacements of each MDD module was recorded as shown in figures 68-71. These displacements were recorded from static, no-load measurements at the indicated traffic pass level.

(1) Lane 1, items 1 and 2. The positive displacements at the 12-in. depth in figures 68 (control) and 69 (reinforced) were caused by lateral movement of the base and/or subgrade. The lateral movement caused the MDD hole and rod to bend, causing the MDD module at the 12-in. depth to move up the rod indicating a positive displacement even though one may not have occurred. The bent rods were noticed when the top MDD modules were removed in order to adjust the MDD modules at the 12-in. depth. The MDD modules used had approximately 0.6 in. of travel and then had to be readjusted for additional travel. The MDD modules were initially set to handle approximately 0.5 in. of downward travel and 0.1 in. of upward travel. The apparent upward displacements in figures 68 and 69 for the 12-in. depth quickly over ranged the 0.1 in. of travel allowed and no further displacements could be recorded until the MDD module was readjusted. After the 12-in. MDD modules were adjusted two or three times, the rod running through the modules was bent too much to allow for further adjustments. These data show that there was a significant amount of lateral movement at the 12-in. depth for both the reinforced and nonreinforced items in lane 1. The 2-in. displacements in figures 68 and 69 compare closely with the average permanent surface depressions in figure 29 for L1I1 and L1I2. There were no significant displacements at the 24-in. depth for either item. The MDD data for lane 1, items 1 and 2 indicate that rutting in both of these items was related to the base/subgrade interface and was affected by movement of base and/or subgrade material near the interface. A lack of significant subgrade rutting in the typical cross section data (figures 33 and 34) for these items supports the MDD data showing movement of interface material. Figure 33 (control) suggests mainly base material movement while figure 34 (reinforced) indicates base and maybe some subgrade material movement.

(2) Lane 2, items 1 and 2. Figures 70 and 71 show the MDD permanent displacement data for items 1 and 2, respectively. The data indicate only minor displacements (<170 mils) at the 20-in.-deep base/subgrade interface for both items. The 20-in. data in figure 70 (control) indicate base/subgrade interface material movement occurring at 600 passes and increasing

significantly at 2750 passes (affecting the 32-in. data). The 20-in. data in figure 71 (reinforced) indicate minor base/subgrade interface movement starting at about 250 passes and remaining small throughout the remainder of traffic. The MDD data indicate that approximately 40-45 percent of the total displacements occurred between the surface and 11-in. depth and 20 percent or less occurred below the base/subgrade interface. A lack of significant subgrade rutting in the typical cross section data (figures 37 and 38) for these items supports the MDD data showing movement of the interface material and some possible densification of the base material.

NONDESTRUCTIVE TESTS

Nondestructive tests were performed on each traffic lane with the Dynatest model 8000 falling weight deflectometer (FWD). The FWD is an impact load device that applies a single-impulse transient load of approximately 25-30 millisecond duration. With this trailer-mounted device, a dynamic force is applied to the pavement surface by dropping a weight onto a set of rubber cushions which results in an impulse loading on an underlying circular plate 17.8 in. in diameter in contact with the pavement. The applied force and the pavement velocities are respectively measured with load cells and velocity transducers. Deflections are determined by integrating the velocity-time signatures. The drop height of the weights can be as high as 15.7 in. to produce a force up to approximately 25,000 lb. The system is controlled with a micro computer which also records the output data. Velocities were measured and deflections computed at the center of the load plate and at distances of 12, 24, 36, 48, 60 and 72 in. from the center of the plate in order to obtain deflection basin measurements. Data were collected at a force level of approximately 15 kips. Impulse stiffness modulus (ISM) values were calculated based on the slope (load/deflection) of the plot of maximum impulse load versus the maximum deflection at the first sensor. An ISM is computed to provide a qualitative stiffness comparison between test points and between the pavement test items.

Figure 72 shows the average ISM value for each test item before traffic was applied. No noticeable difference in ISM could be detected between reinforced and unreinforced items. The FWD did not detect any significant difference in ISM values between the 6 and 10-in. base course items in lane 1. For the 3 CBR subgrade items, the different base course thicknesses were reflected in the ISM values. FWD tests were not conducted after traffic due to fear of damaging the FWD equipment on the rutted pavement.

LABORATORY MEASUREMENTS OF GEOGRID PROPERTIES

Laboratory measurements were made on the geogrid products used in the field tests in an attempt to determine geogrid property requirements for base reinforcement in flexible pavement applications. Table 4 presents a summary of the measurements. The secant modulus was determined according to ASTM D 4595 "Standard test method for tensile properties of geotextiles by the wide-width strip method." Six samples of each geogrid product were tested in each the machine and cross machine direction. The maximum secant modulus listed represents a secant modulus measured at the point along the stress strain curve where the maximum slope of the curve starts to decrease. The maximum secant modulus for the geogrids tested occurred between 0.5 and 1.0 percent elongation. The geometric properties were obtained by randomly measuring 4 cells in each of the of the 12 samples used in the wide-width tensile test. The rib width and thickness varied significantly in some of the geogrids. The value listed represents the average value for the rib. The stability secant modulus values listed were obtained from the "Grid Aperture Stability by In-Plane Rotation" test (Appendix A) developed by Dr. Thomas Kinney of Geosynthetic Services of Alaska.

Junction (node) strength tests were not conducted because none of the products were damaged during test section construction or traffic testing. Endurance properties to survive installation were adequate for all products. Also, since the polymer composition of all the products was either polypropylene or polyester, their long-term endurance in the pavement structure was considered good since these polymers have been buried long term in other pavement applications with no significant deterioration.

Table 4

Summary of Laboratory Measurements of Geogrid Properties

PROPERTY	SS-1		SS-2		GEOGRID X		FORTRAC 35/20-20		GB-3022		MIRAGRID 5T	
	MD	XD	MD	XD	MD	XD	MD	XD	MD	XD	MD	XD
GEOMETRY												
APERTURE SIZE (IN.)	0.99	1.46	0.95	1.42	1.11	1.63	0.69	0.73	0.73	0.67	1.24	1.31
CELL AREA (SQ. IN.)	2.42		2.24		2.80		0.857		0.783		3.04	
APERTURE OPENING (SQ. IN.)	1.45		1.35		1.81		0.50		0.49		1.62	
OPEN AREA (%)	60		60		65		59		62		53	
RIB WIDTH (IN.)	0.176	0.173	0.170	0.163	0.162	0.149	0.109	0.111	0.108	0.075	0.164	0.305
RIB THICKNESS (IN.)	0.040	0.031	0.062	0.050	0.046	0.037	0.042	0.047	0.031	0.046	0.034	0.035
JUNCTION THICKNESS (IN.)	0.115		0.164		0.114		0.060		0.043		0.038	
STRENGTH												
SECANT MODULUS (LB./IN.)												
MAX SECANT MODULUS (%)	2206 (0.9)	2936 (1.0)	3272 (0.9)	3261 (0.8)	3843 (0.5)	4317 (0.6)	2563 (1.0)	2023 (0.7)	3007 (0.7)	2903 (0.6)	3629 (0.8)	2906 (0.5)
2 %	1826	2370	2572	2526	2263	2868	1931	1252	2053	1672	2292	1255
5 %	1205	1564	1725	1742	1490	2004	1184	758	1273	1017	1411	866
STABILITY												
SECANT MODULUS (Draft GSA) Torque of 20 cm-kg cm-kg/deg	4.37		8.55		2.97		2.03		3.12		2.12	

MD = MACHINE DIRECTION
XD = CROSS MACHINE DIRECTION

ANALYSIS AND CONCLUSIONS

ANALYSIS

a. Traffic improvement factor. The field test results in terms of traffic passes to produce a 1-in. rut and 1-in. of permanent surface depression (does not include rut upheaval) are shown in table 5. The traffic improvement factor (ratio of reinforced traffic passes to unreinforced traffic passes) are also shown based on a 1-in. rut and 1-in. of permanent surface depression. The traffic improvement factor ranged from 0.9 (no improvement) up to 22.4 times more traffic to produce a 1-in. rut and 16.3 for 1-in. surface depression. Since the failure criteria for flexible pavements is usually a 1-in. rut, the traffic improvement factor based on rut depth should be used in evaluating the geogrid performance.

b. Depth of placement. The depth of placement of the geogrid reinforcement in the pavement structure is critical to the traffic improvement factor. Figure 73 shows a plot of geogrid placement depth versus traffic improvement factor (based on 1-in. rut depth) for lanes 1 and 2. The optimum depth of the geogrid reinforcement for the 30,000-lb tire load (17.25 in. tire width) was approximately 8 in. (2-in. AC over 6-in. base over geogrid). Results from the literature review of this study (Webster [1]) present data that show a traffic improvement factor of less than 1 occurred when the geogrid was placed at a depth of 4 in. (4-in. base over geogrid) using the same tire loaded to 35,000 lb at a tire pressure of 100 psi. For FAA pavements of light aircraft, a 2-in. minimum surfacing course is required. Also, a minimum 4-in. base course thickness should be required over geogrid reinforcement in order to protect the geogrid during construction. Therefore, for flexible pavements for light aircraft reinforced with geogrid, the minimum depth of geogrid placement should be 6 in.

The geogrid should always be placed at the bottom of the base course. Test results in figure 28 show that geogrid reinforcement at the bottom of the base was more effective than in the middle of base for 14-in.-thick base layers surfaced with 2 in. of AC.

c. Thickness design criteria. Results of test lanes 1 and 2 were used to develop thickness relationships between the unreinforced and reinforced test items. Figure 74 plots the results of pavement thickness versus traffic passes for a 1-in. rut failure for lane 1 (8 CBR subgrade) and lane 2 (3 CBR subgrade). Lines extended through these data points were used to map out the shaded zone which was used to develop equivalent thicknesses between the unreinforced and reinforced conditions. The shaded zone was not extended below the recommended minimum geogrid placement depth of 6 in. Also, a slightly conservative approach was used when shading the data from lane 2 (3 CBR). The shaded band width at the 12- to 14.5-in. depth was forced to match that of lane 1 (8 CBR) data. The vertical differences in the shaded areas were used to plot the unreinforced thickness versus the equivalent reinforced thickness, as shown in figure 75. For example, in figure 74 a 10.8-in. depth or less on the unreinforced line (top of shaded area) equates to a 6-in. depth on the reinforced line (bottom of shaded area). Thus, in figure 75 an unreinforced thickness of 10.8 in. or less plots equal to a 6-in. equivalent reinforced thickness. Similarly, in figure 74 for an unreinforced

Table 5

Traffic Improvement Factor

TEST ITEM	DESCRIPTION	TRAFFIC PASSES		TRAFFIC IMPROVEMENT FACTOR	
		1" RUT DEPTH	1" PERMANENT*** SURFACE DEPRESSION	BASED ON 1" RUT DEPTH	BASED ON 1" SURFACE DEPRESSION
L111	CONTROL 10" BASE 6 CBR SUBGRADE	15000 *	8191		
L112	10" BASE SS-2 GEOGRID 6 CBR SUBGRADE	100000 *	14775 *	6.7	2.4
L113	6" BASE SS-2 GEOGRID 6 CBR SUBGRADE	15000 *	18630 *	22.4	16.3
L114	CONTROL 6" BASE 6 CBR SUBGRADE	670	1162		
L211	CONTROL 18" BASE 3 CBR SUBGRADE	1131	1641		
L212	18" BASE SS-2 GEOGRID 3 CBR SUBGRADE	1432	2281	1.3	1.4
L213	12" BASE SS-2 GEOGRID 3 CBR SUBGRADE	282	444	3.1	2.8
L214	CONTROL 12" BASE 3 CBR SUBGRADE	90	160		
L311	14" BASE GB-3022 GEOGRID 3 CBR SUBGRADE	170	340	1.6	1.9
L312 **	14" BASE SS-2 GEOGRID MID-BASE 3 CBR SUBGRADE	230	475	2.2	2.6
L313	14" BASE SS-2 GEOGRID 3 CBR SUBGRADE	500	650	4.7	3.6
L314	14" BASE SS-1 GEOGRID 3 CBR SUBGRADE	285	463	2.7	2.6
L411	14" BASE LB0201/AMP GEOGRID 3 CBR SUBGRADE	100	172	0.9	1.0
L412	14" BASE MIRAGRID 5T GEOGRID 3 CBR SUBGRADE	97	175	0.9	1.0
L413	14" BASE FORTRAC 35/20-20 GEOGRID 3 CBR SUBGRADE	117	225	1.1	1.2
L414	CONTROL 14" BASE 3 CBR SUBGRADE	106	181		

* EXTRAPOLATED VALUES

** ALL GEOGRIDS WERE POSITIONED BETWEEN THE BASE AND SUBGRADE EXCEPT LANE 3 ITEM 2.

***DOES T INCLUDE UPHEAVAL

NOTE: TEST ITEMS L111-L214 HAD DISTRIBUTED TRAFFIC AND L311-L414 HAD CHANNELIZED TRAFFIC

depth of 14.5 in. on either unreinforced line (top of shaded area) equates to a 12-in. depth on both reinforced lines (bottom of shaded areas). Therefore, in figure 75 an unreinforced thickness of 14.5-in. plots equivalent to a 12-in. reinforced thickness. These thickness values represent the total pavement thickness requirements (2-in. AC surface plus base course).

The following illustrates how the design criteria in figure 75 can be used. For example, using the FAA design curves for flexible pavements for light air craft (Figure 76) for a 7.5 CBR subgrade and 24,000-lb gross aircraft weight, the required pavement thickness is 12.3 in. Using figure 75 with an unreinforced thickness of 12.3 in., an equivalent geogrid reinforced thickness would be 8.5 in. The reinforced pavement would consist of 2 in. of AC surface, 6.5-in. base, geogrid, over the subgrade. The savings in base thickness would be 3.8 in.

d. Geogrid improvement mechanisms. The improvement mechanisms for geogrid reinforced base courses for flexible pavements are essentially the same as those for geogrid reinforced aggregate surfaced pavements as reported in the literature review of this study[1].

(1) Grid Interlock with Aggregate Base Material. By interlocking with the base layer aggregate, geogrids reduce permanent lateral displacements which accumulate with traffic passes. L1I4 (2-in. AC, 6-in. base, 8 CBR subgrade) without reinforcement failed due to lateral flow of the base material originating at the base/subgrade interface (See figures 36 and 49-52). The geogrid in L1I3 (2-in. AC, 6-in. base, geogrid, 8 CBR subgrade) prevented this type of failure (see figure 35). Failure in this item was forced to occur through densification or consolidation of the pavement layers and rutting of the subgrade. The presence of the geogrid forced a different (and stronger) failure mode.

(2) Subgrade Confinement. The geogrid confines the subgrade material below the base preventing or limiting the amount of subgrade rutting upheaval from penetrating into or through the base material. Without geogrid confinement, rutting upheaval can penetrate through the base layer as shown in figures 50-52.

(3) Separation. For the 3 and 8 CBR subgrades tested, the geogrid was not needed for separation of the base layer and subgrade. No significant amount of aggregate sinking into the subgrade occurred in the items tested. Control items failed due to lateral displacements of the aggregate at the base/subgrade interface rather than aggregate sinking into the subgrade.

(4) Tensioned Membrane Effect. Once lateral displacement of the base is prevented and the geogrid is successful in confining or separating the base and subgrade, the pavement failure mechanism due to additional traffic is rutting of the subgrade or densification or consolidation of the pavement layers. Surface rutting can be transmitted to the subgrade as increased traffic passes causes permanent subgrade deformation under the wheel path with subgrade heave outside the wheel path. The result of this type of rutting caused by a distributed traffic pattern can be seen in figures 35 and 39. As the base becomes thicker for the same strength subgrade, the amount of rutting reflecting from the pavement surface to the subgrade decreases. This can be

shown by comparing figures 35 and 34 for the 8 CBR subgrade and figures 39 and 38 for the 3 CBR subgrade. When the geogrid reinforcement depth is near its optimum placement depth under relatively thin bases, the tensioned membrane effect resulting from the geogrid being stretched due to traffic load rutting may be realized. In this case the geogrid secant modulus at low strains may be an important property. Actual strains in the geogrids were not measured in the field test sections so no definitive conclusion on the importance of the tensioned membrane effect and secant modulus can be drawn.

e. Geogrid physical properties versus performance. Attempts at relating the geometry and strength properties shown in table 4 for the various geogrid products tested in lanes 3 and 4 to the traffic improvement factors listed in table 6. Results of this effort were mostly unsuccessful. However, a draft index test "Grid Aperture Stability by In-Plane Rotation" developed by Dr. Thomas Kinney, Geosynthetic Services of Alaska (APPENDIX A) produced a secant aperture stability modulus at a torque of 20 cm-kg which showed good correlation with the Traffic Improvement Factor from the field test results (Figure A1).

The performance of the various geogrid products tested ranged from no improvement up to a 40 percent reduction in total pavement thickness requirement. The relatively rigid sheet-type geogrid (SS-2) performed the best of all products tested. The lighter weight version of this product performed second best. However, one other sheet-type product and one woven-type product with good strength properties failed to provide any measurable performance improvement. The remaining woven-type products provided marginal performance improvement.

Based on the geogrid properties shown in table 4, the traffic improvement factors listed in table 5, visual inspection of geogrids tested, and engineering judgment, the judgments listed in table 6 are offered regarding geogrid properties for base reinforcement.

CONCLUSIONS

Based on the results of the literature review and tests reported herein, the following conclusions are warranted for light aircraft pavements over cohesive subgrades:

a. The validity of geogrid reinforced base courses for flexible pavements for light aircraft has been verified by the full-scale traffic tests described in this report. The total pavement design thickness can be reduced by the amounts shown in figure 75 when a geogrid reinforcement product equivalent to the SS-2 geogrid is used.

b. The geogrid performance is a function of depth of placement. For flexible pavements for light aircraft the minimum placement depth should be 6 in. (2-in. AC surface and 4-in. aggregate base).

c. For subgrade strengths greater than a 1.5 CBR, the geogrid reinforcement performs best when placed between the base course and subgrade.

Table 6

Geogrid Properties Affecting Base Reinforcement

Geogrid Item	Property	Judgment
Rib	Thickness	Thicker is better.
Rib	Stiffness	Stiffer is better. Need test to measure stiffness.
Rib	Shape	Square or rectangular are better than rounded or curved shapes.
Aperture	Size	Related to base aggregate size. Optimum size not known. .75 to 1.5 in. probably good target range.
Aperture	Shape	Round or square is better.
Aperture	Rigidity	Stiffer is better.
Junction	Strength	Need some minimum strength. All geogrids tested were adequate.
Grid	Secant Modulus (ASTM D 4595)	Need minimum secant modulus value. Optimum not known. Should use that of SS-2 as minimum.
Grid	Stability	The "Grid Aperture Stability by In-Plane Rotation" test developed by Dr. Thomas Kinney shows good potential for traffic performance relationships. A minimum secant aperture stability modulus at a specified torque may be a good index test requirement.

d. The improvement mechanisms for geogrid reinforcement over subgrade strengths greater than 1.5 CBR include grid interlock with aggregate base material, subgrade confinement, and to some extent a tensioned membrane effect when placed under relatively thin base courses.

e. The optimum geogrid property requirements for maximum performance are not totally understood at this time. The geogrid properties affecting base reinforcement shown in table 6 need further study in order to more fully understand optimum geogrid properties required for developing generic specifications for base reinforcement.

REFERENCES

1. Webster, S. L. 1991 (May). "Geogrid Reinforced Base Courses for Flexible Pavements for Light Aircraft, Literature Review and Test Section Design," DOT/FAA/RD-90/28, U.S. Department of Transportation, Federal Aviation Administration, Washington, DC. (Also WES Miscellaneous Paper GL-92-6)

2. U.S. Department of Transportation, "Standards for Specifying Construction of Airports," AC: 150/5370-10A, 1989 (Feb). Federal Aviation Administration, Washington, DC.

3. ASTM. 1989. Annual Book of ASTM Standards, Section 4 Construction, Vol. 04.08 Soil and Rock, Building Stones; Geotextiles, Philadelphia, PA.

4. Scullion, T., Uzan, J., Yazdani, J. I., and Chan, P. 1988 (Sep). "Field Evaluation of the Multi-Depth Deflectometers," Texas Transportation Institute, Texas A&M University, College Station, TX.

5. U.S. Department of Transportation, "Airport Pavement Design and Evaluation," AC: 150/5320-6C, 1978 (Dec). Federal Aviation Administration, Washington, DC.

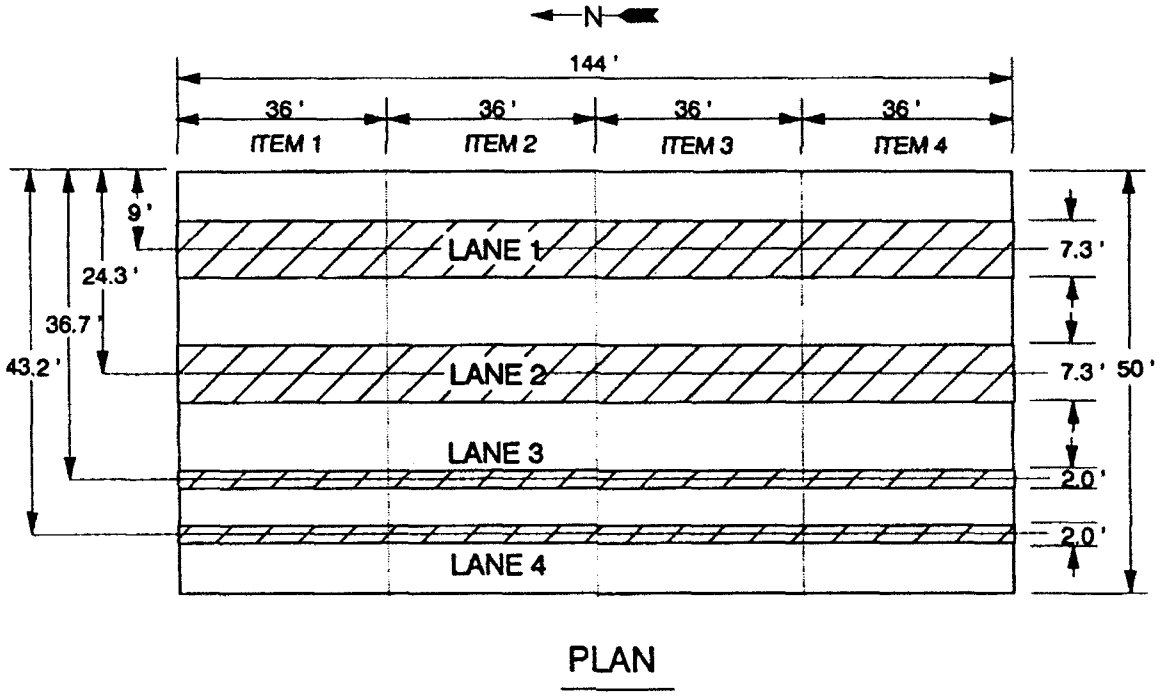

PLAN

Figure 1. Layout of geogrid test section

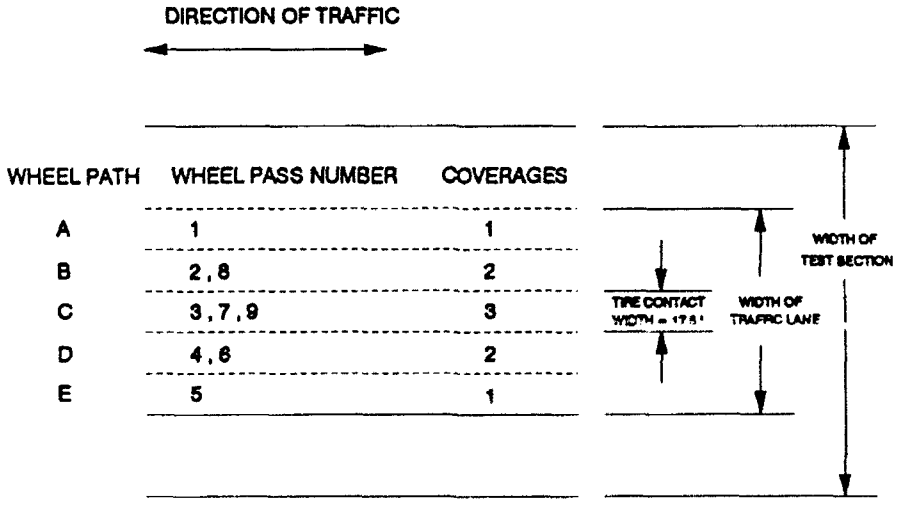

Figure 2. Traffic pattern for test Lanes 1 and 2

GEOGRID REINFORCEMENT / BASE COURSE / SUBGRADE STRENGTH		NO REINFORCEMENT		SS-2 GEOGRID	
		THICK	THIN	THICK	THIN
8 CBR		Lane 1 Item 1 2" AC 10" Base	Lane 1 Item 4 2" AC 6" Base	Lane 1 Item 2 2" AC 10" Base SS-2	Lane 1 Item 3 2" AC 6" Base SS-2
3 CBR		Lane 2 Item 1 2" AC 18" Base	Lane 2 Item 4 2" AC 12" Base	Lane 2 Item 2 2" AC 18" Base SS-2	Lane 2 Item 3 2" AC 12" Base SS-2

Figure 3. Experimental design for traffic Lanes 1 and 2

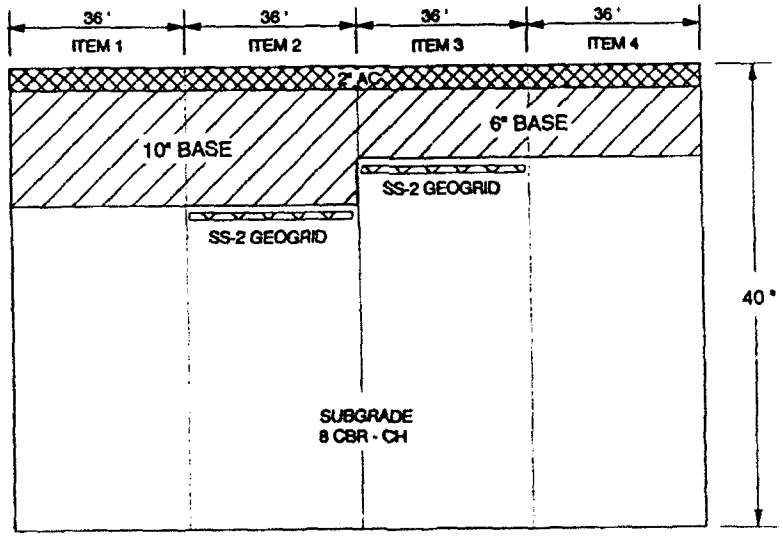

Figure 4. Profile of traffic Lane 1

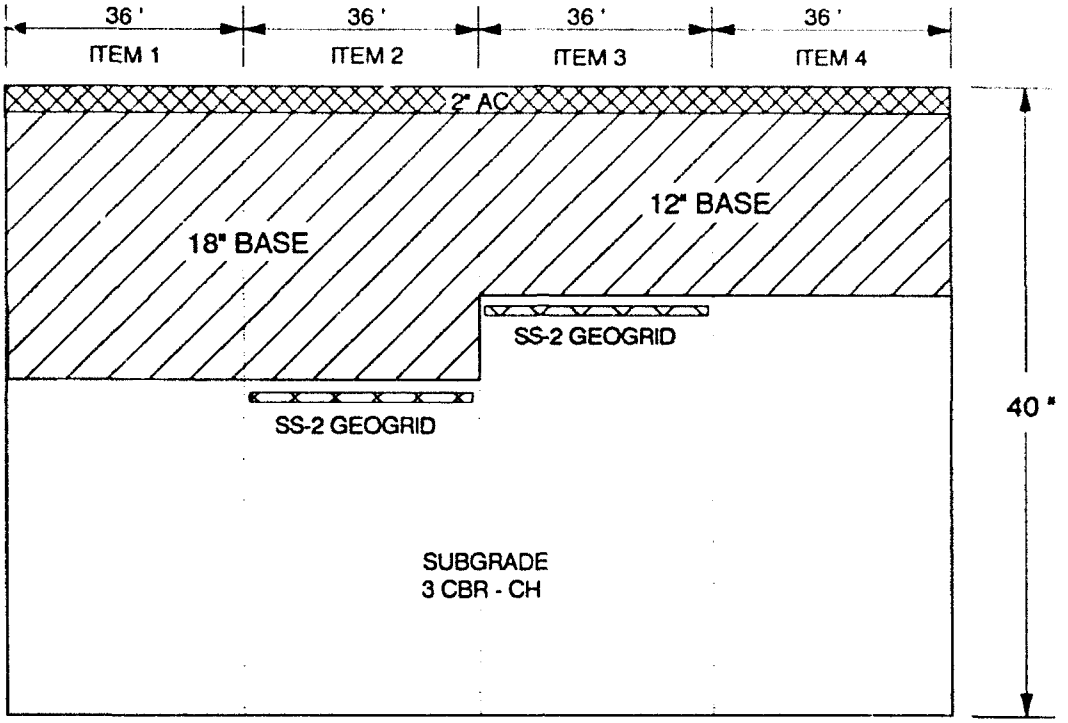

Figure 5. Profile of traffic Lane 2

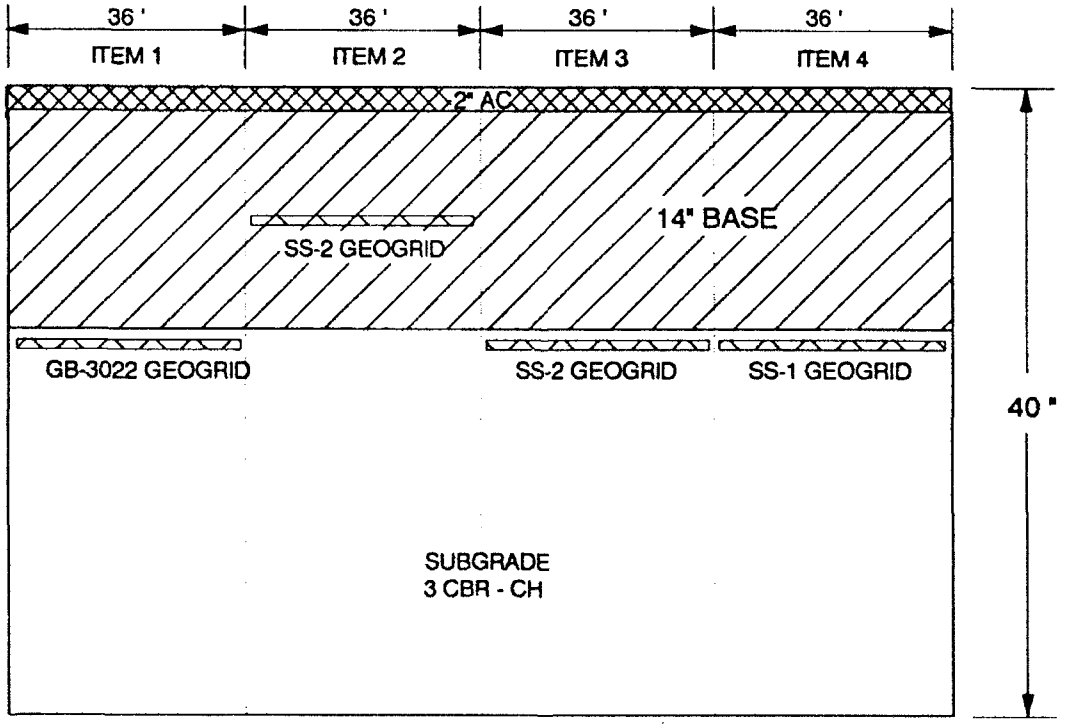

Figure 6. Profile of traffic Lane 3

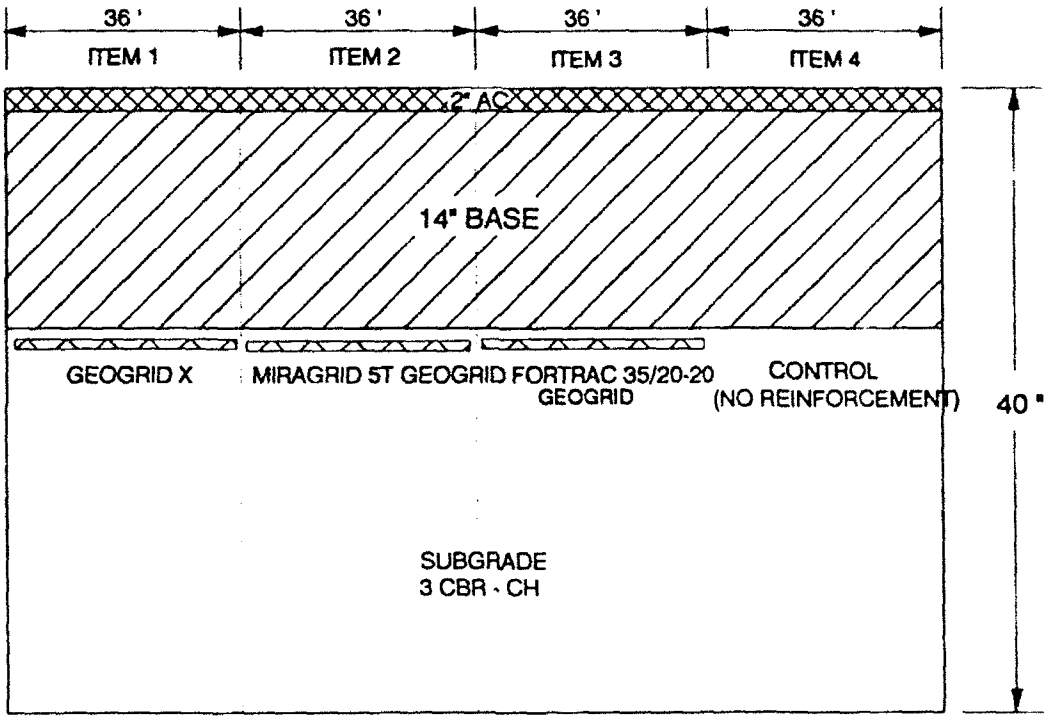

Figure 7. Profile of traffic Lane 4

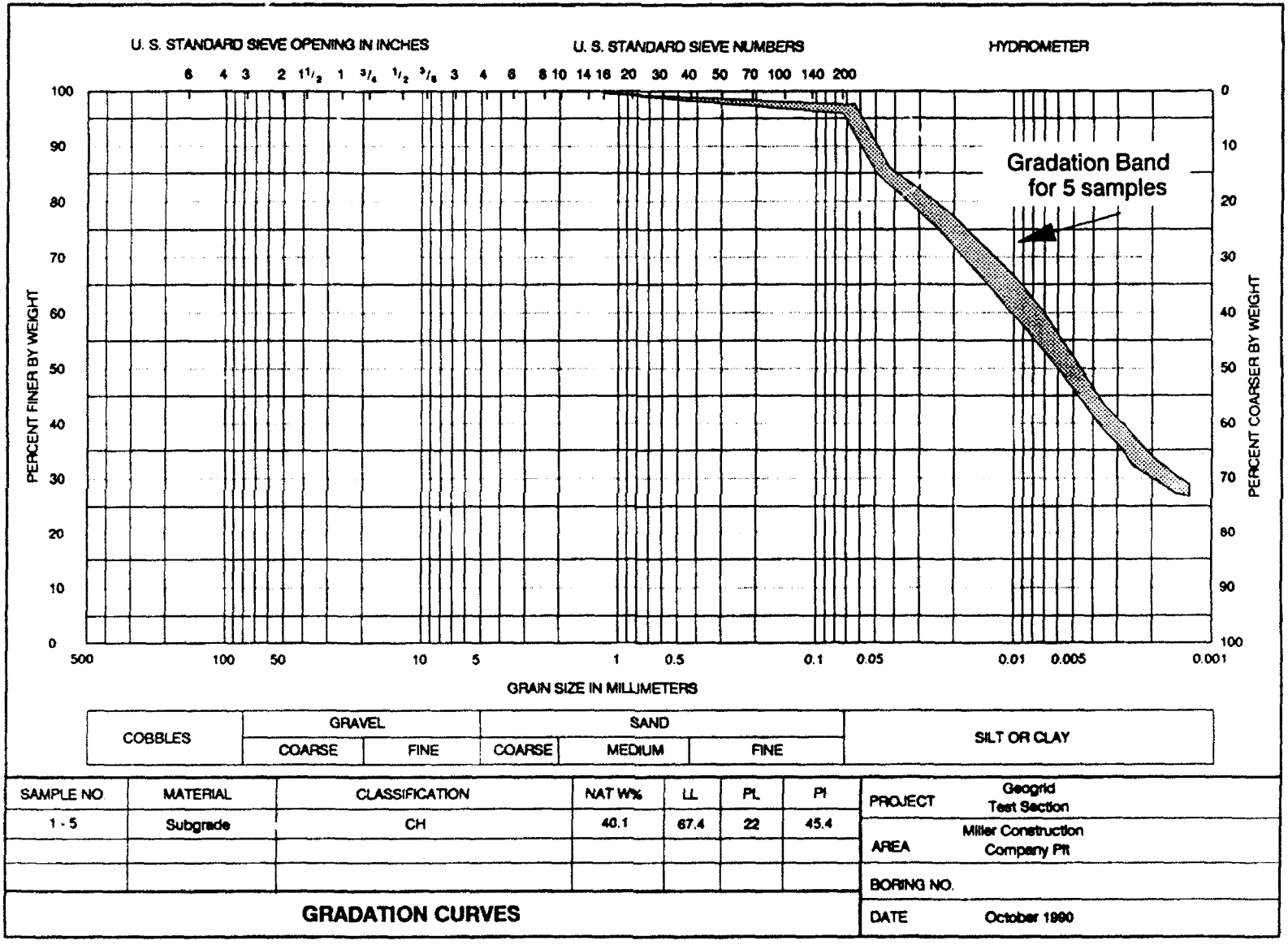

SAMPLE NO.	MATERIAL	CLASSIFICATION	NAT W%	LL	PL	PI
1 - 5	Subgrade	CH	40.1	67.4	22	45.4

GRADATION CURVES

PROJECT	Geogrid Test Section
AREA	Miller Construction Company Pit
BORING NO.	
DATE	October 1990

Figure 8. Classification data for subgrade material

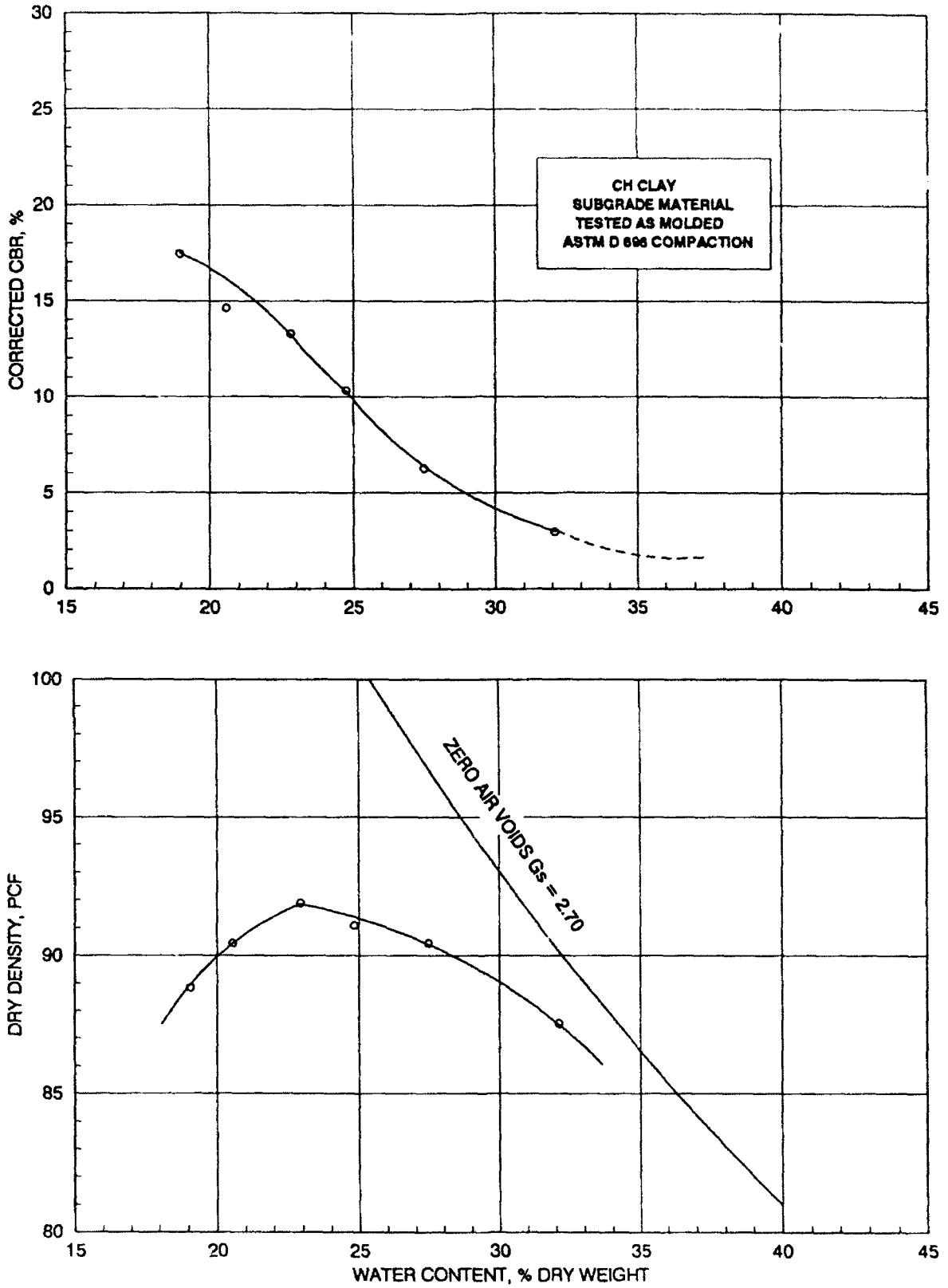

Figure 9. CBR, density, and water content data for heavy clay subgrade material (tested as molded)

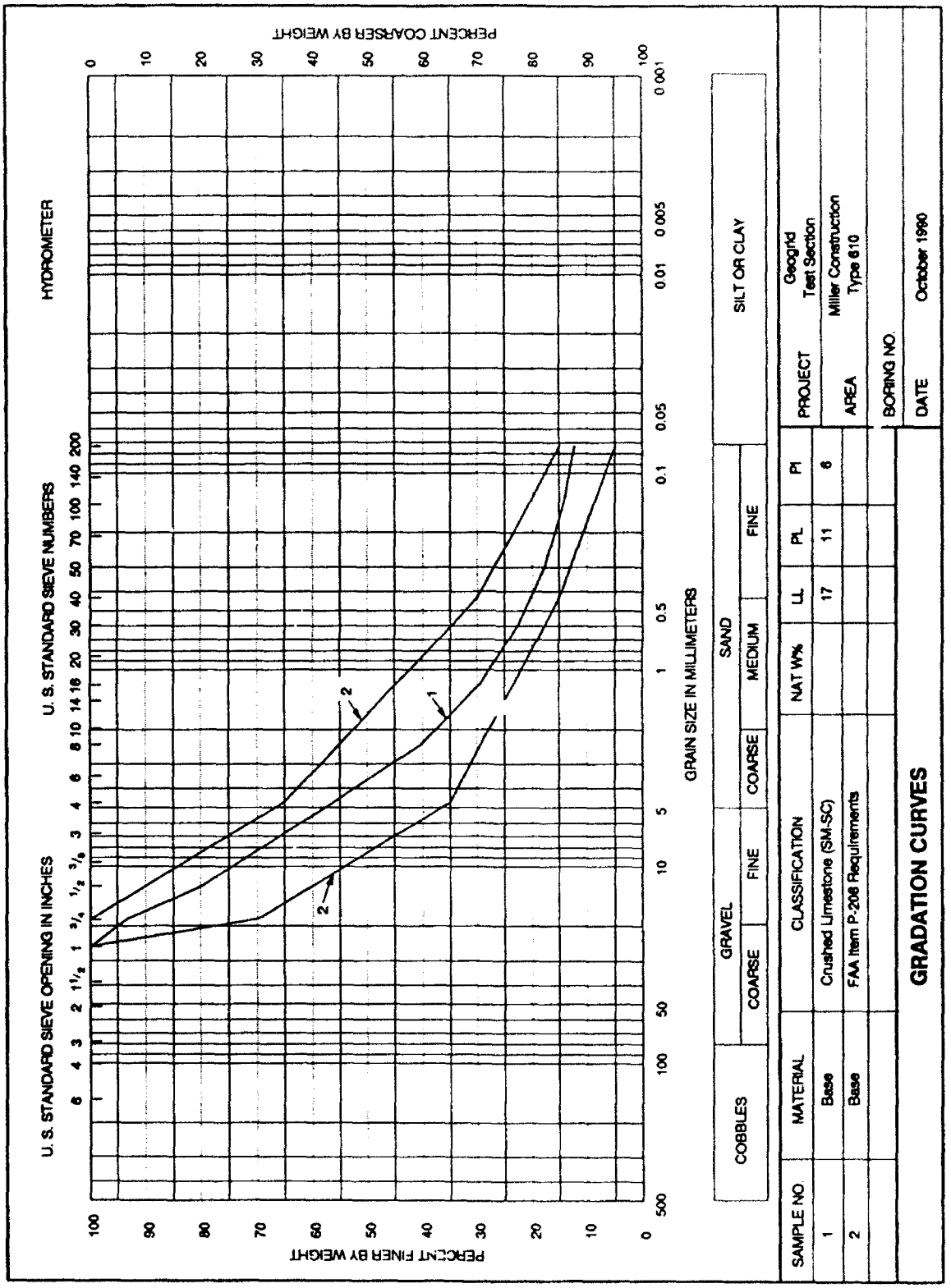

Figure 10. Classification data for base course material

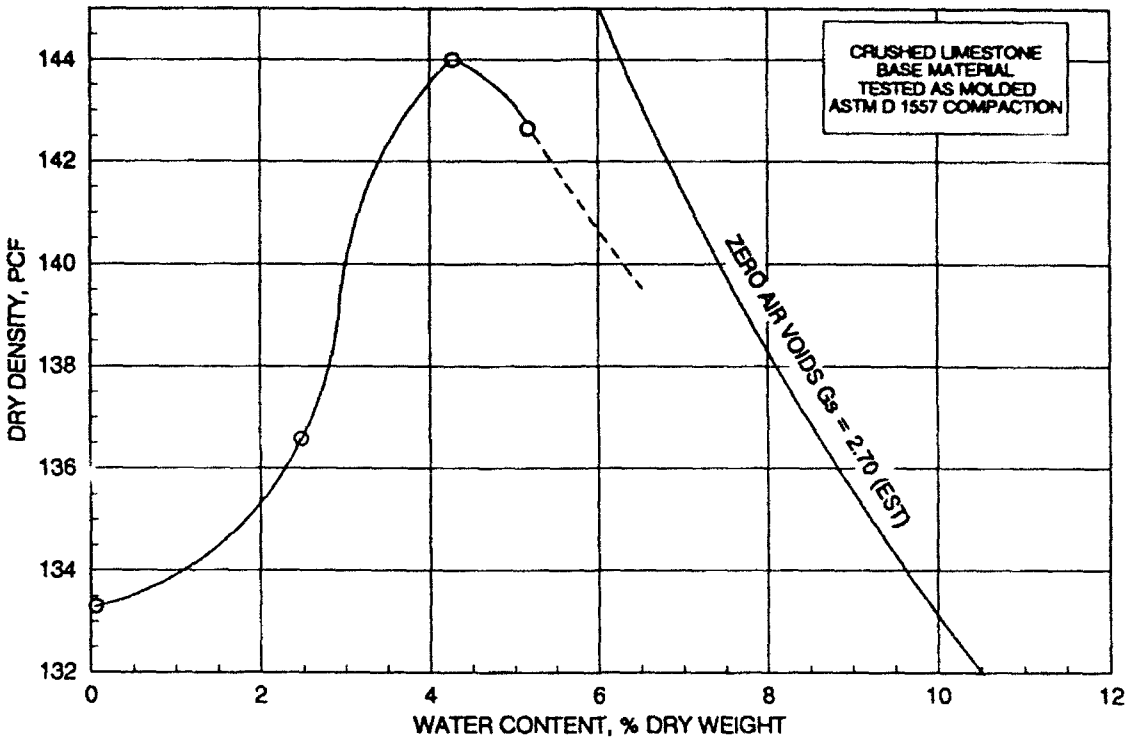

Figure 11. Density, and water content data for crushed limestone base course material (tested as molded)

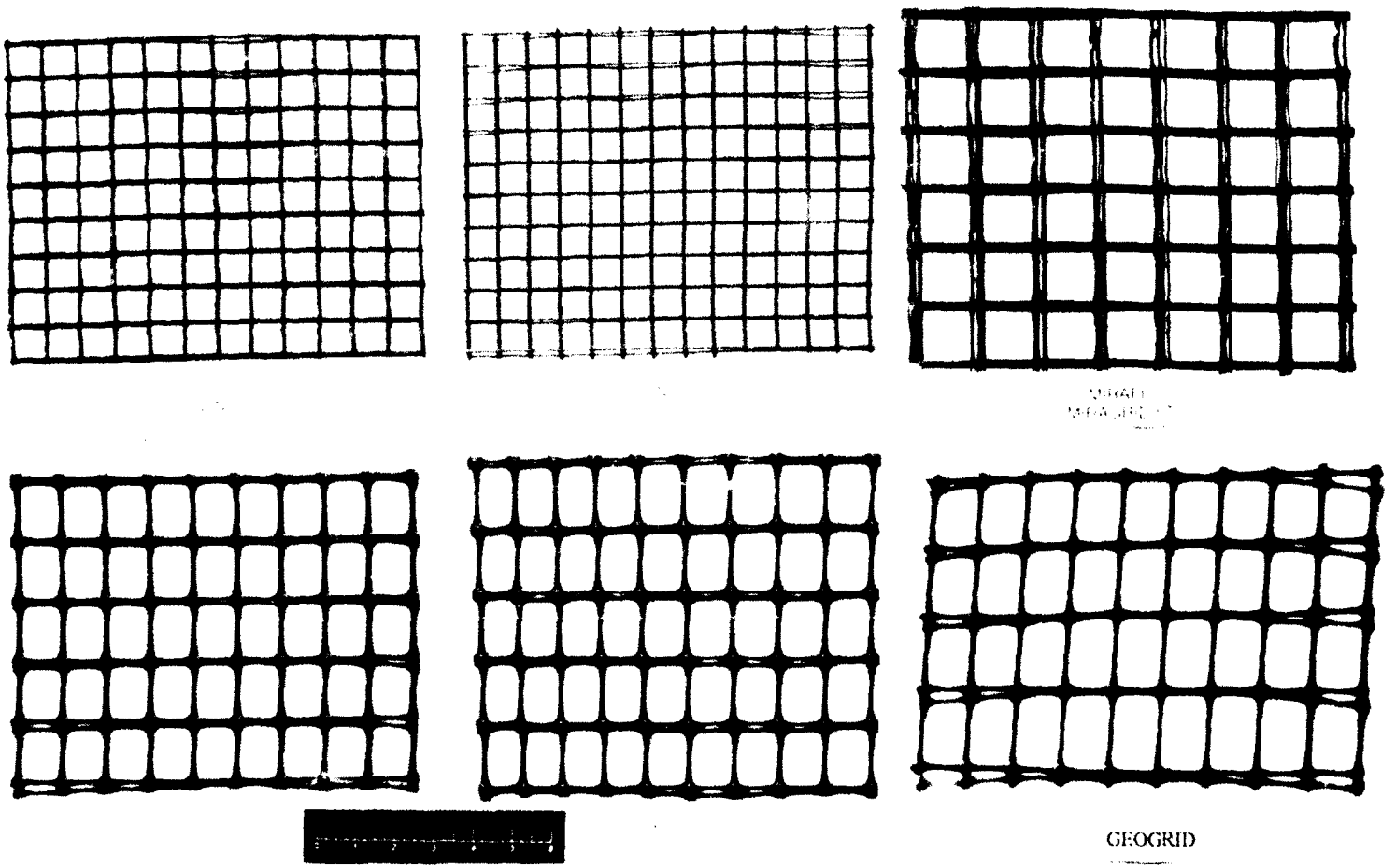

Figure 12. Geogrids used in the field test section

Figure 13. Final subgrade surface prior to geogrid installation

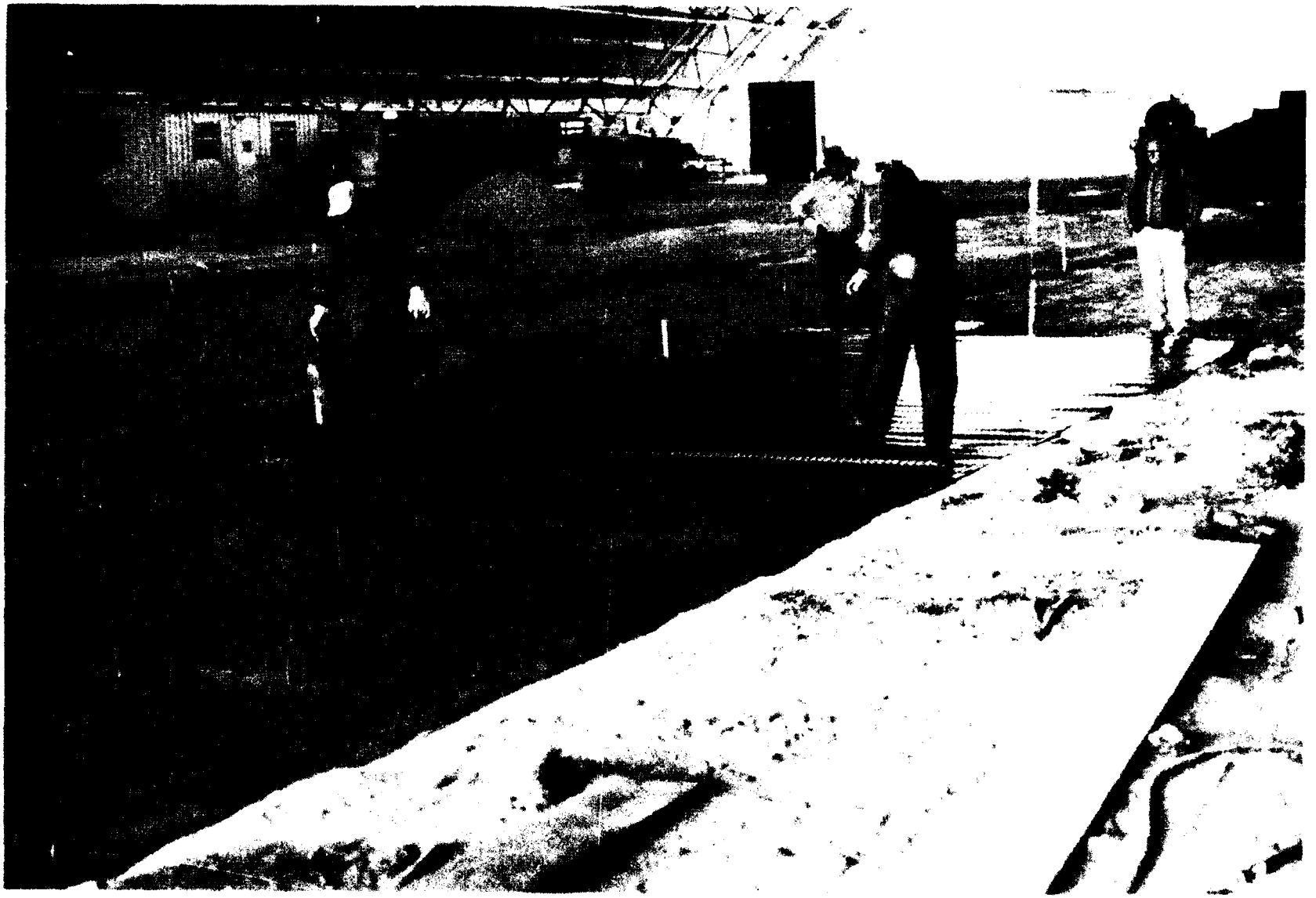

Figure 14. Installing geogrid on the subgrade

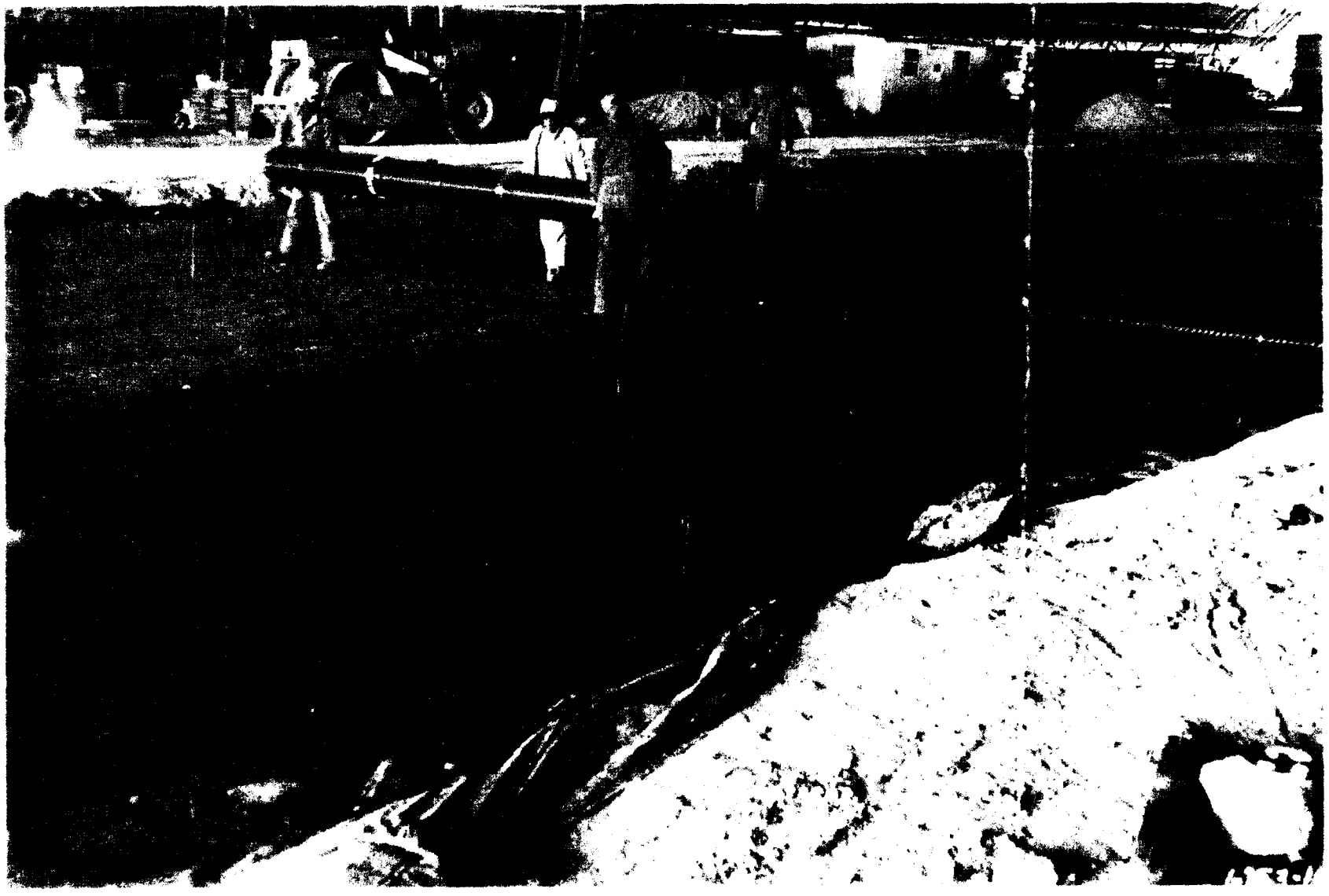

Figure 15. Geogrid installed on the subgrade

Figure 16. Installing crushed limestone base course

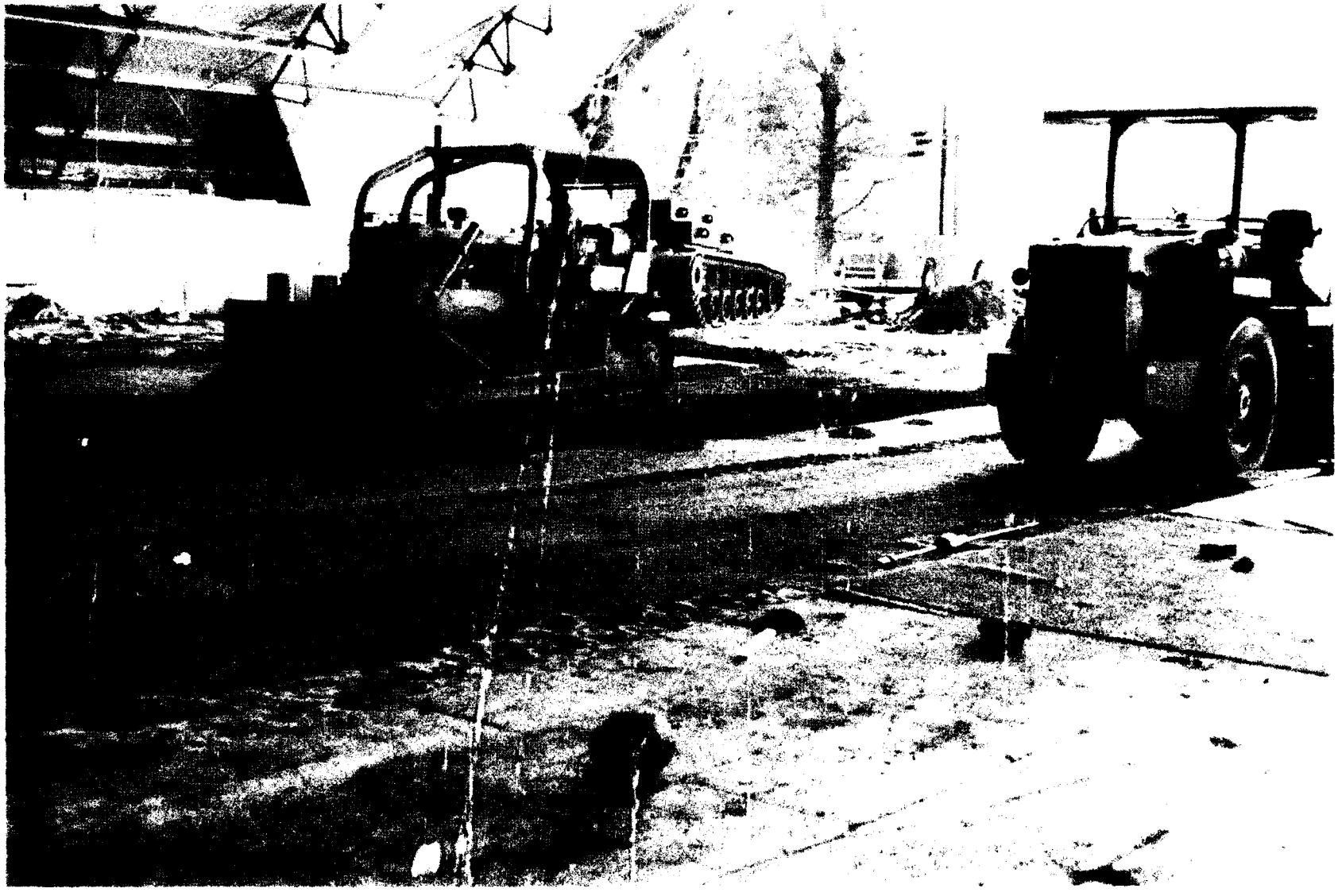

Figure 17. Spreading and compacting base course material

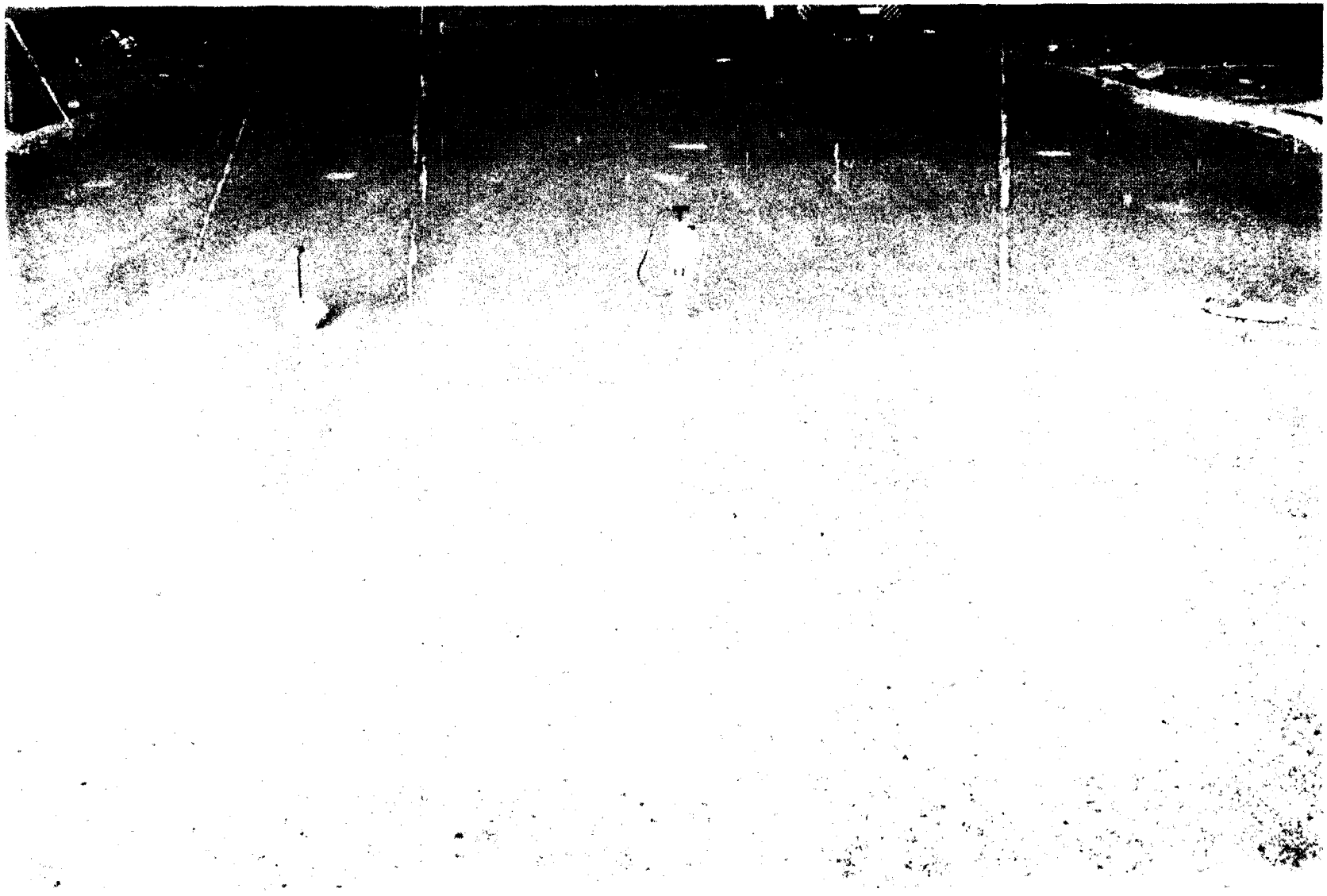

Figure 18. Base course surface prior to installing AC surfacing

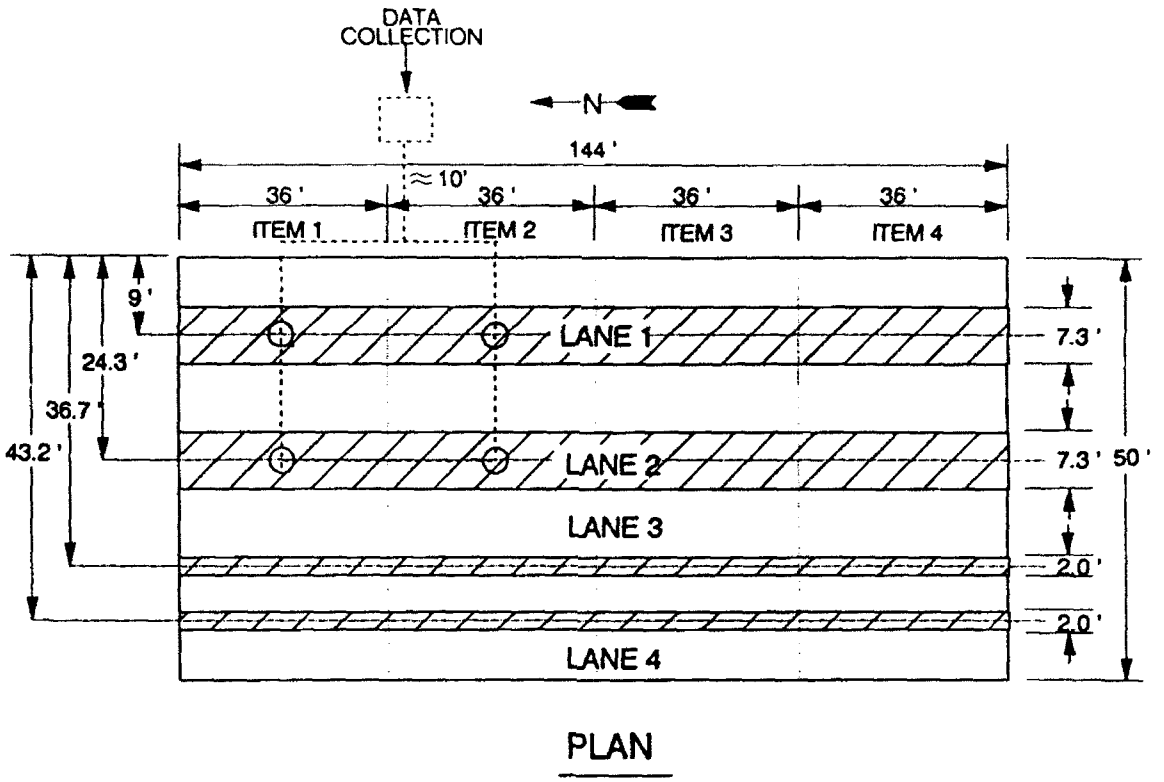

Figure 19. Layout of MDD test locations

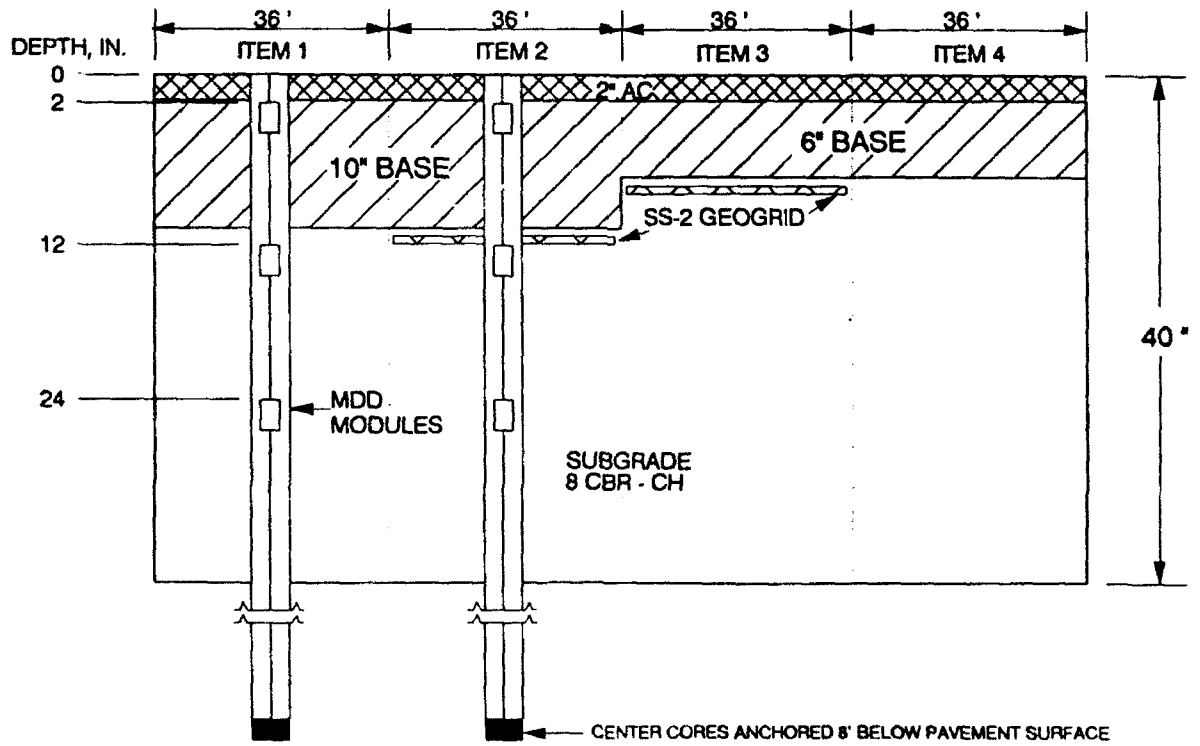

Figure 20. Profile of MDD module test locations for traffic Lane 1

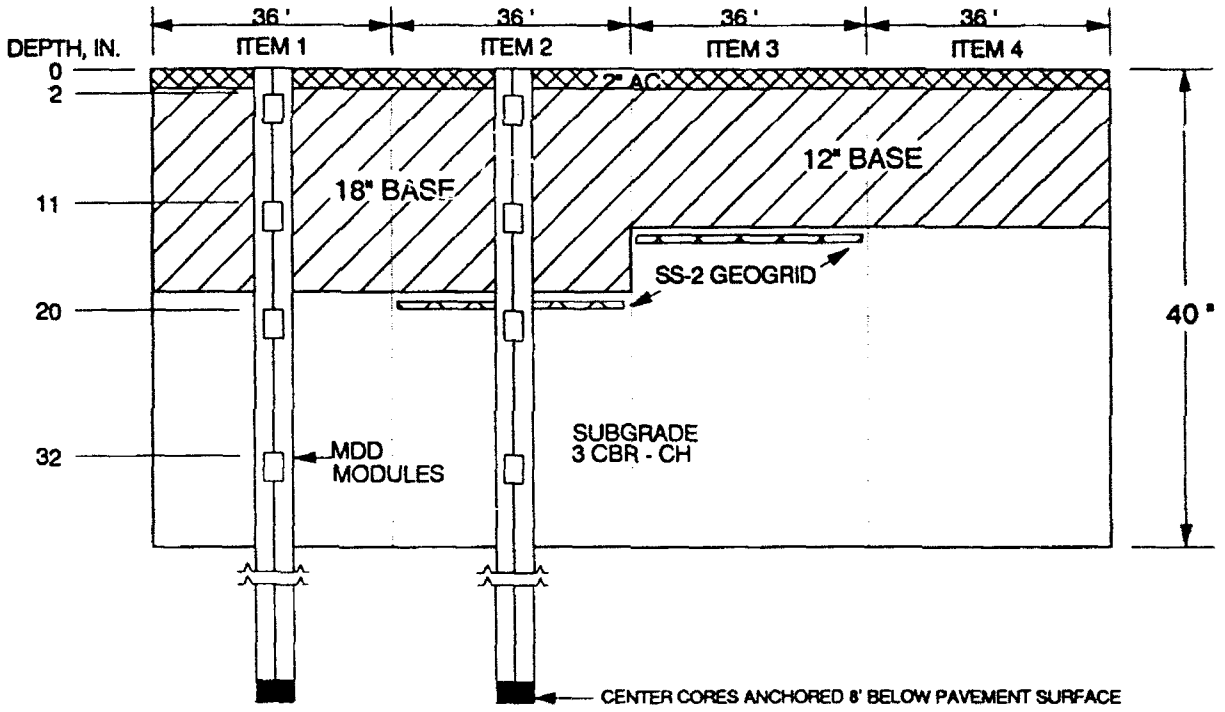

Figure 21. Profile of MDD module test locations for traffic Lane 2

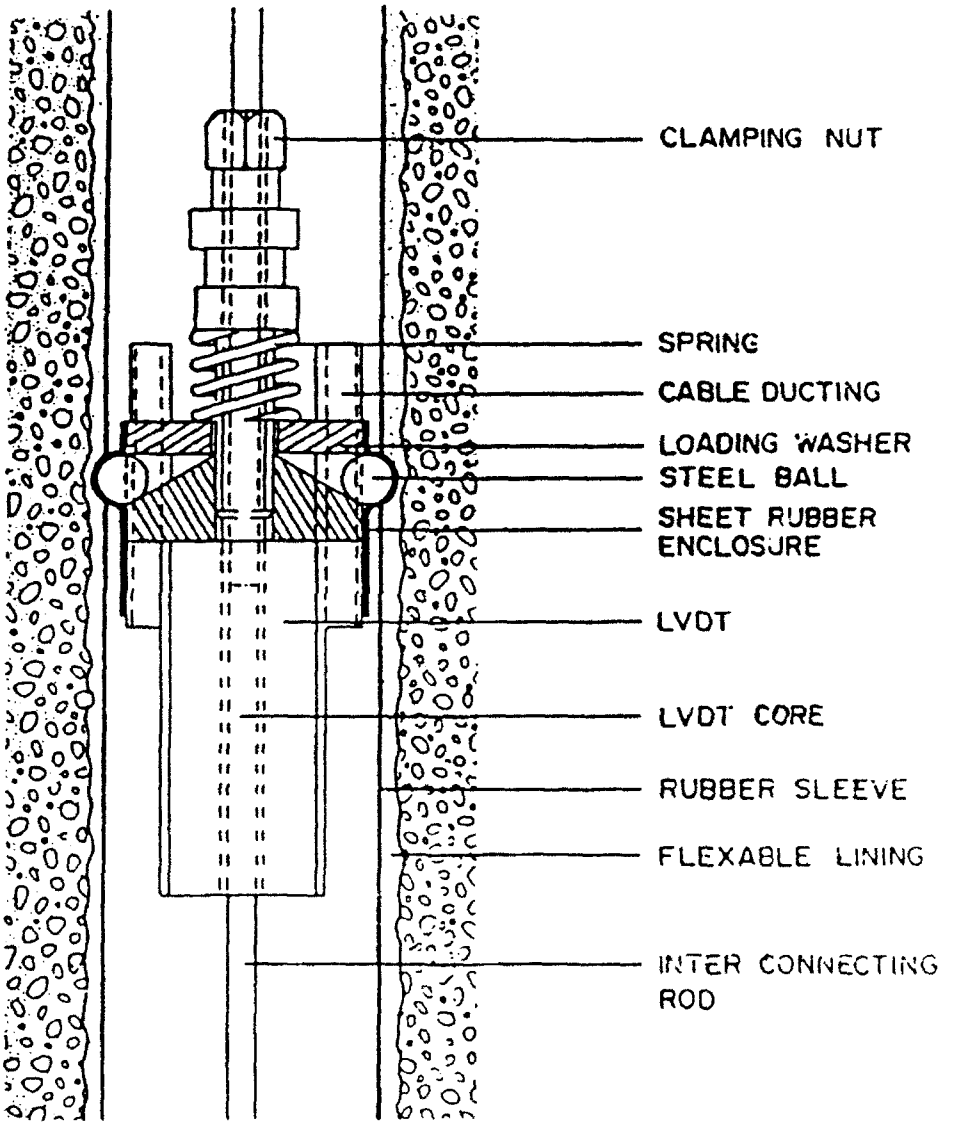

Figure 22. Components of MDD module[4]

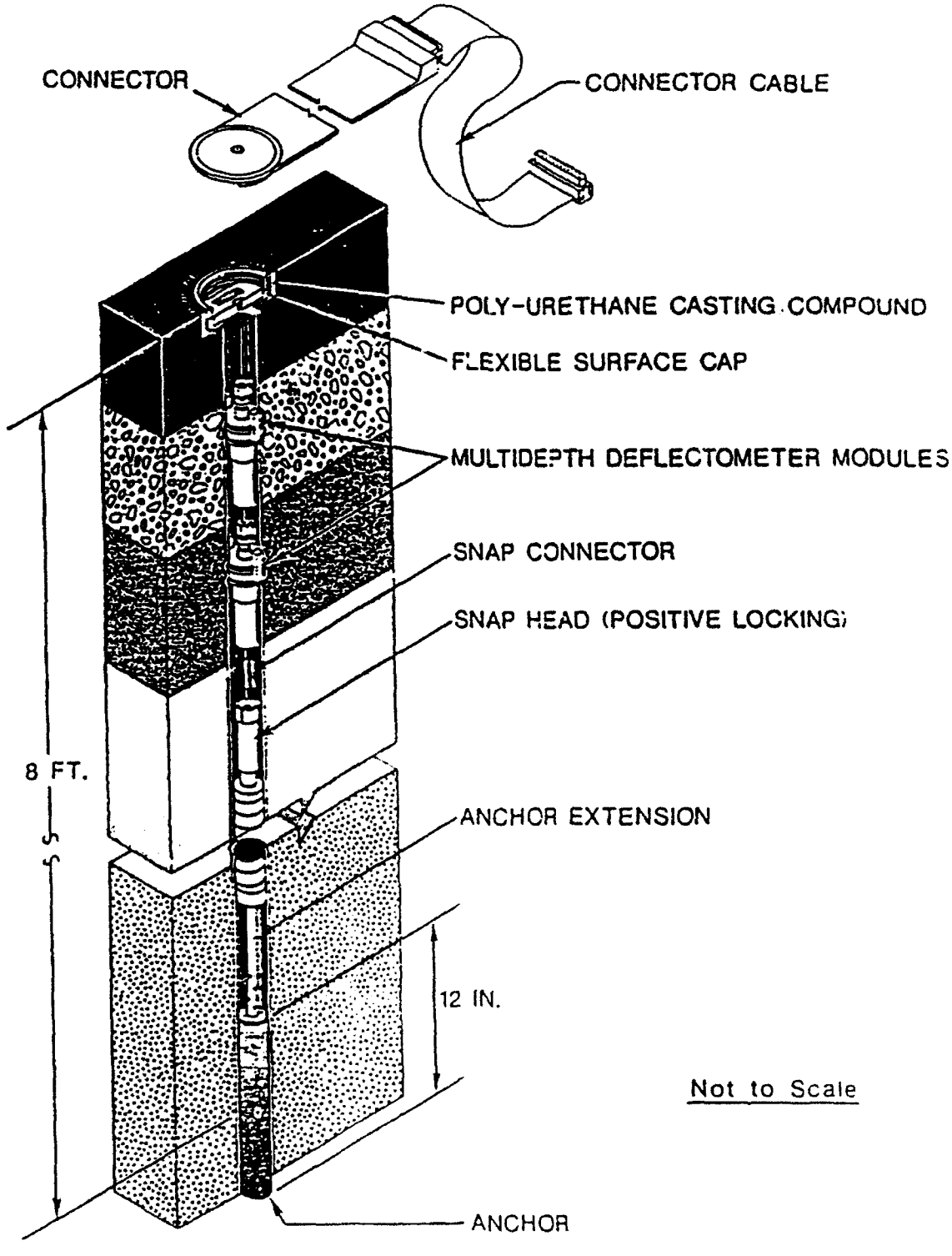

Figure 23. Typical cross section of MDD after installation[4]

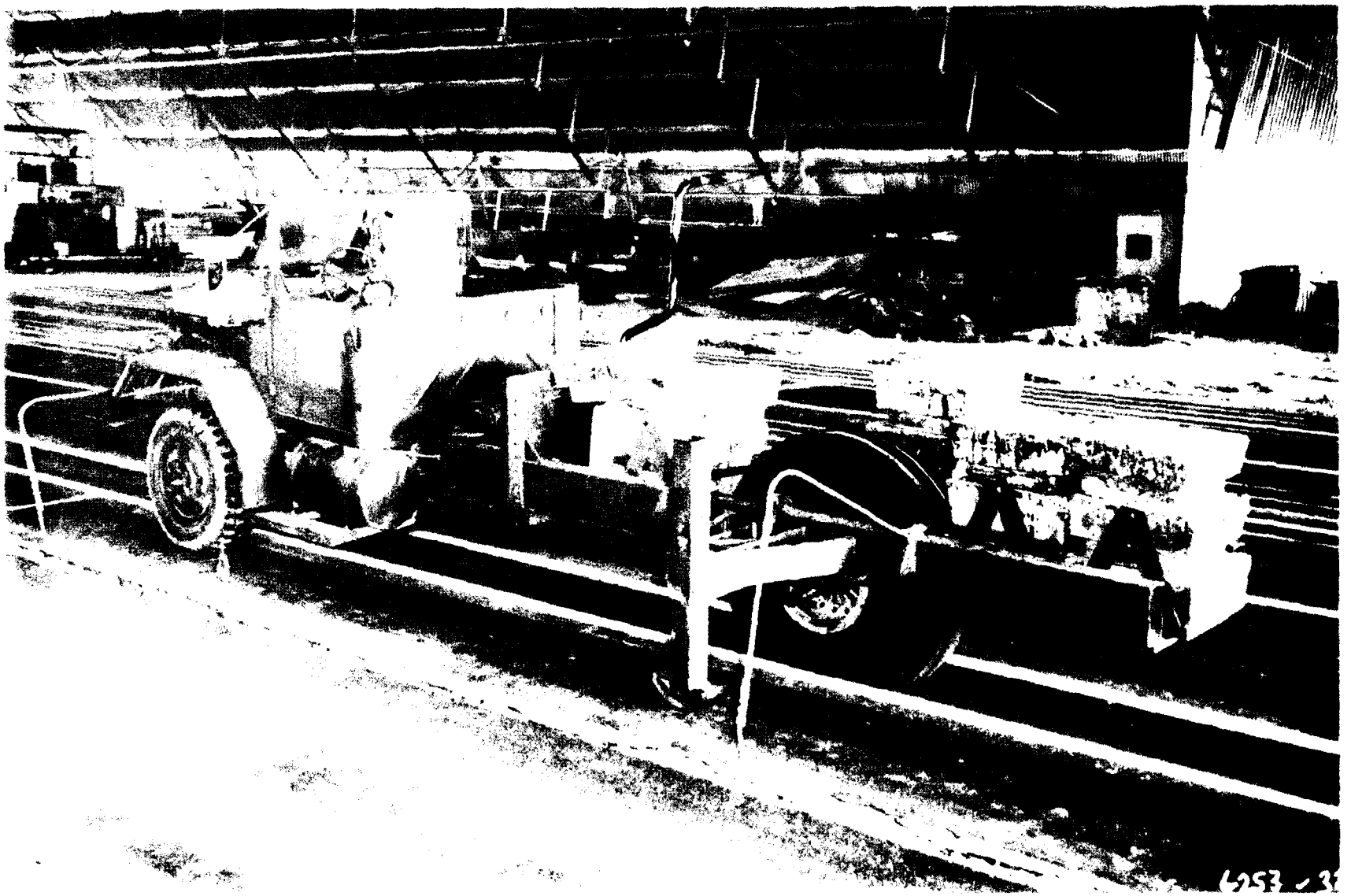

Figure 24. 30-kip single-wheel test cart

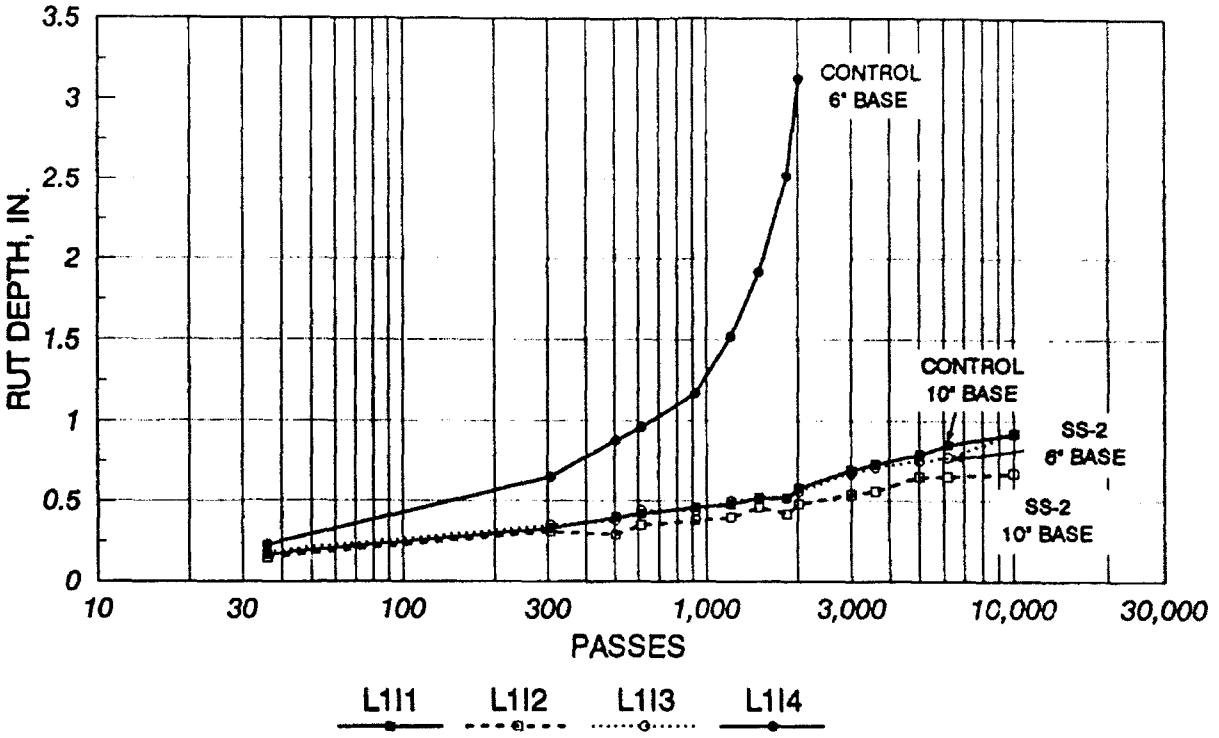

Figure 25. Rut depth measurements for Lane 1

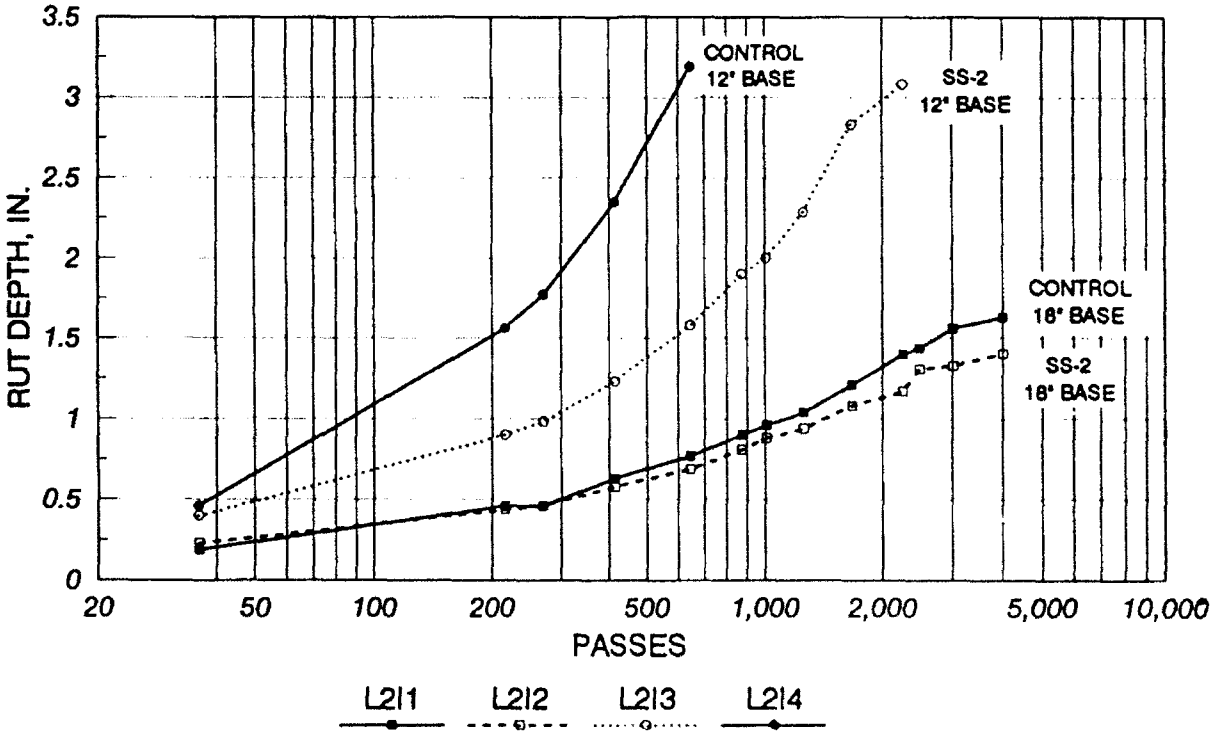

Figure 26. Rut depth measurements for Lane 2

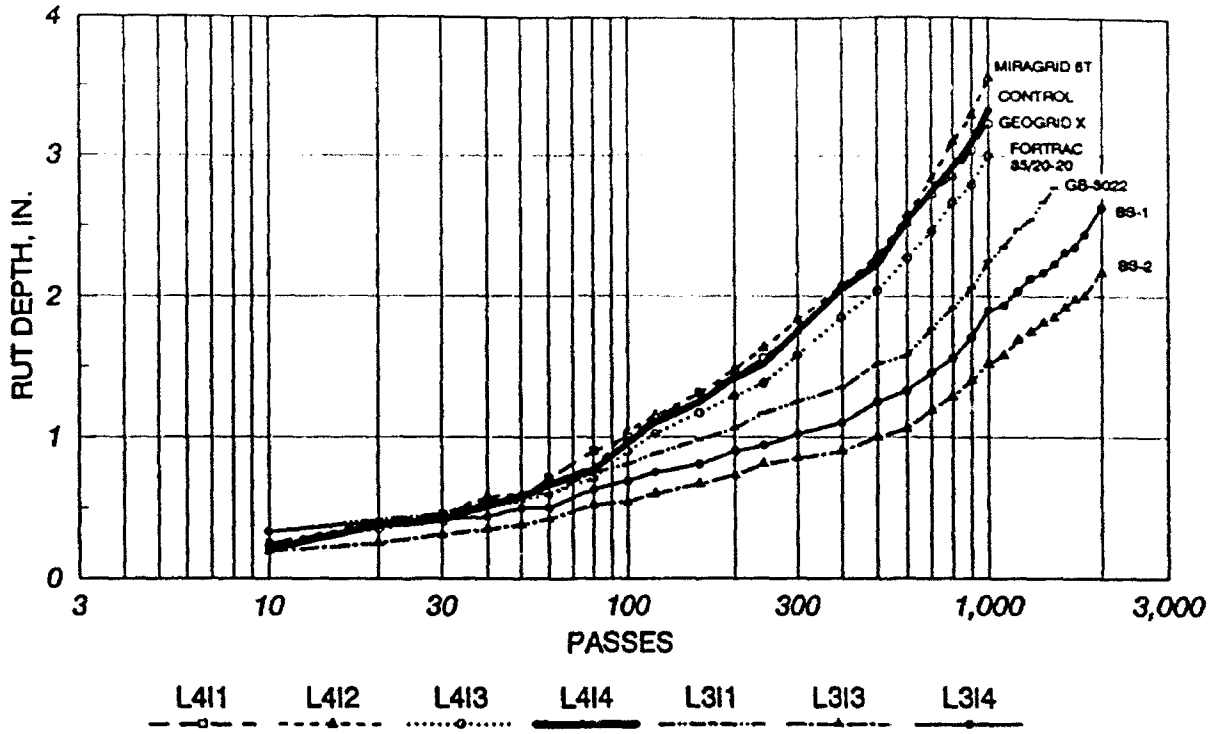

Figure 27. Rut depth measurements for Lanes 3 & 4

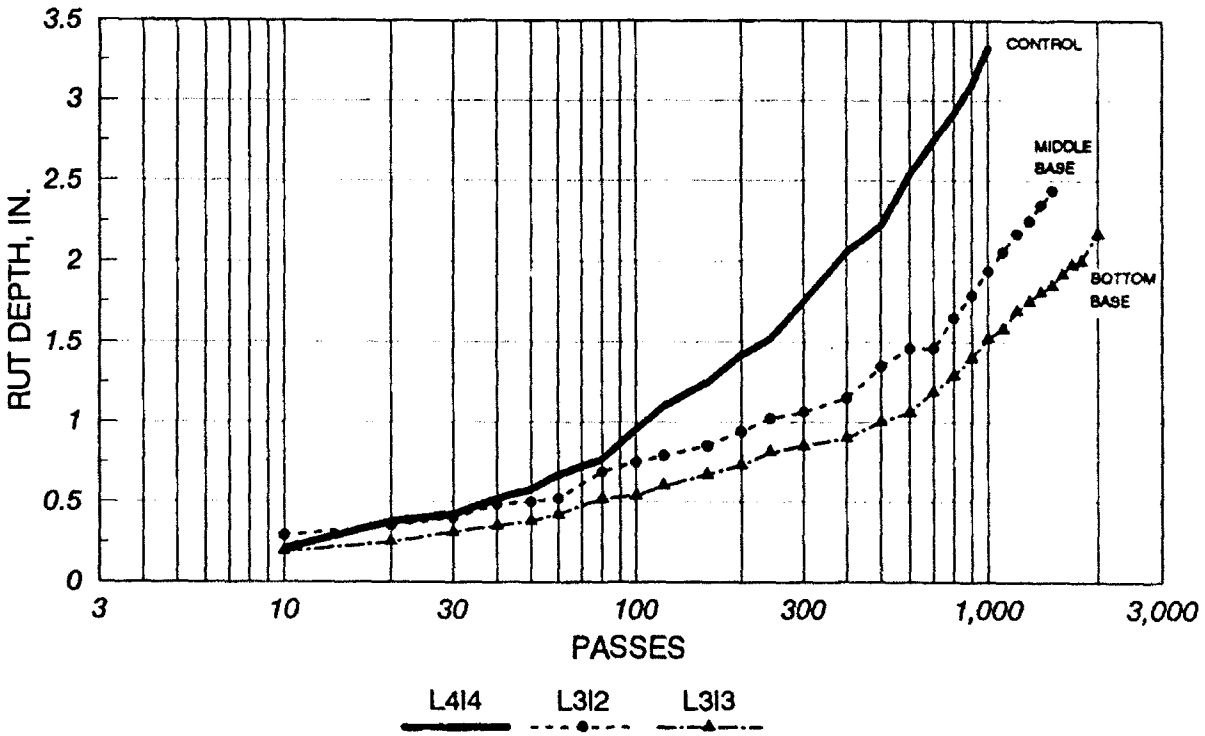

Figure 28. Comparison of geogrid placed in the middle of the base and at the bottom of the base

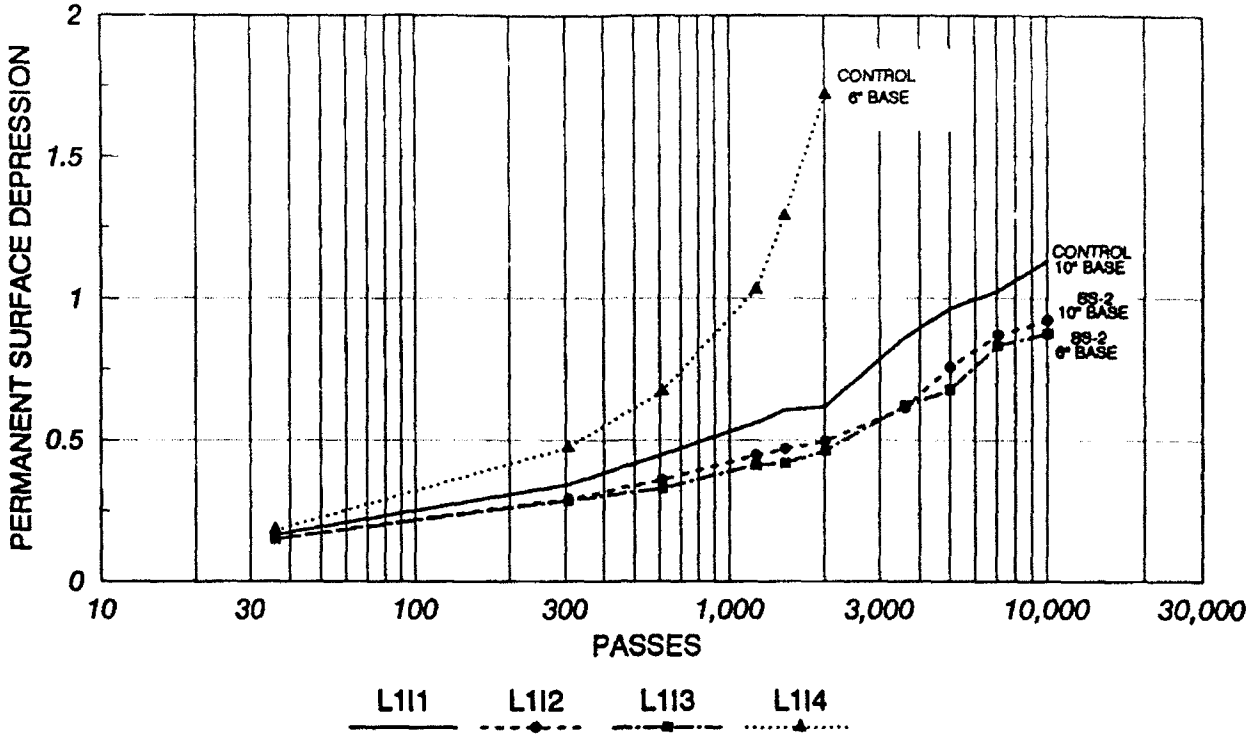

Figure 29. Permanent surface depression for Lane 1

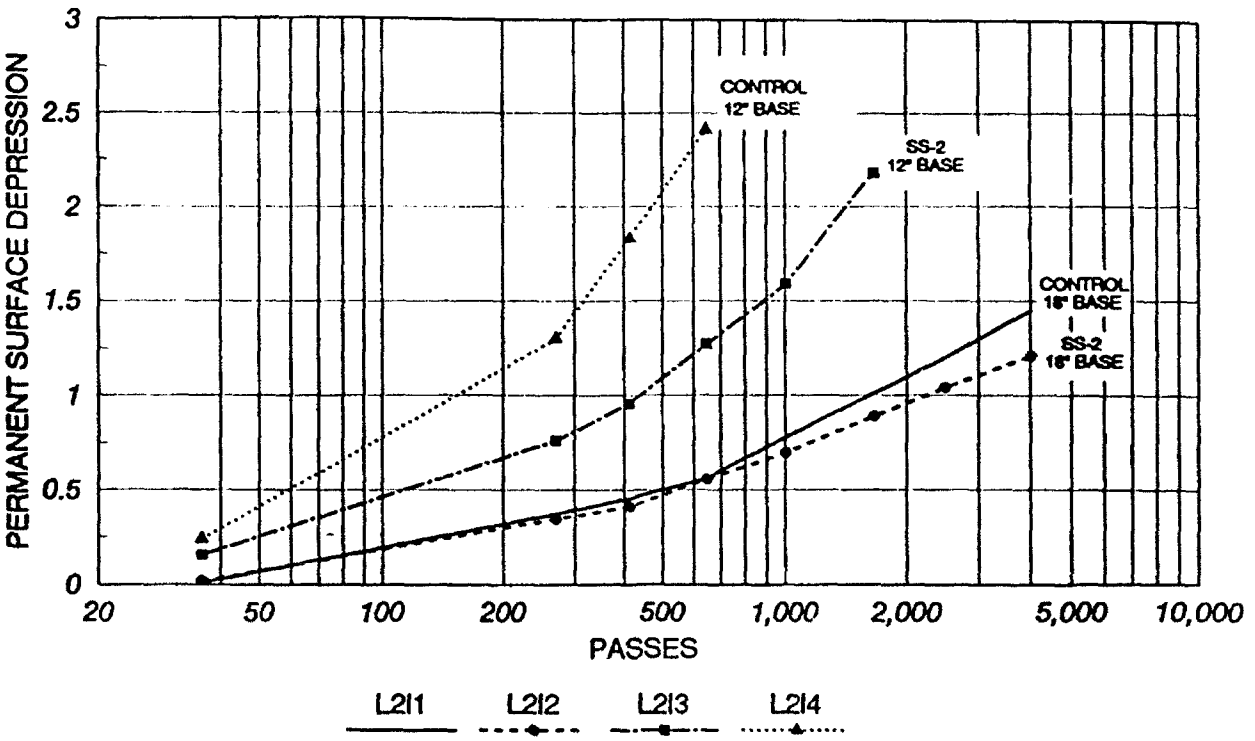

Figure 30. Permanent surface depression for Lane 2

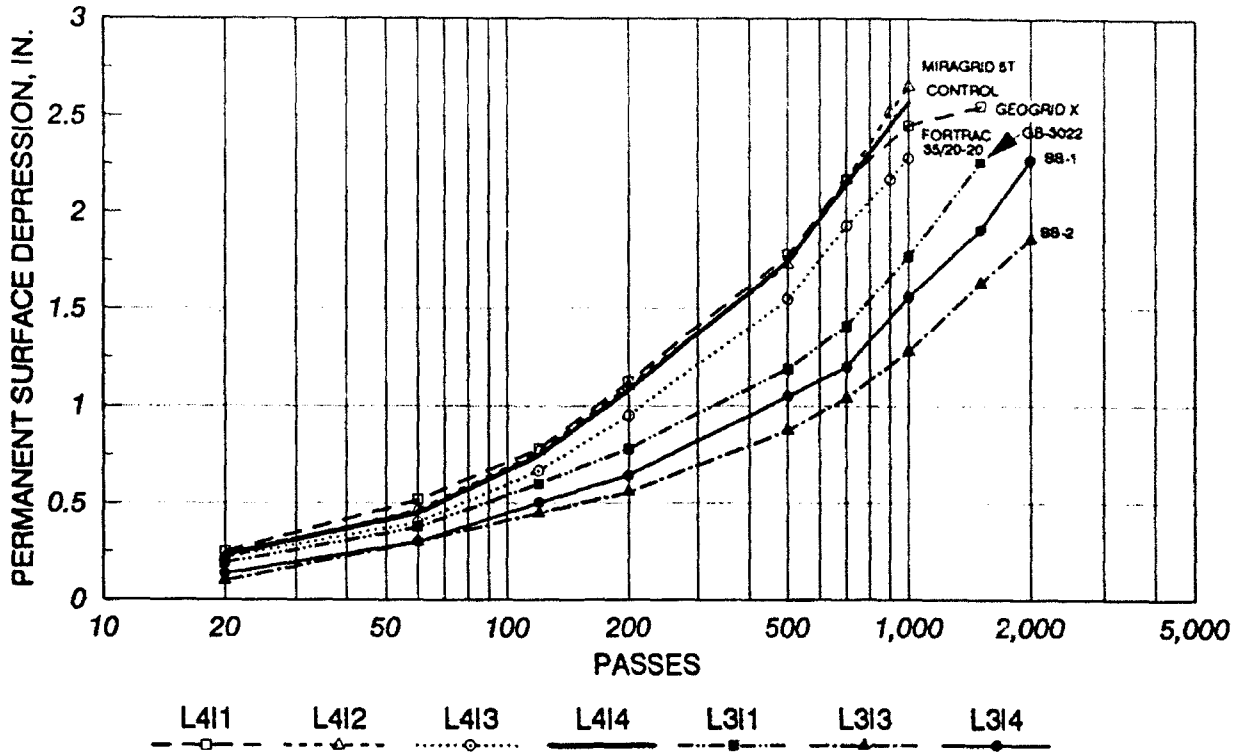

Figure 31. Permanent surface depression for Lanes 3 & 4

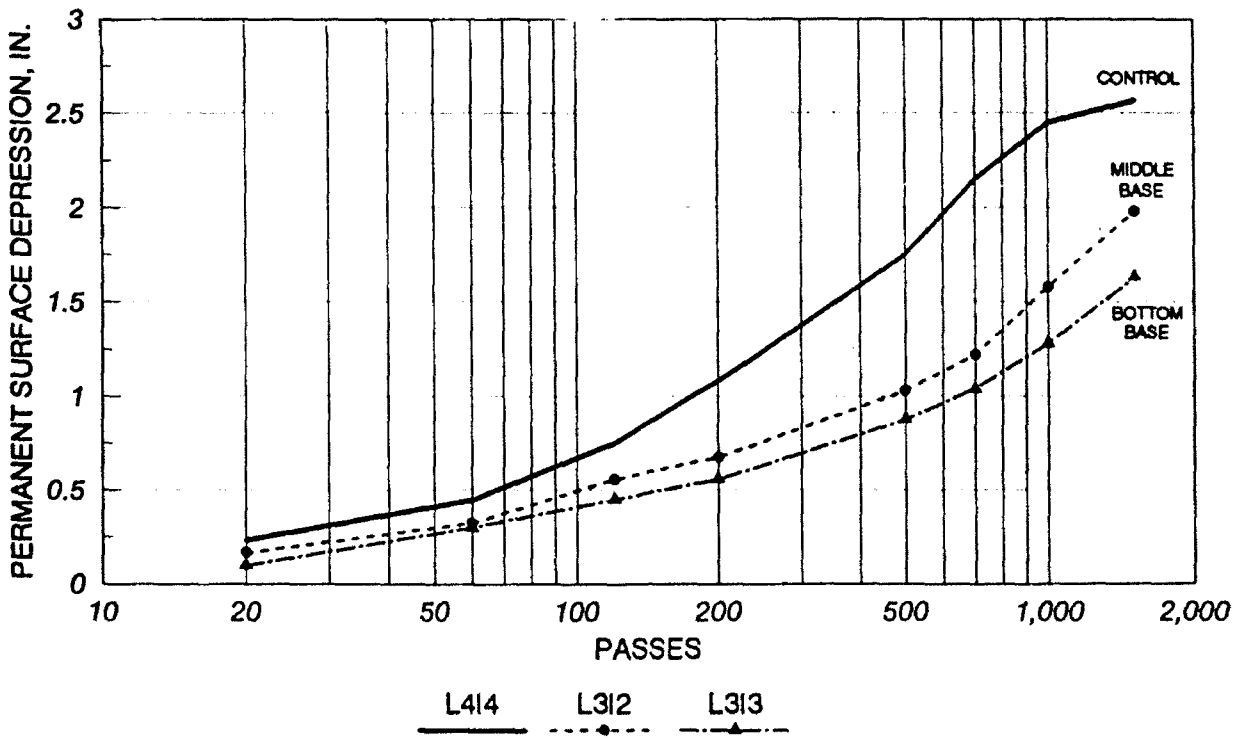

Figure 32. Comparison of geogrid placed in the middle of the base and at the bottom of the base

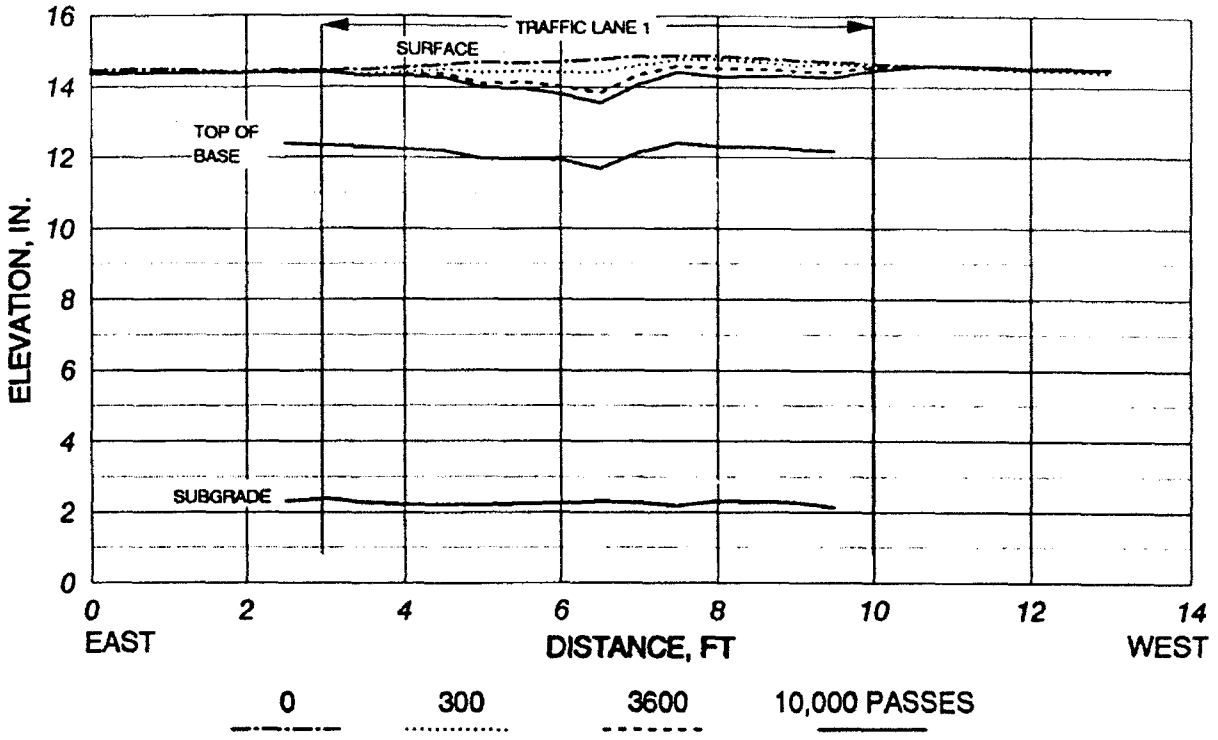

Figure 33. Typical cross section, Lane 1, Item 1 (control, 2 in. AC, 10 in. base)

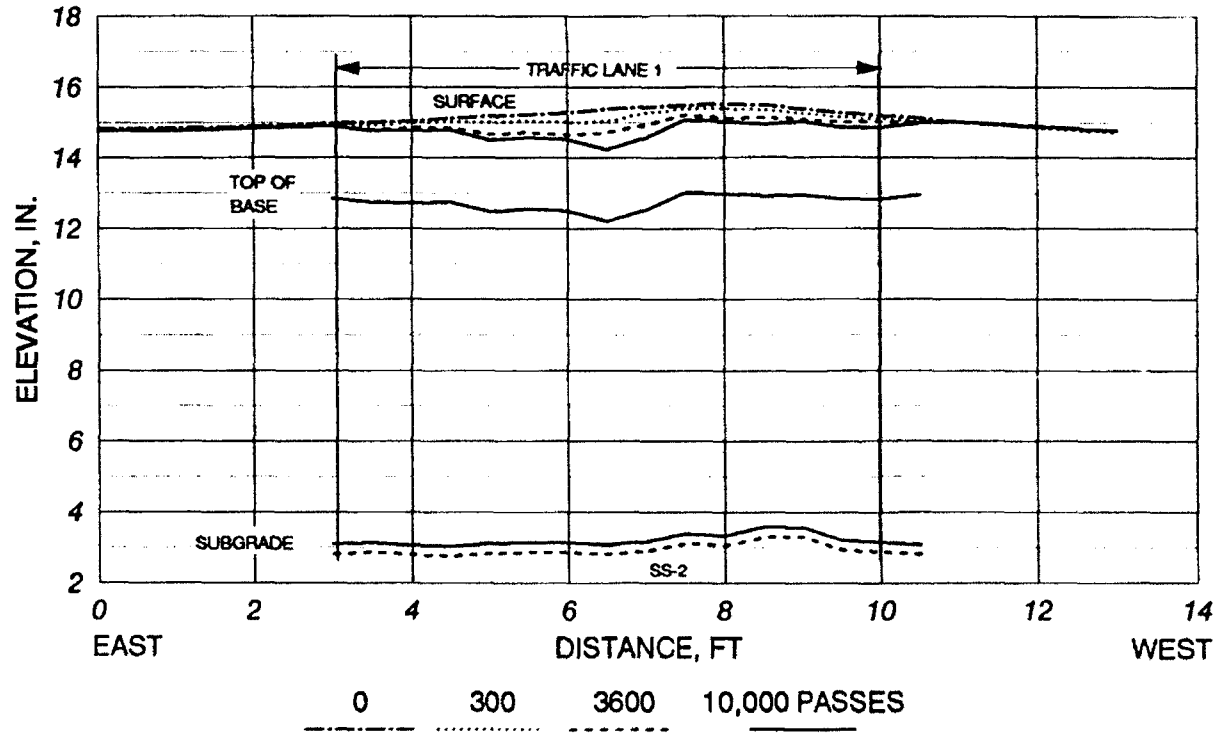

Figure 34. Typical cross section, Lane 1, Item 2 (2 in. AC, SS-2, 10 in. base)

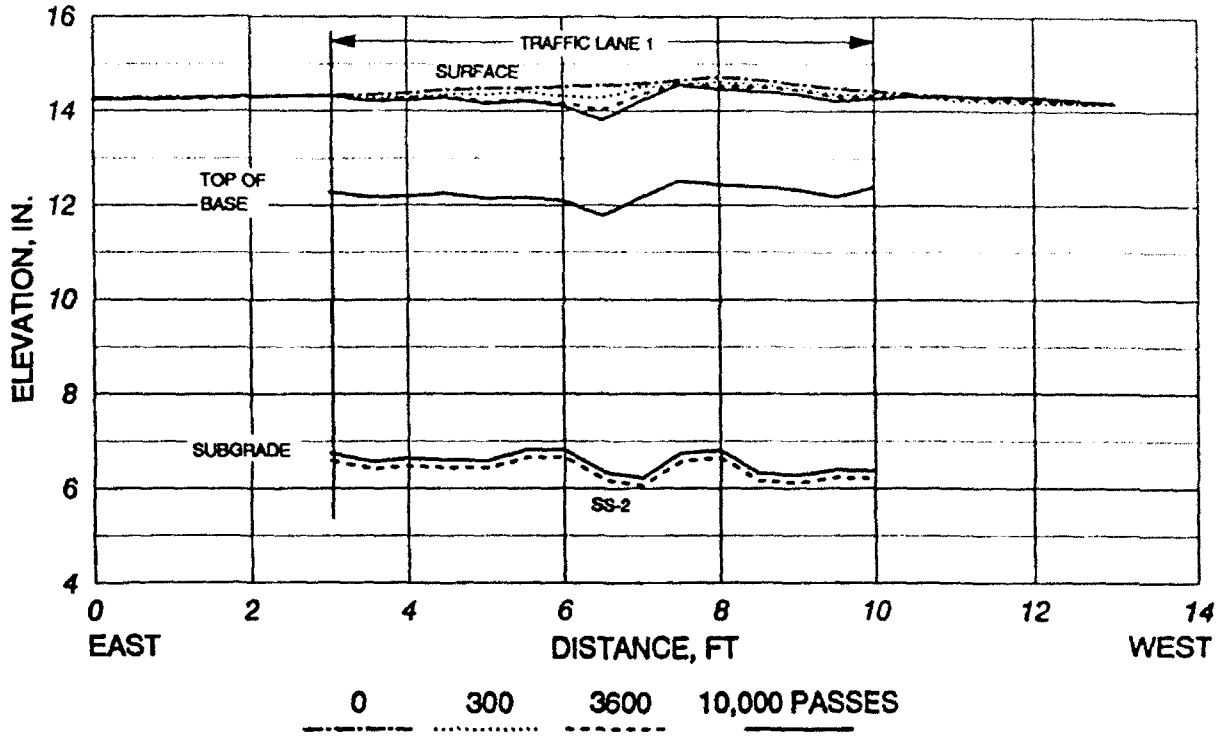

Figure 35. Typical cross section, Lane 1, Item 3
(2 in. AC, SS-2, 6 in. base)

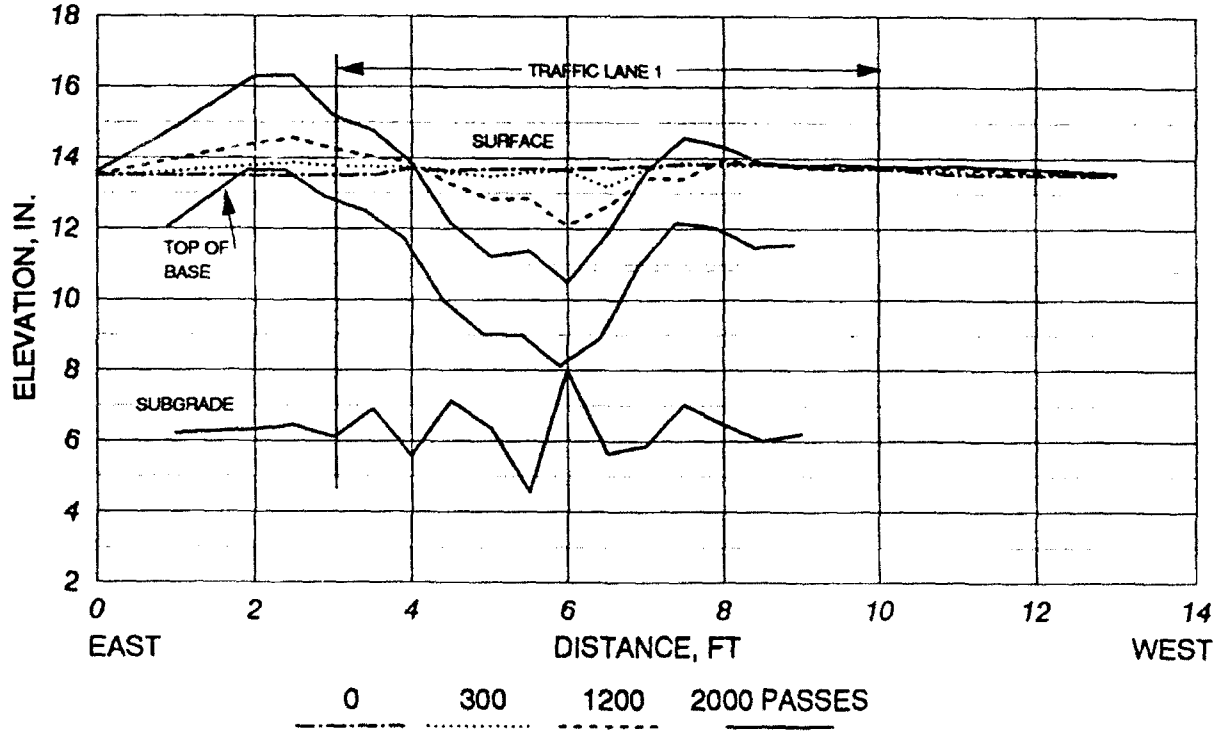

Figure 36. Typical cross section, Lane 1, Item 4
(control, 2 in. AC, 6 in. base)

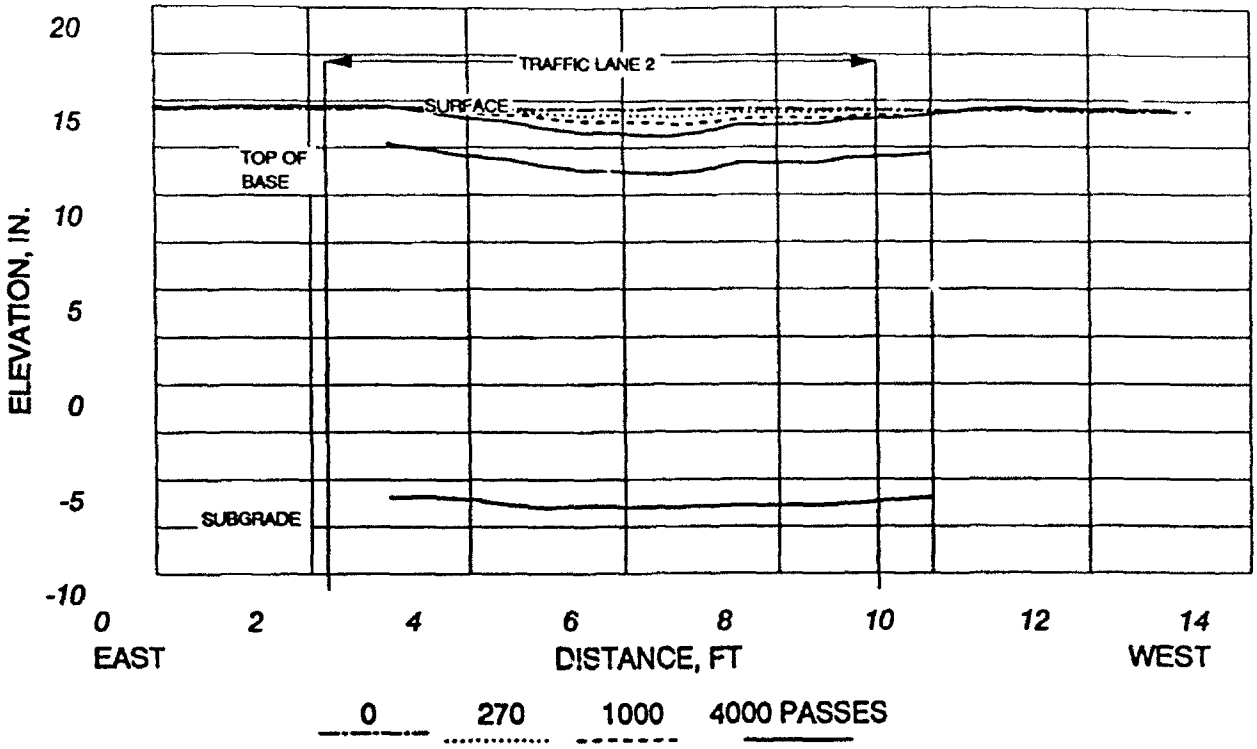

Figure 37. Typical cross section, Lane 2, Item 1 (control, 2 in. AC, 18 in. base)

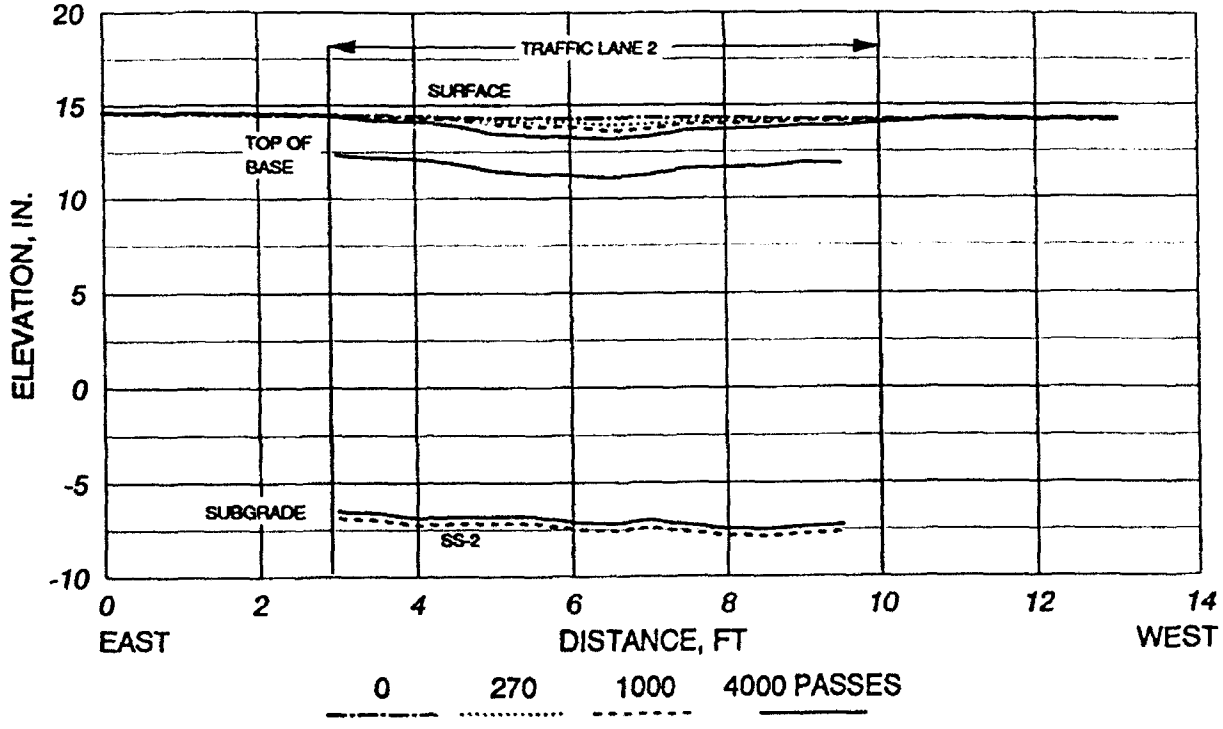

Figure 38. Typical cross section, Lane 2, Item 2 (2 in. AC, SS-2, 18 in. base)

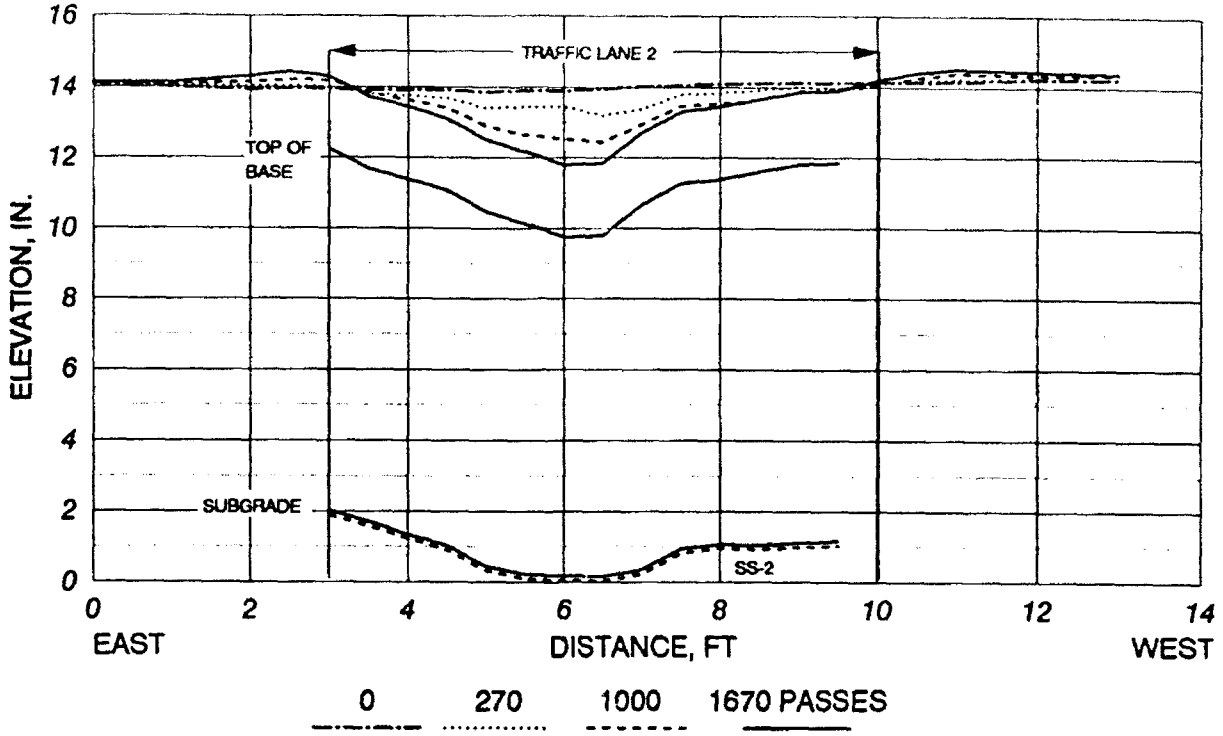

Figure 39. Typical cross section, Lane 2, Item 3 (2 in. AC, SS-2, 12 in. base)

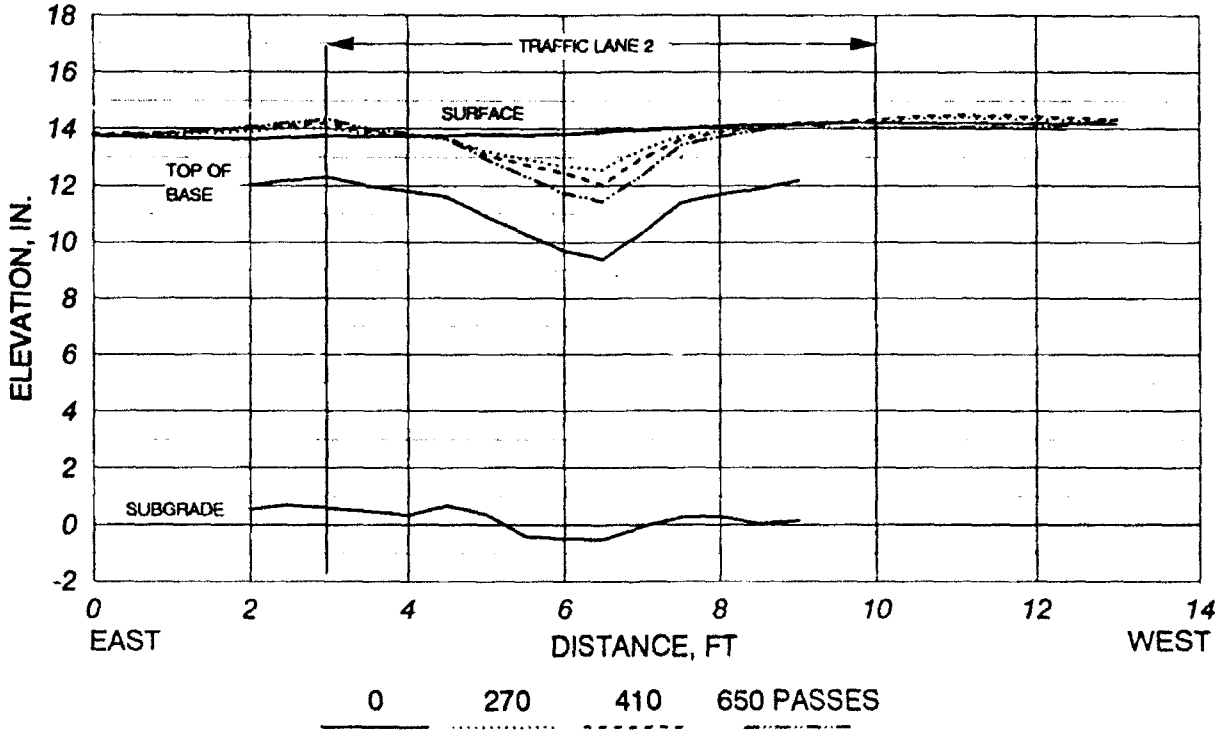

Figure 40. Typical cross section, Lane 2, Item 4 (control, 2 in. AC, 12 in. base)

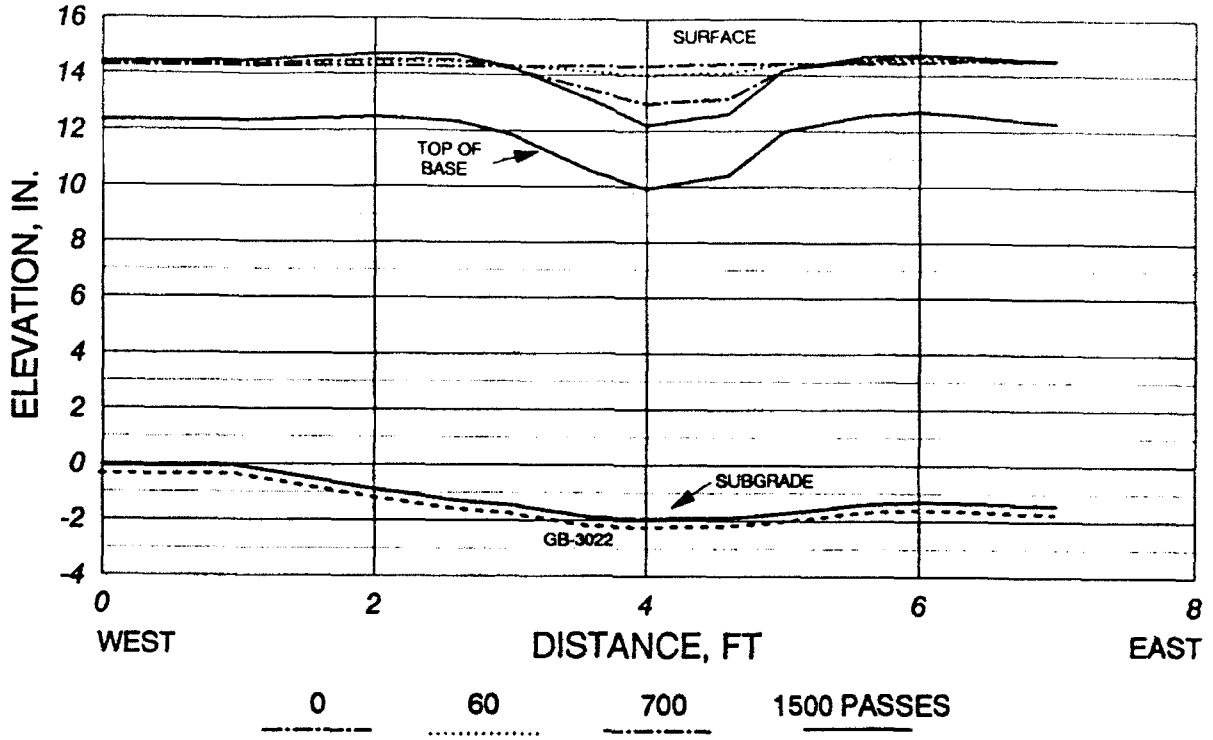

Figure 41. Typical cross section, Lane 3, Item 1 (GB-3022)

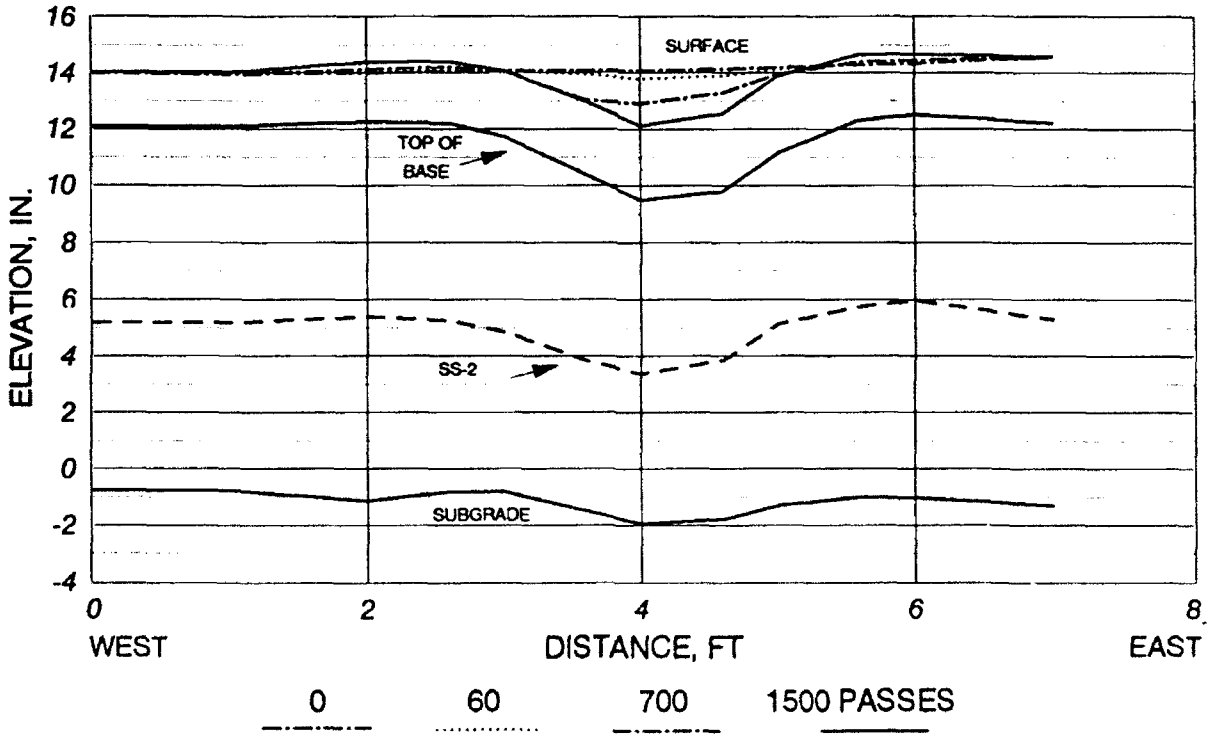

Figure 42. Typical cross section, Lane 3, Item 2 (SS-2 middle of base)

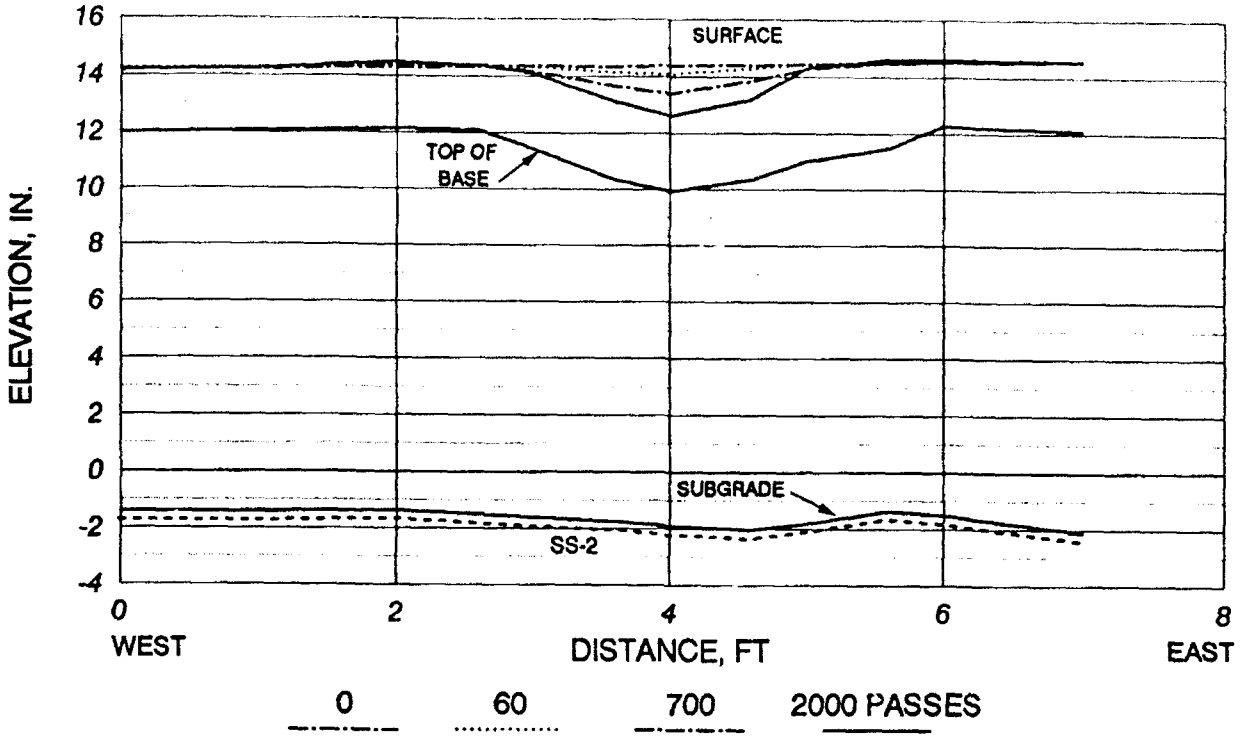

Figure 43. Typical cross section, Lane 3, Item 3 (SS-2)

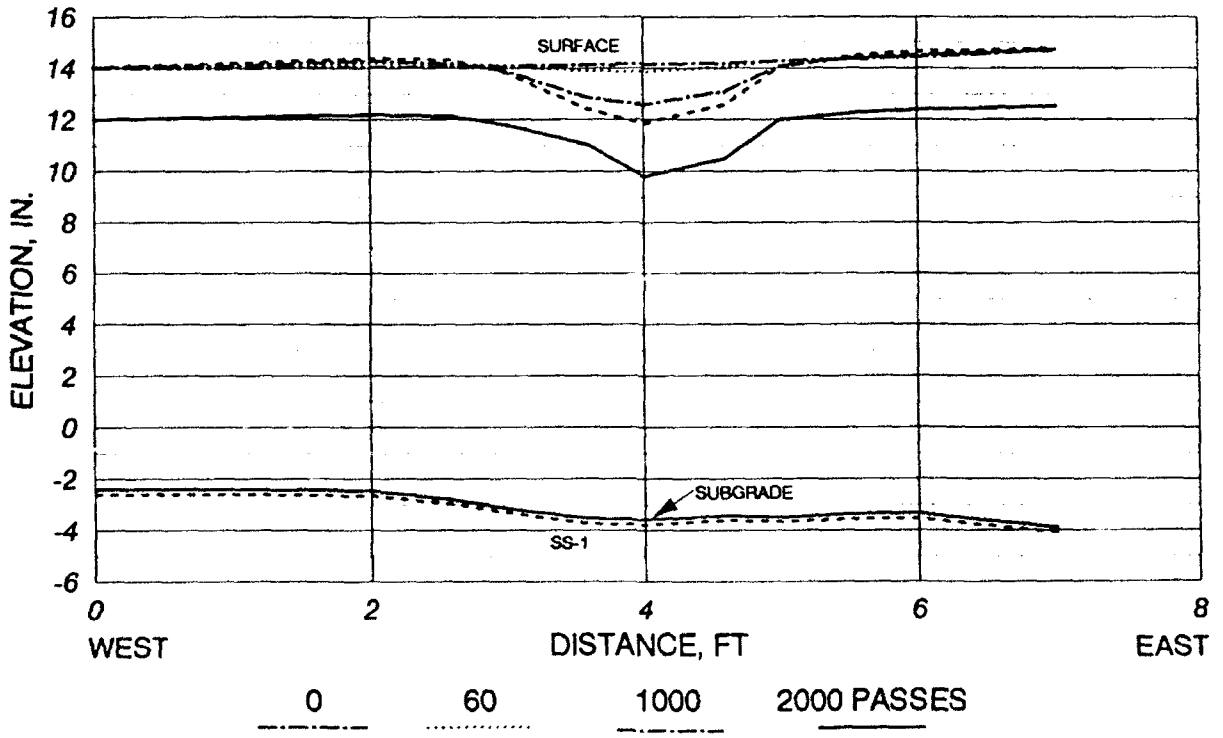

Figure 44. Typical cross section, Lane 3, Item 4 (SS-1)

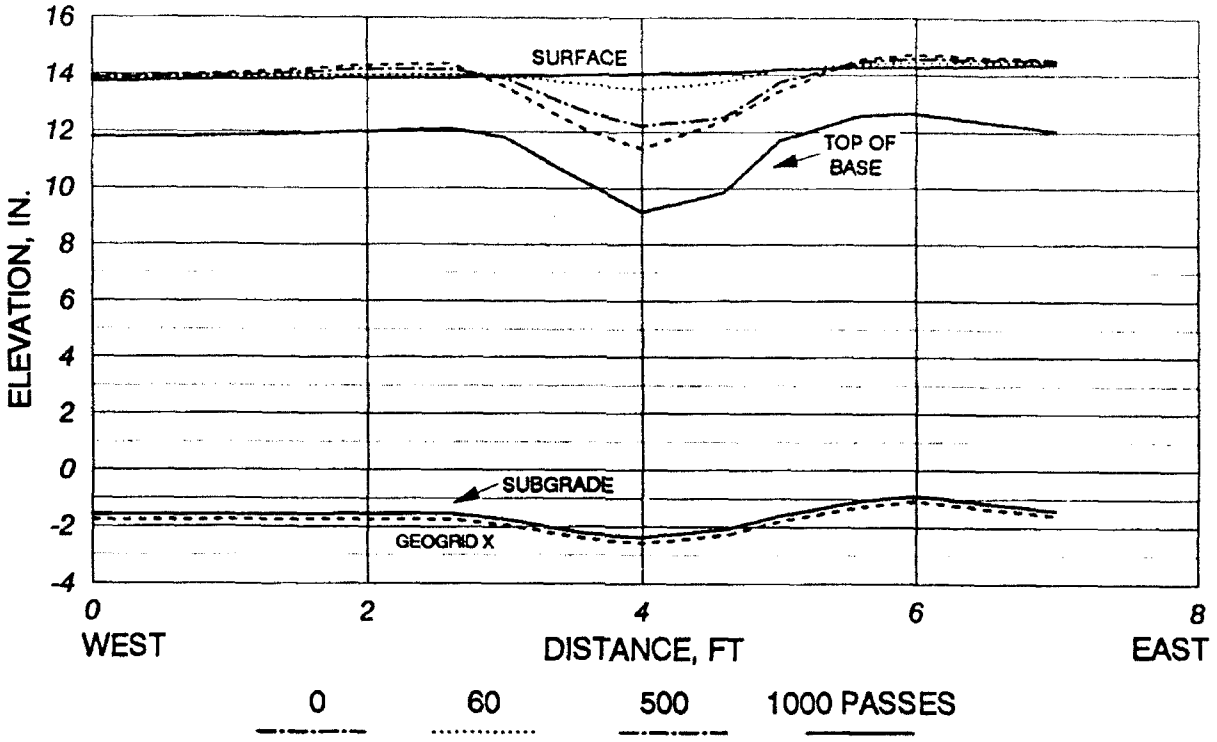

Figure 45. Typical cross section, Lane 4, Item 1 (Geogrid X)

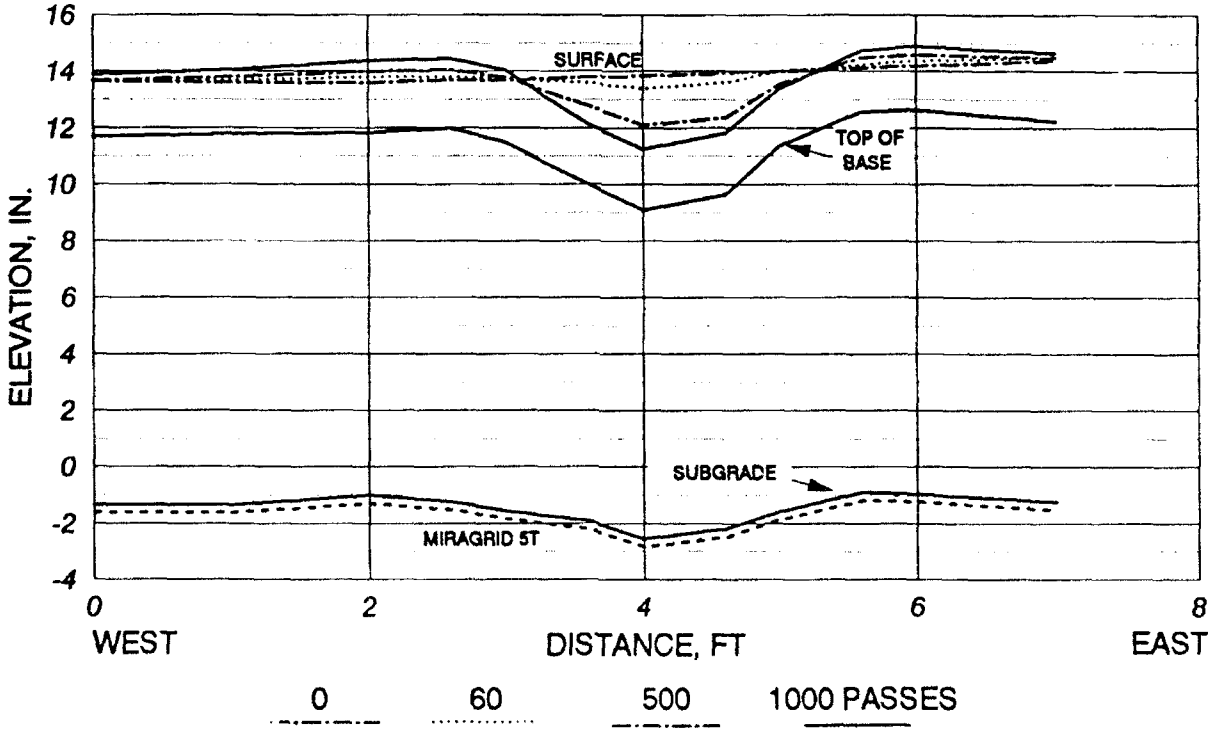

Figure 46. Typical cross section. Lane 4, Item 2 (Miragrid 5T)

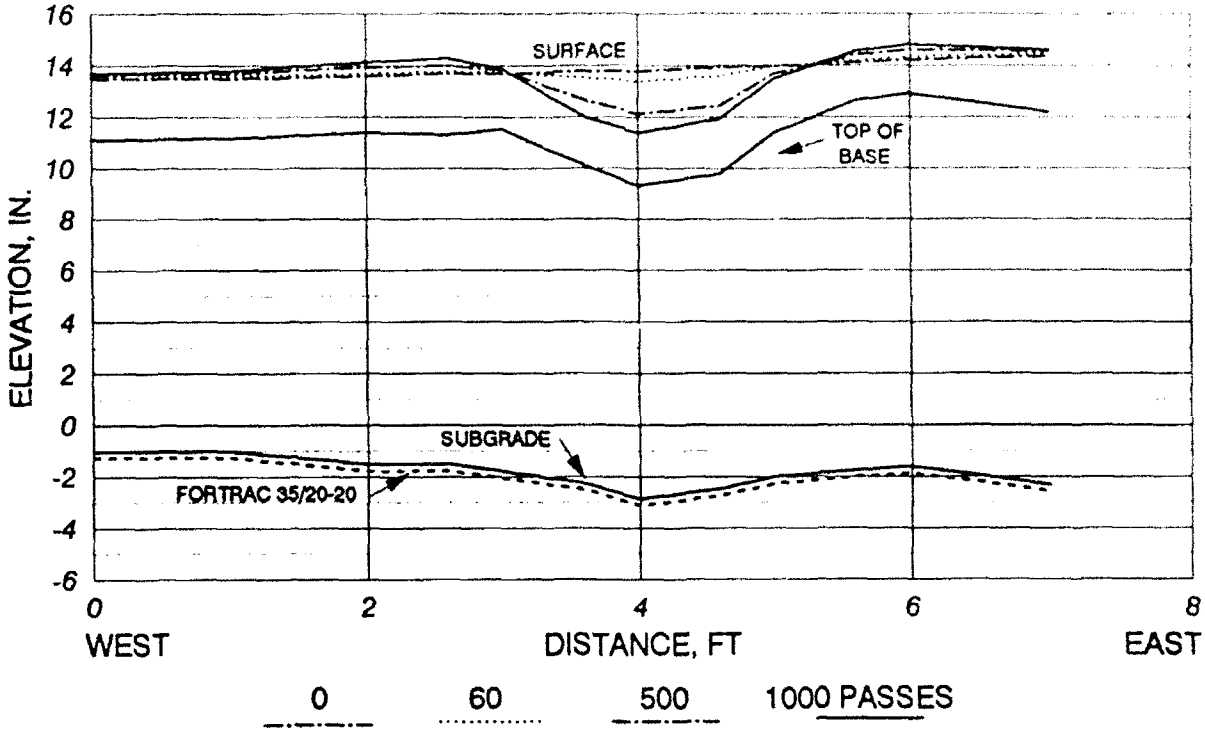

Figure 47. Typical cross section, Lane 4, Item 3 (Fortrac 35/20-20)

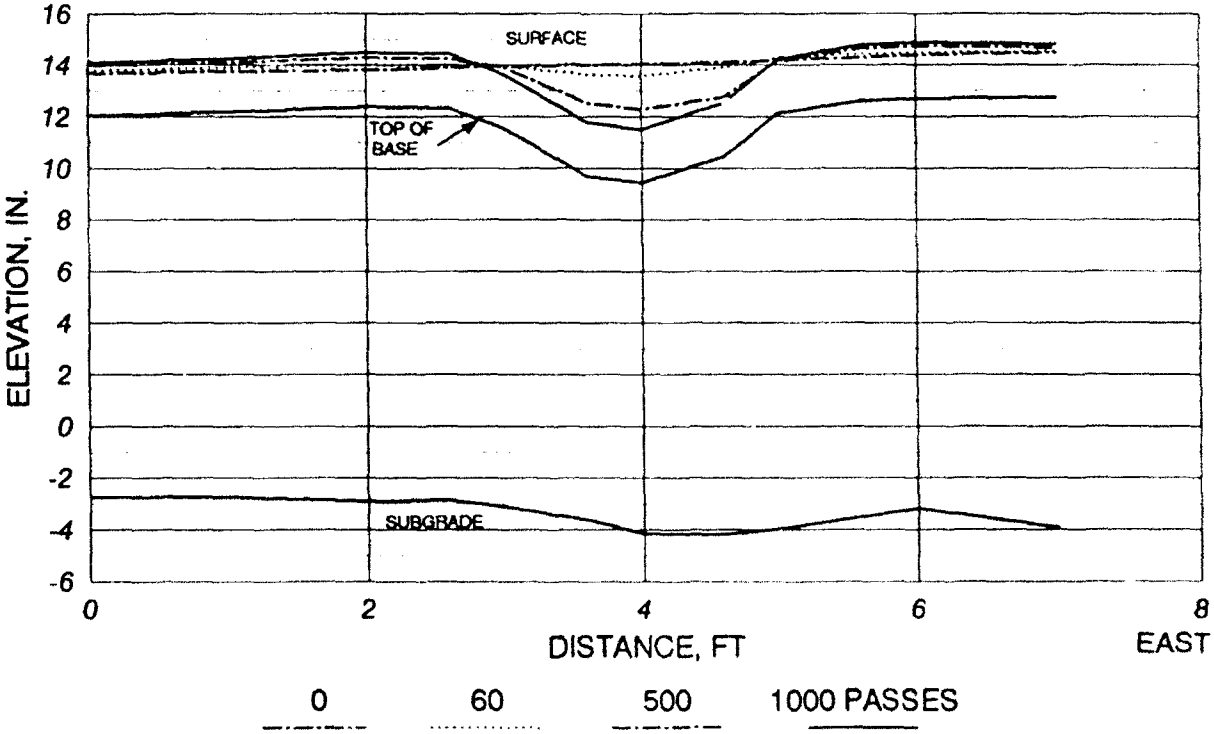

Figure 48. Typical cross section, Lane 4, Item 4 (control)

Figure 49. Lane 1, Item 3 (6-in. base, reinforced) and Item 4 (6-in. base, control) after 2016 passes of traffic

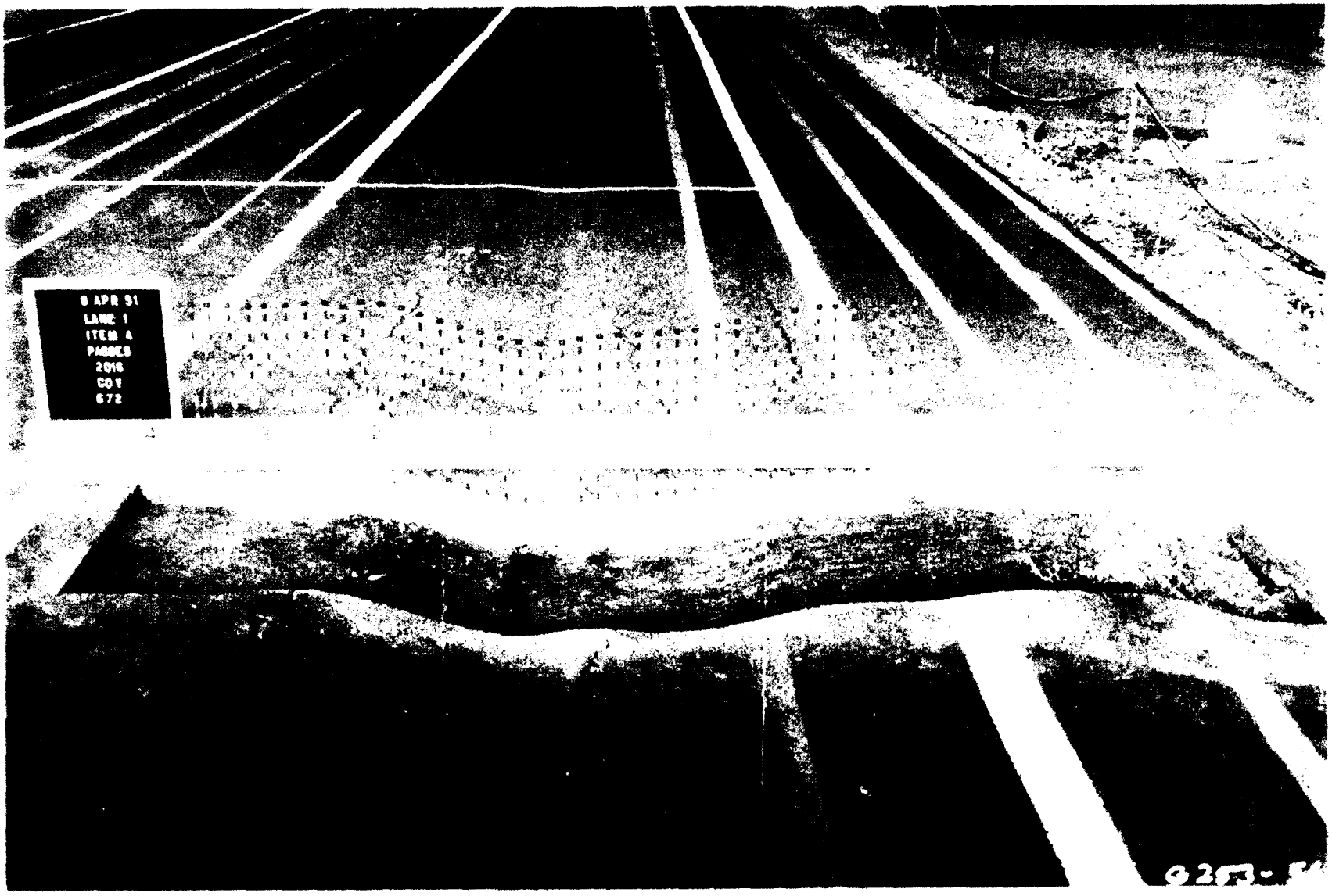

Figure 50. Lane 1, Item 4, the portion of AC surface removed

Figure 31. Trench in Lane 1, Test 1, after base material removed

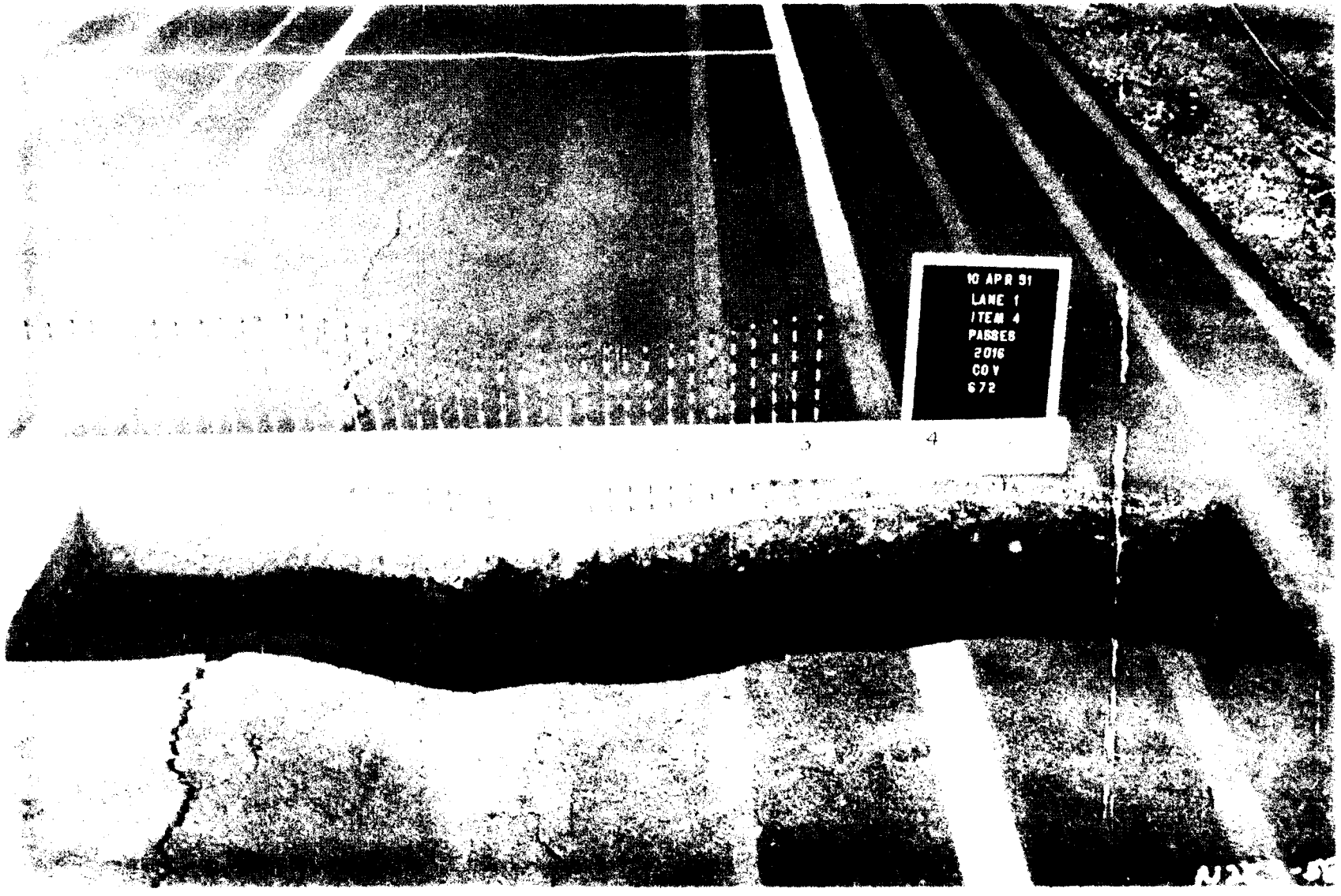

Figure 32. Trench in Lane 1, Item 4 after a portion of subgrade removed

Figure 53. [illegible] (Geogrid 2) on left and [illegible] on right after 1500 passes

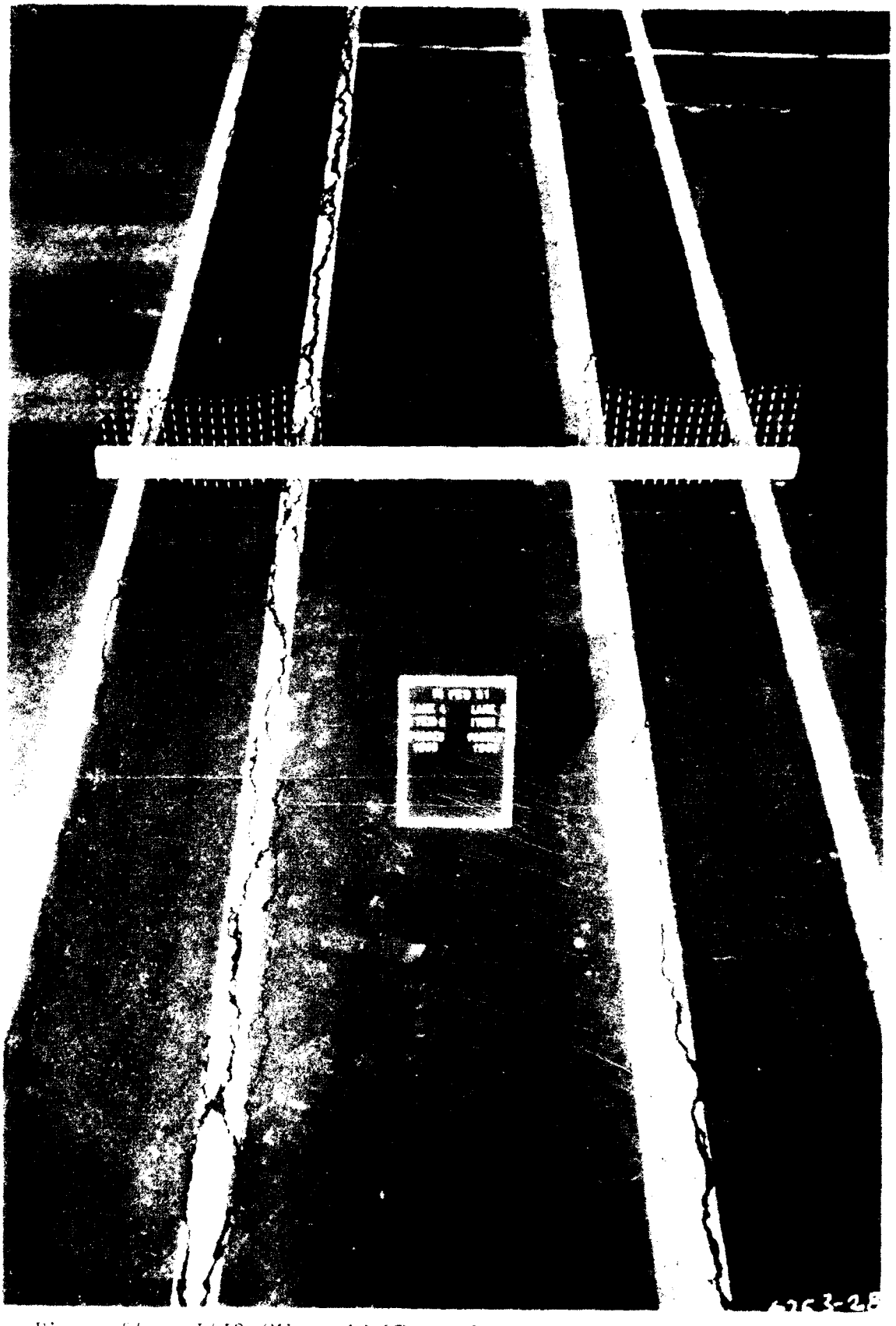

Figure 54. L4I2 (Miragrid 5T) on left and L3I2 (SS-2 mid-base) after 1500 passes

Figure 55. L413 (Fortrac 35/20-20) on left after 1500 passes and L313 (SS-2) on right after 2000 passes

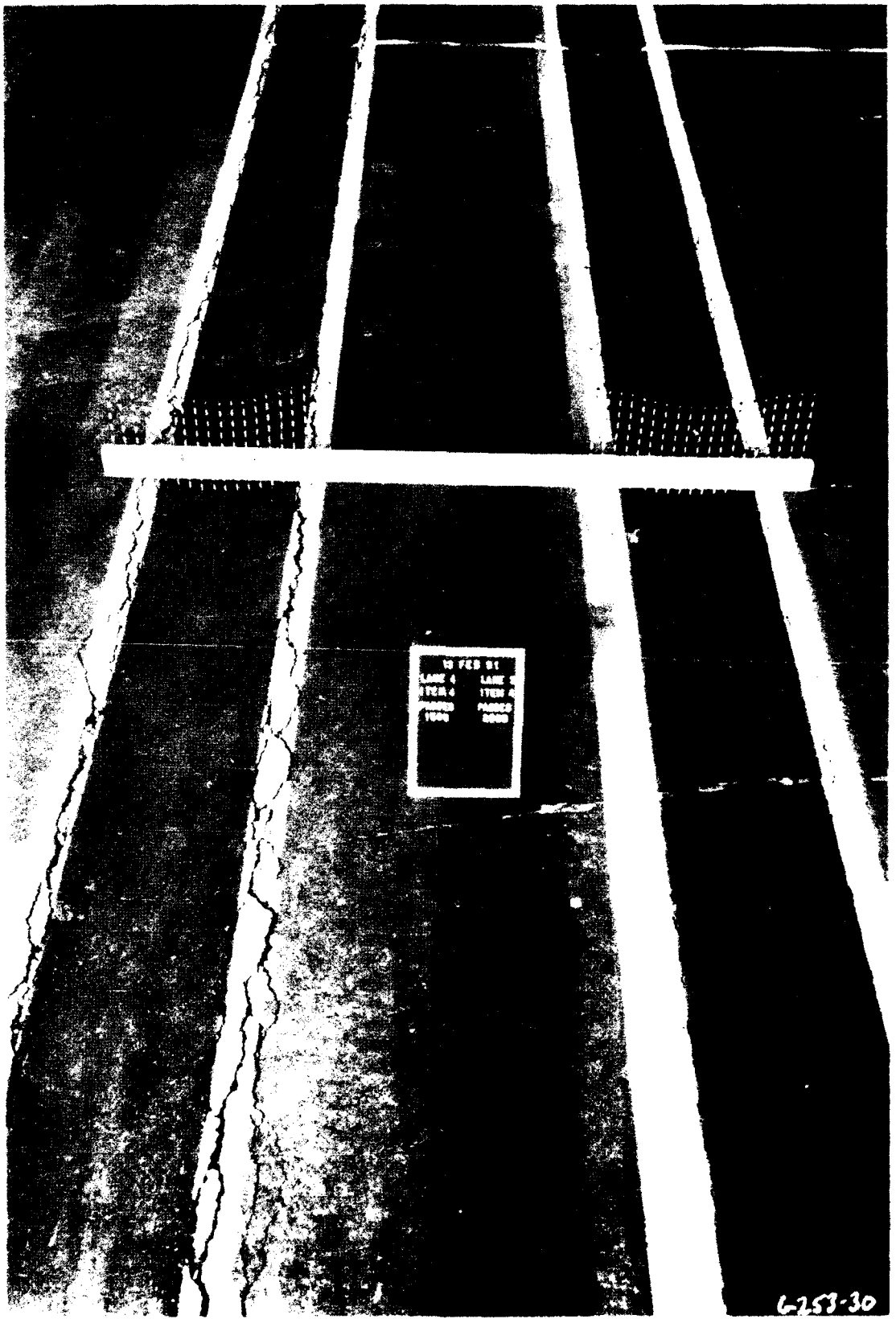

Figure 56. L4I4 (control) on left after 1500 passes and L3I4 (SS-1) on right after 2000 passes

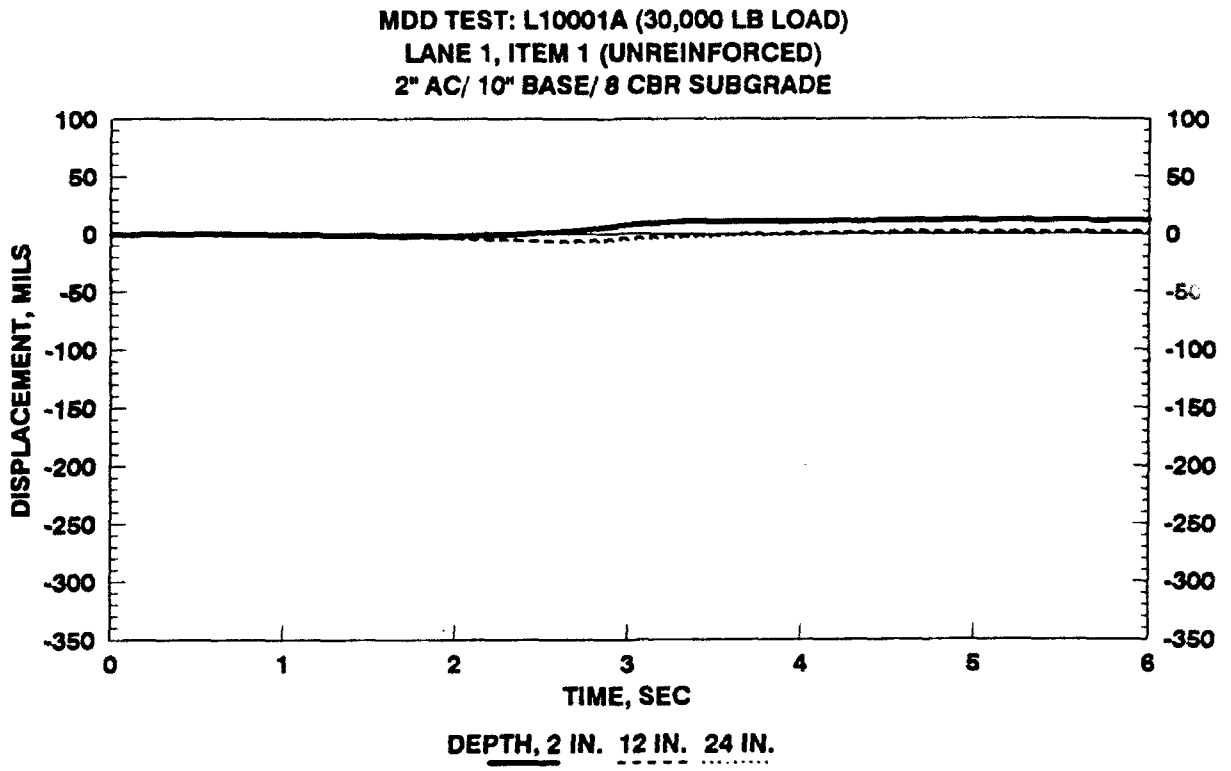

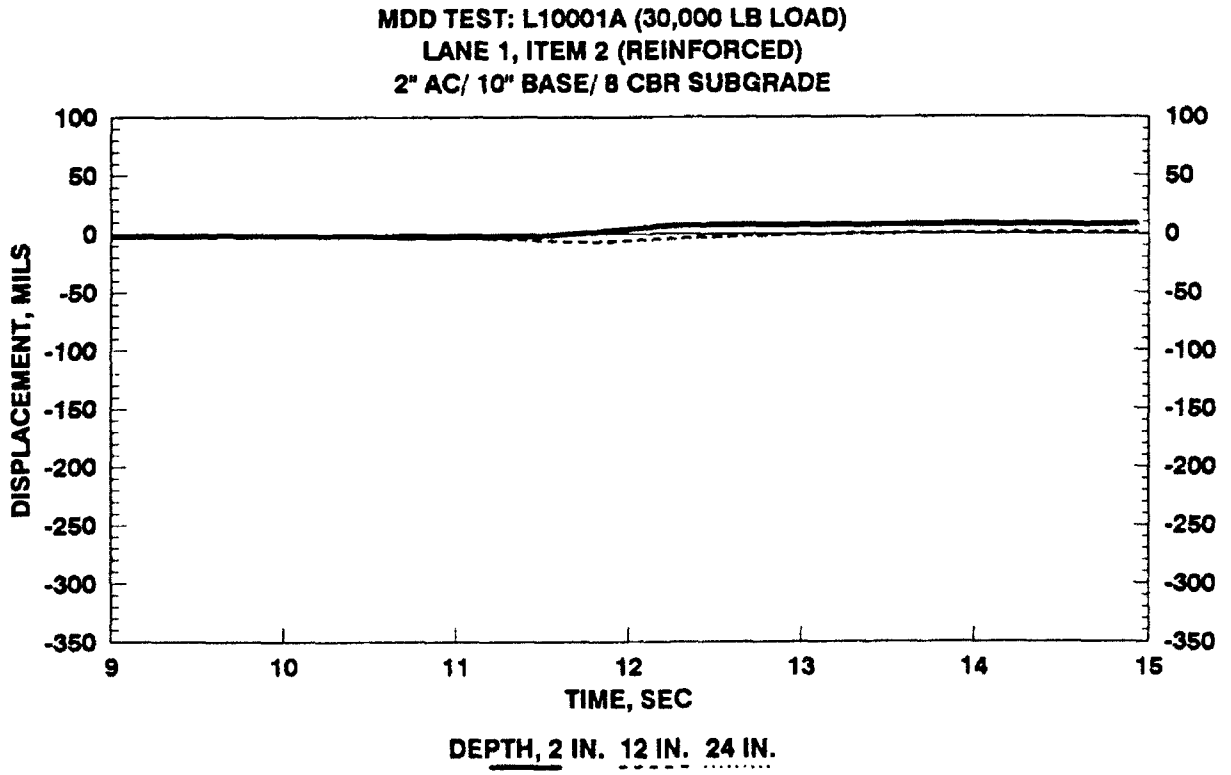

Figure 57. Initial elastic deformations for L1I1 (unreinforced) and L1I2 (Reinforced) Pass 1, Wheel Path A

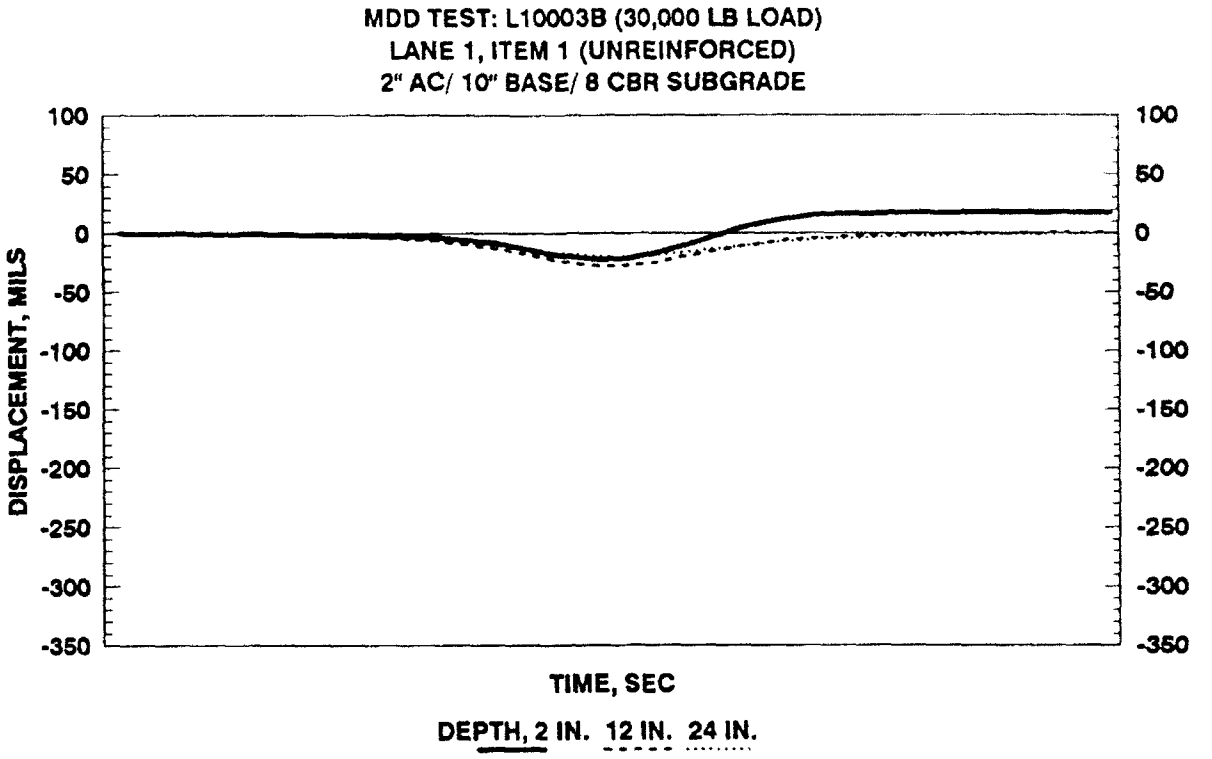

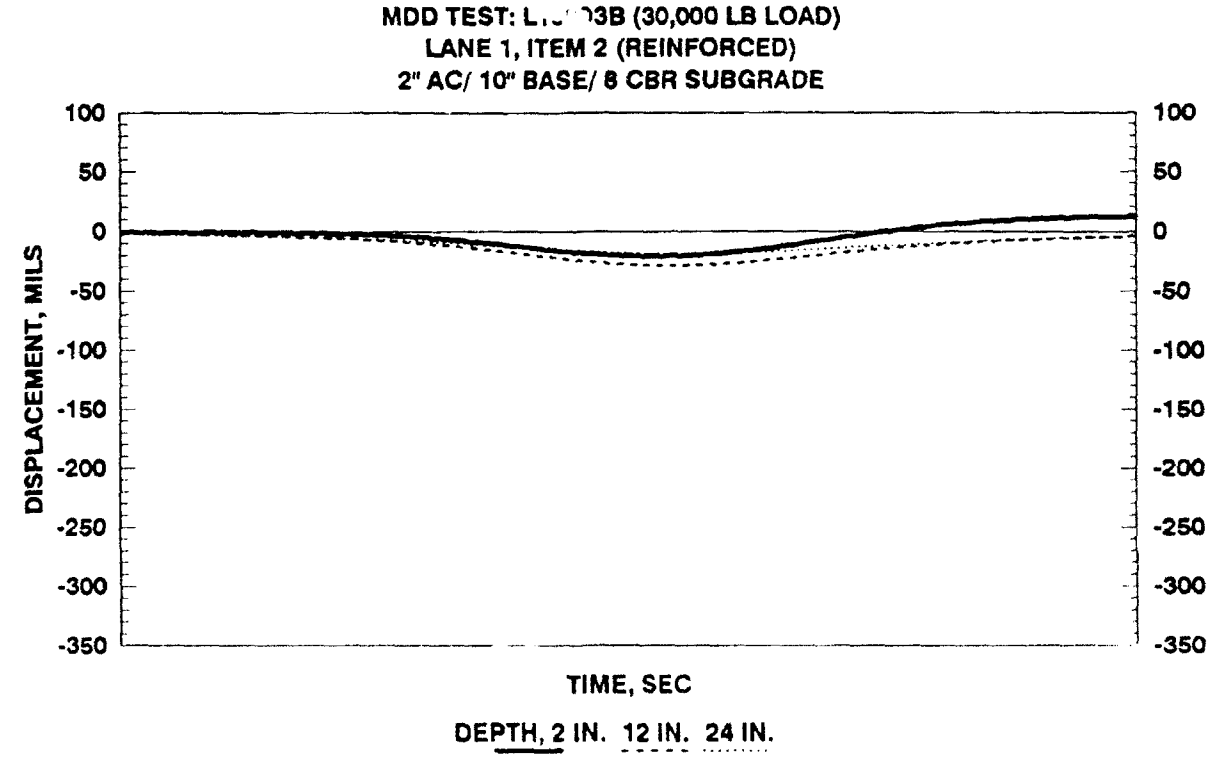

Figure 58. Displacements for pass 3, wheel Path B

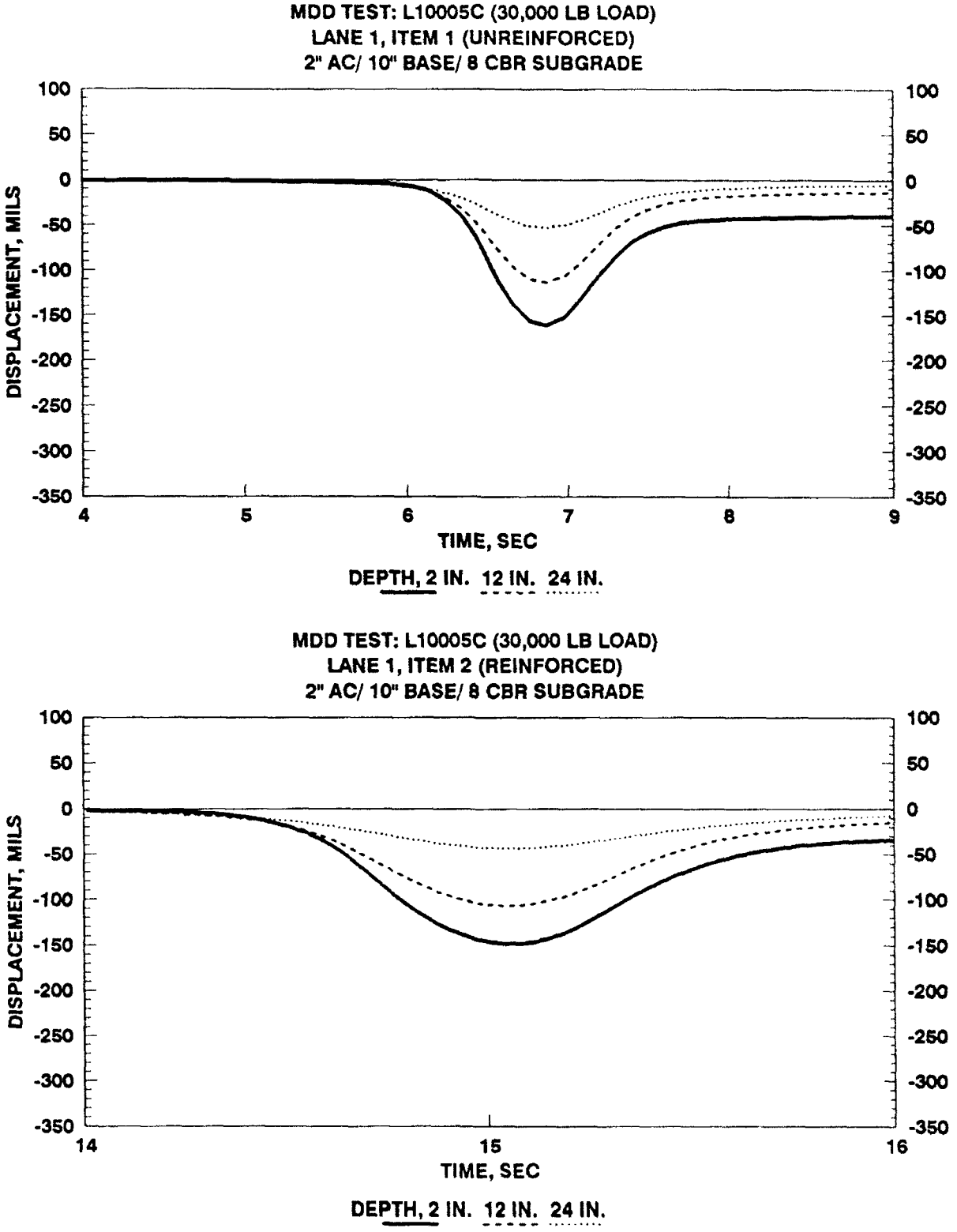

Figure 59. Displacements for pass 5, wheel Path C

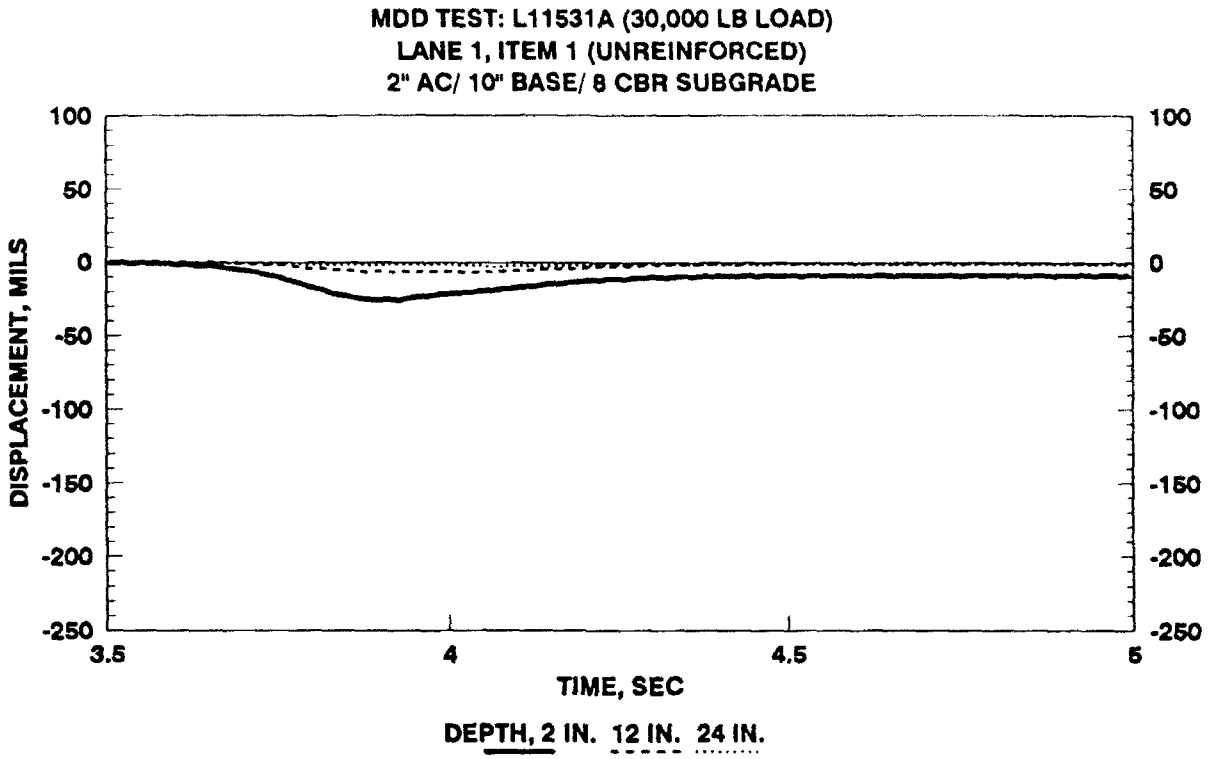

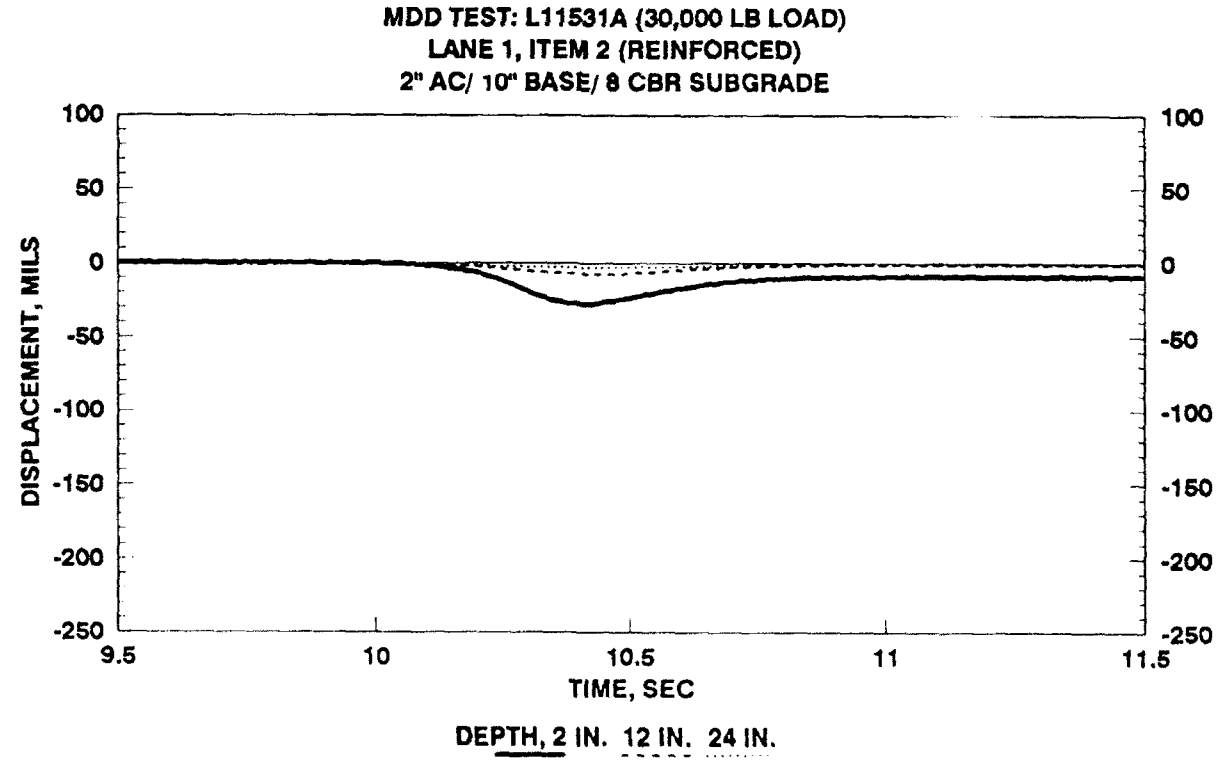

Figure 60. Displacements for pass 1531, wheel Path A

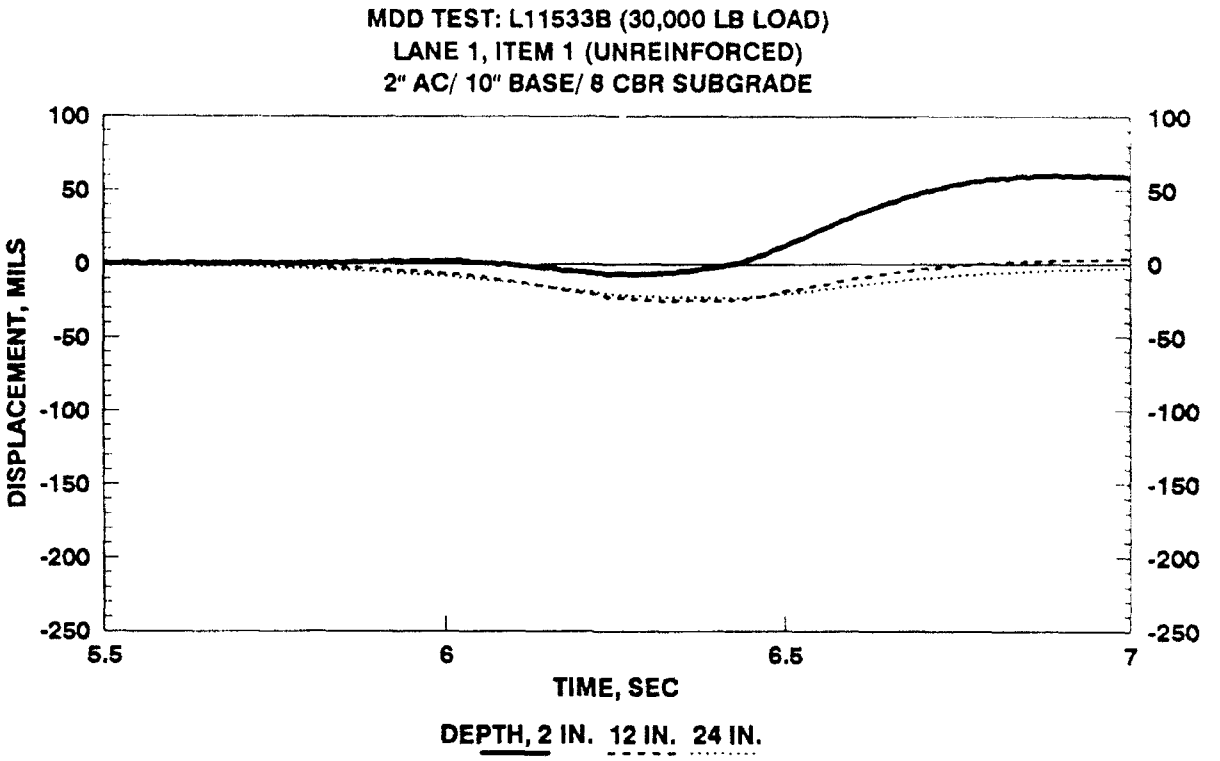

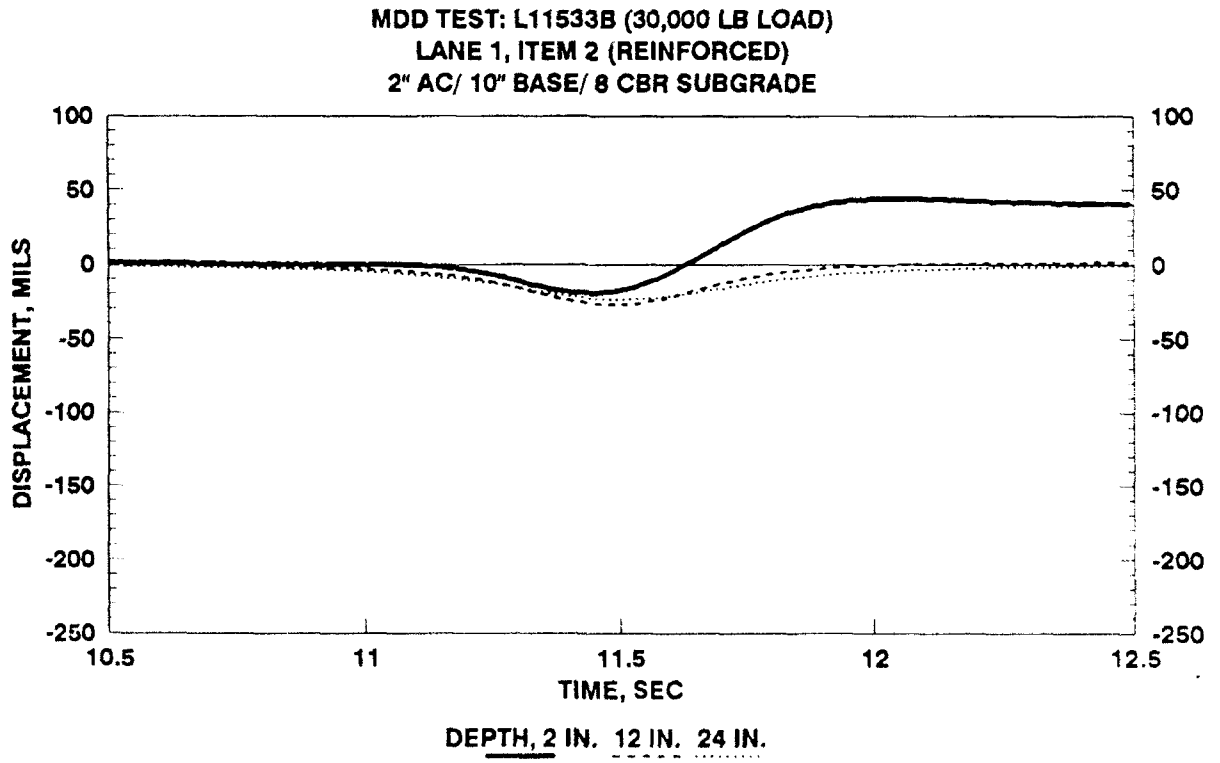

Figure 61. Displacements for pass 1533, wheel Path B

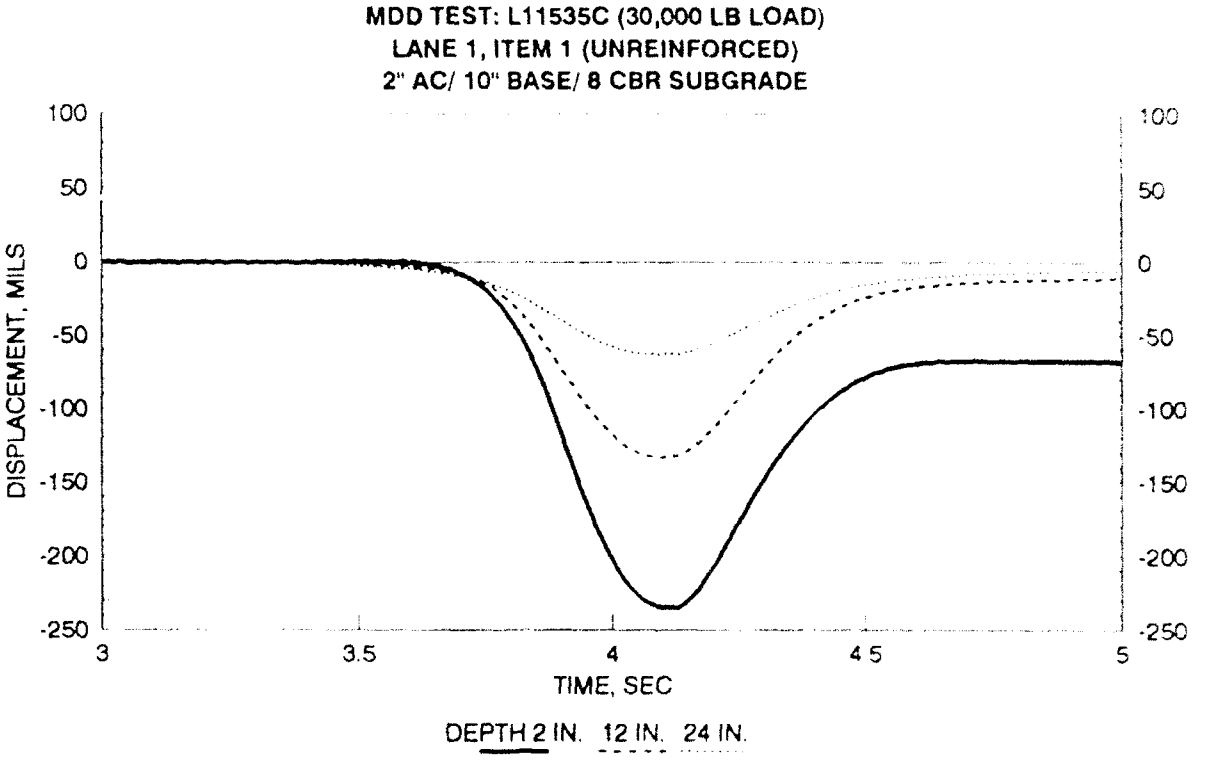

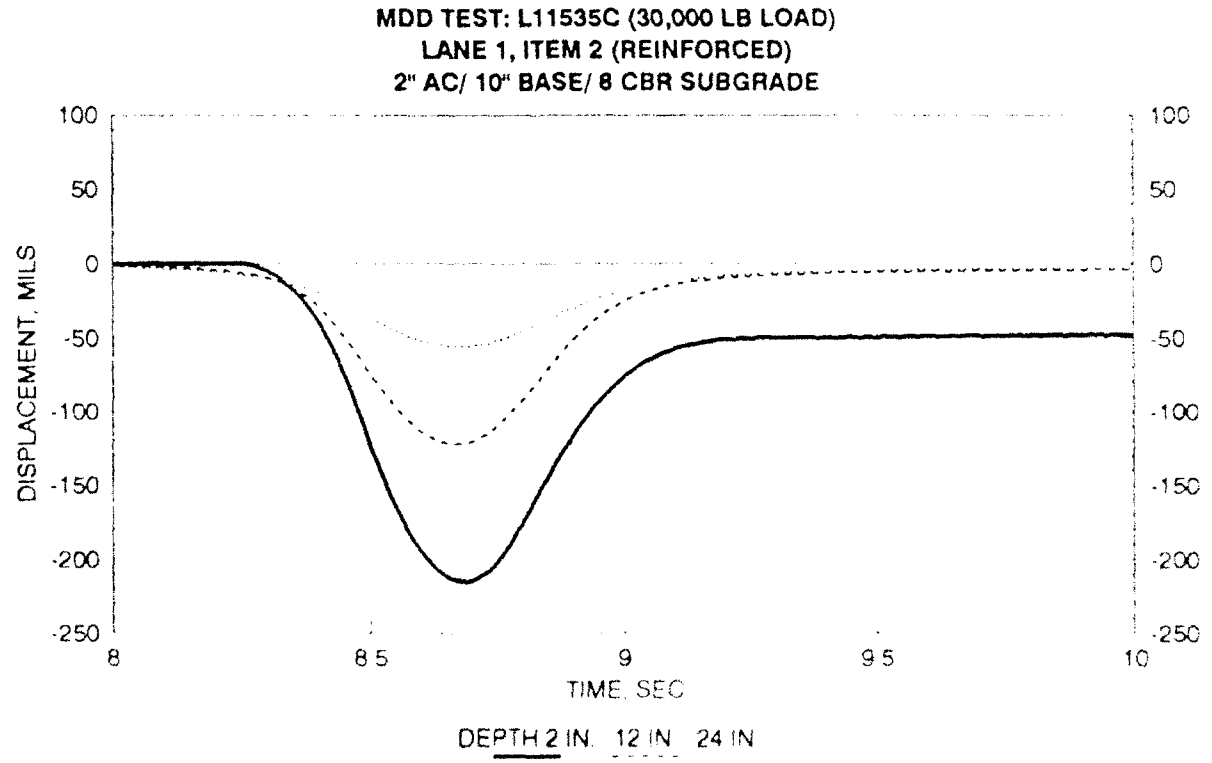

Figure 62. Displacements for pass 1535, wheel Path C

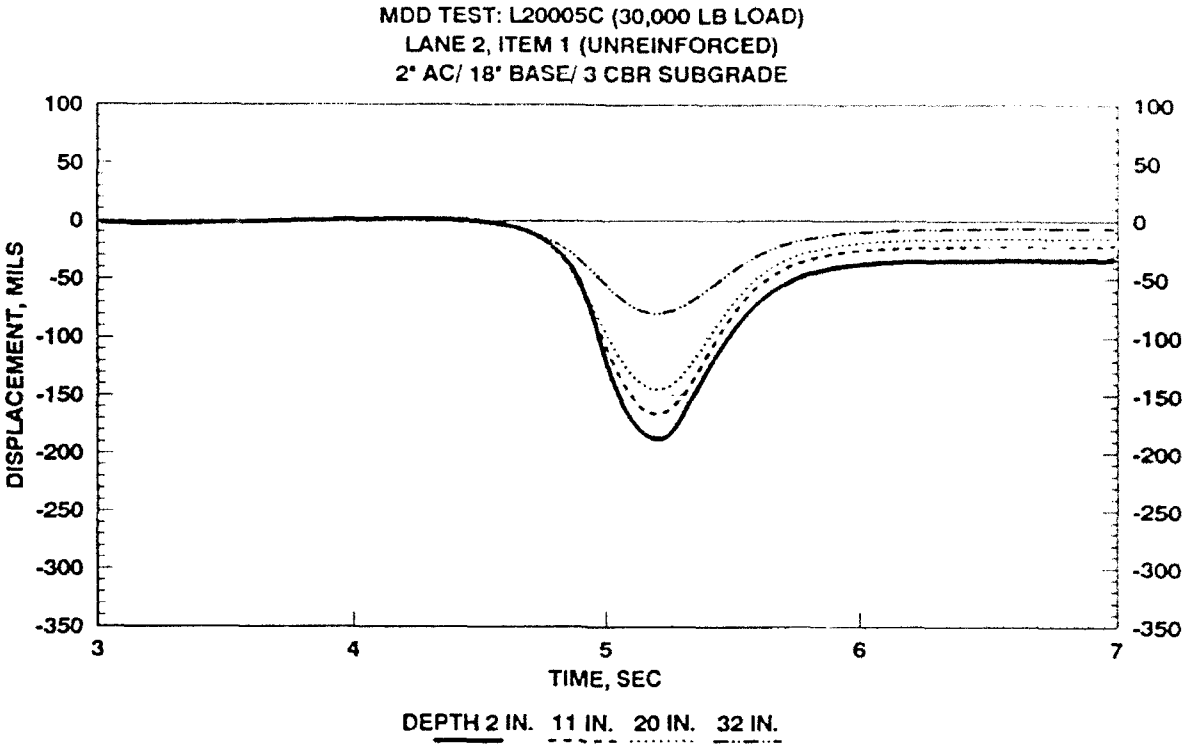

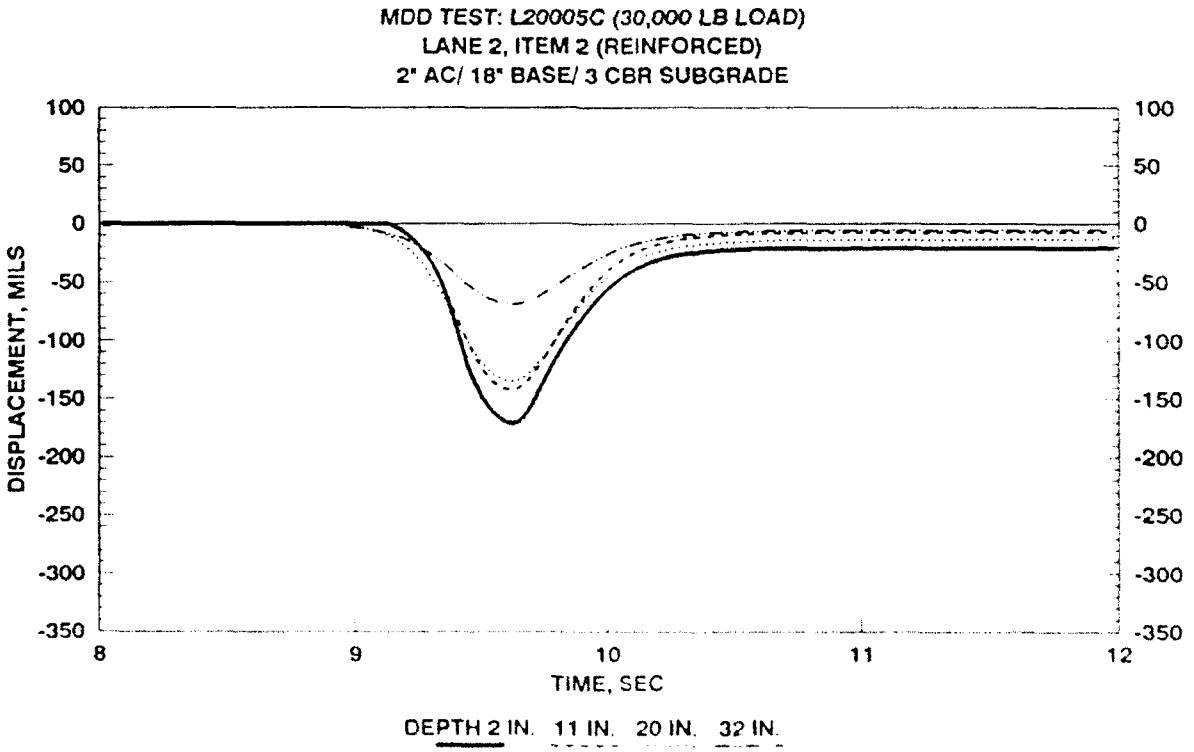

Figure 63. Displacements for L2I1 (unreinforced) and L2I2 (reinforced) for pass 5, wheel Path C

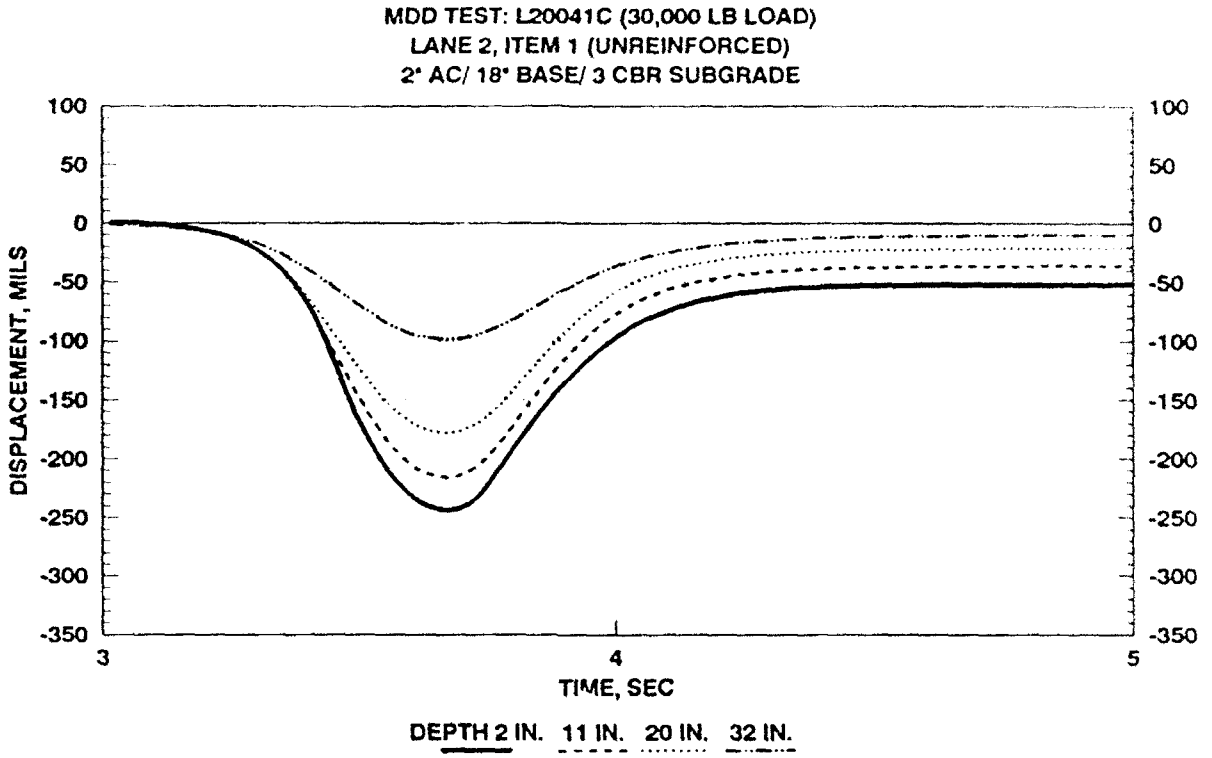

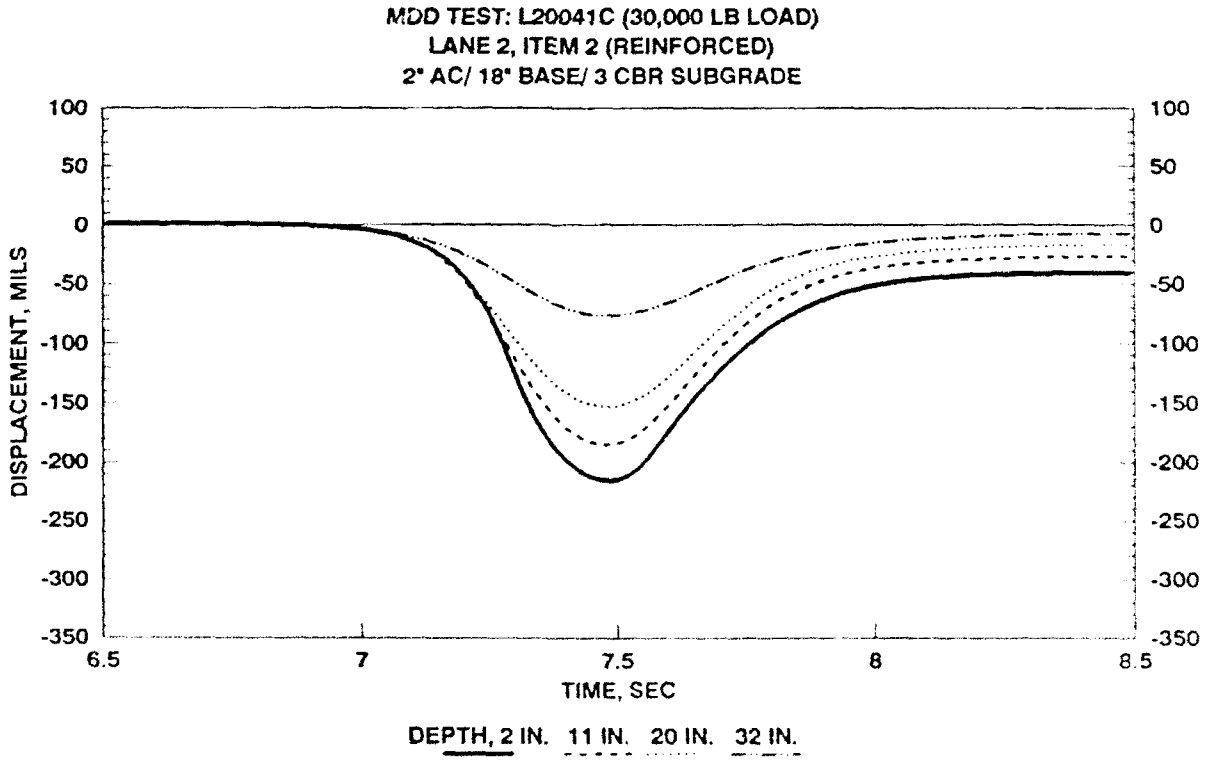

Figure 64. Displacements for pass 41, wheel Path C

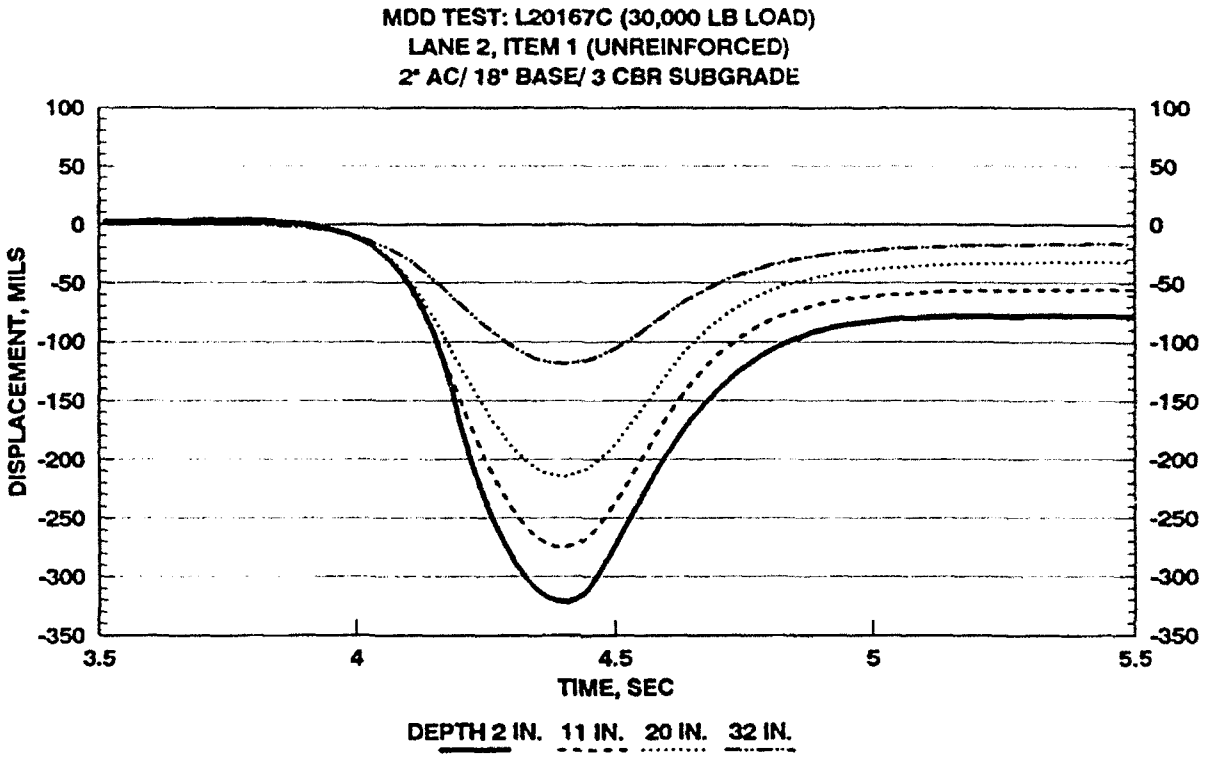

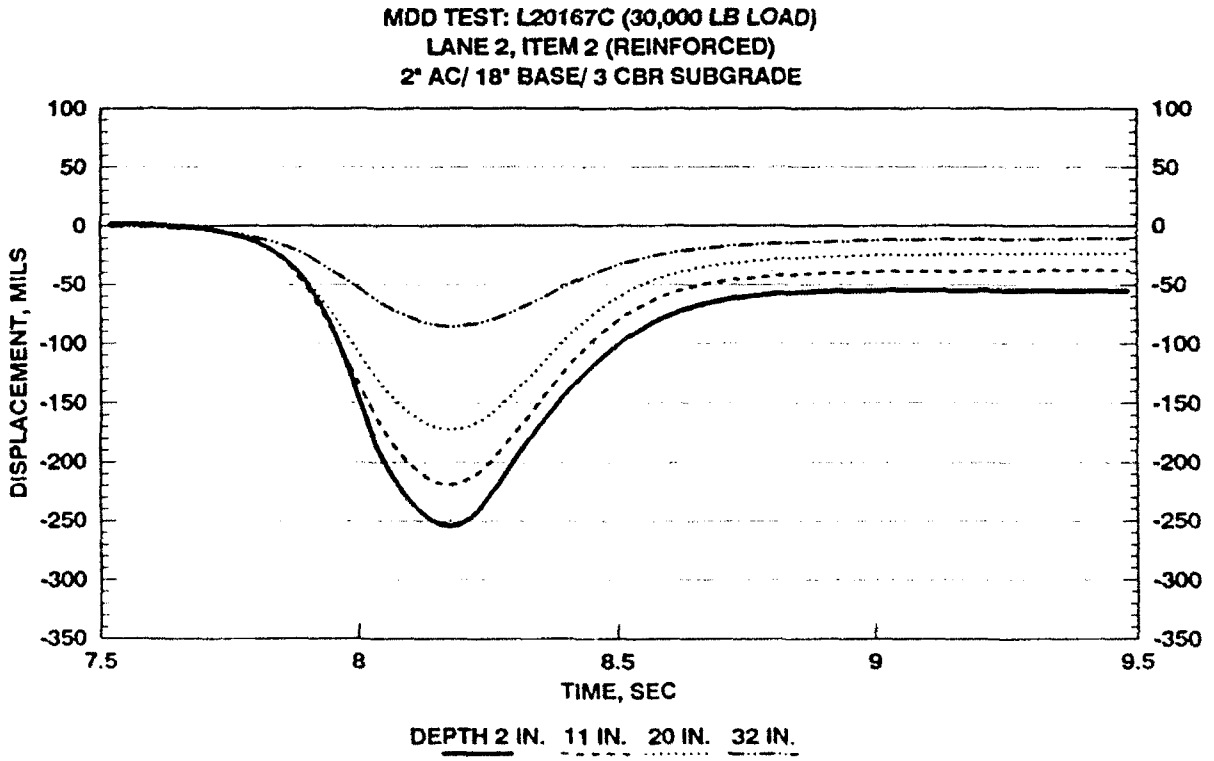

Figure 65. Displacements for pass 167, wheel Path C

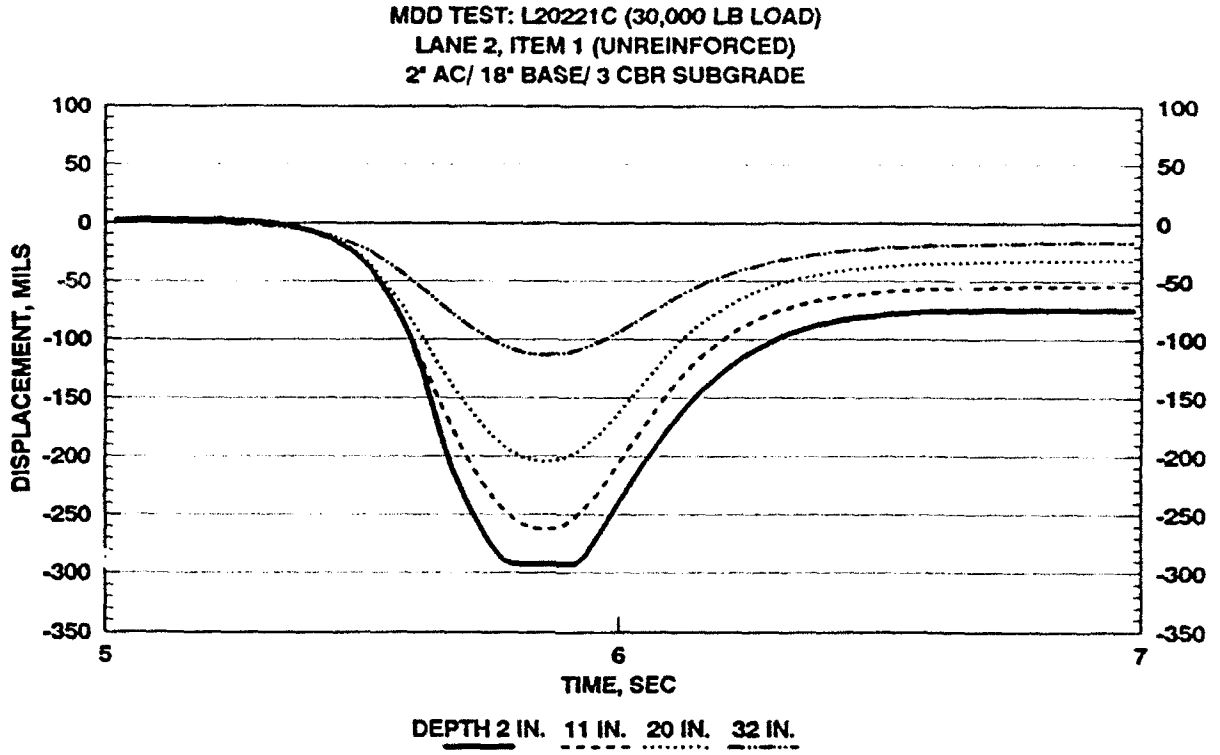

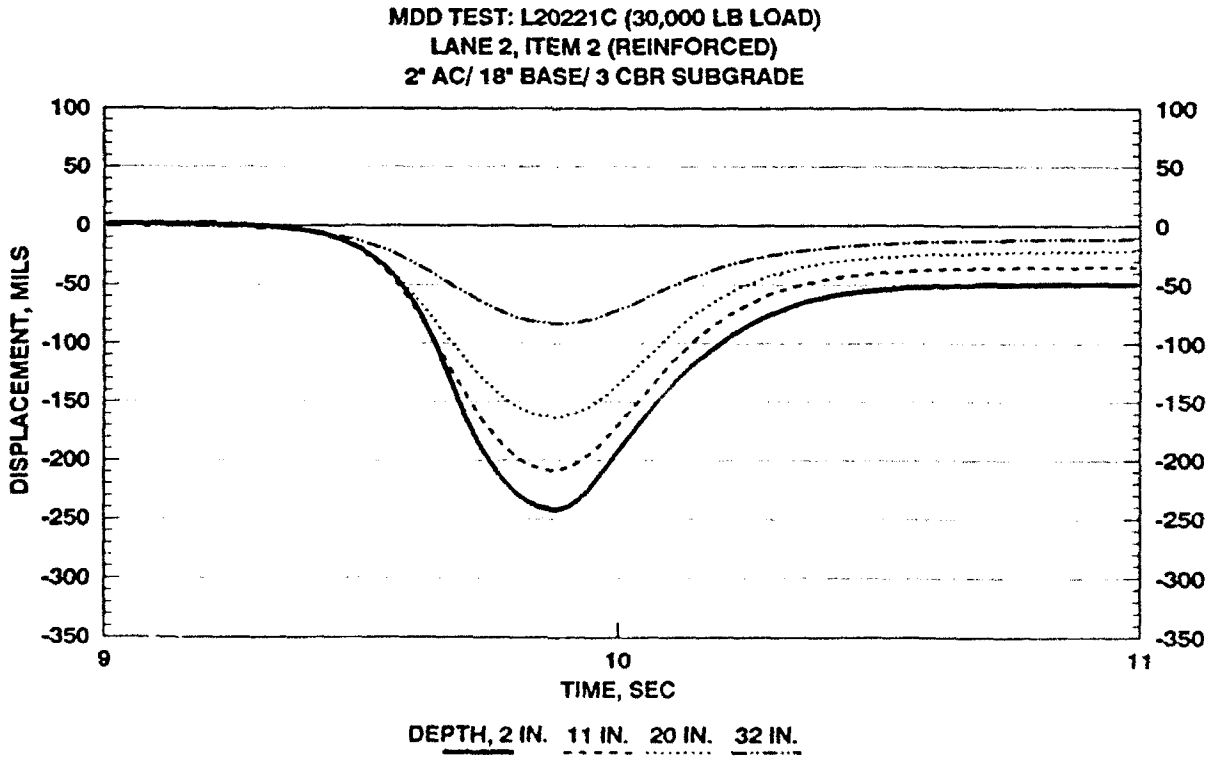

Figure 66. Displacements for pass 221, wheel Path C

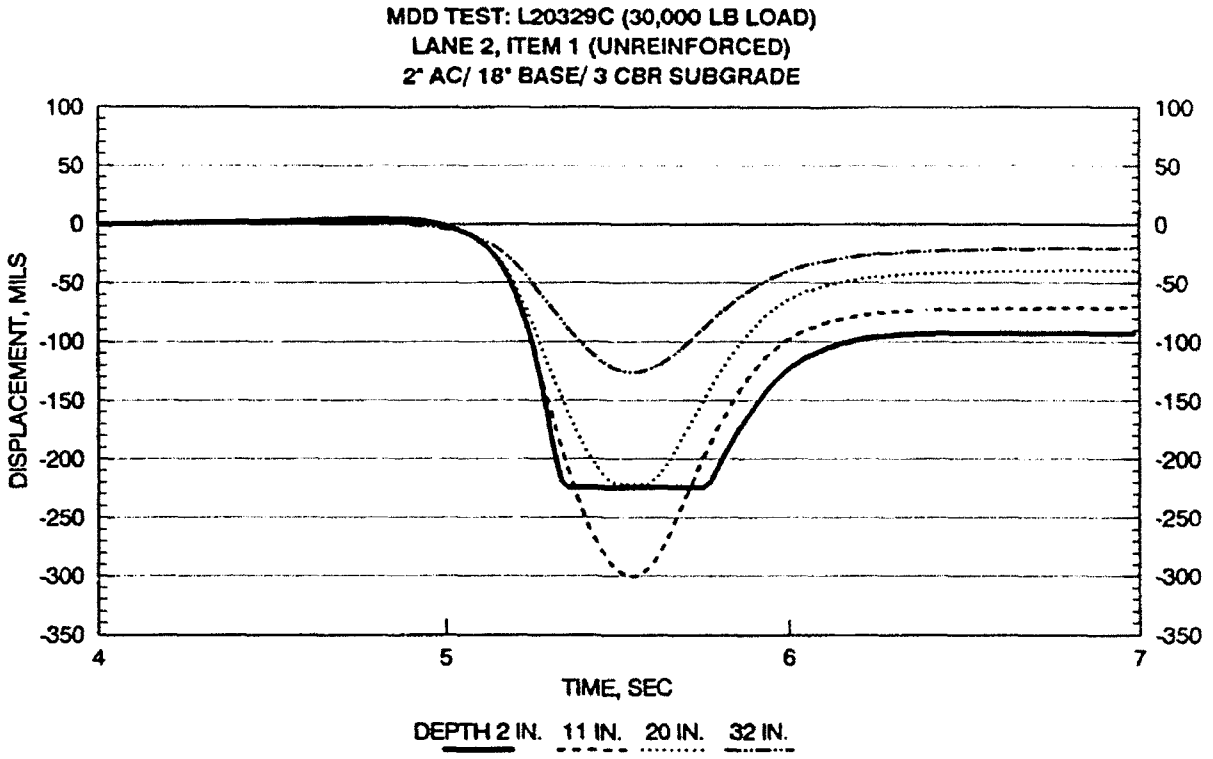

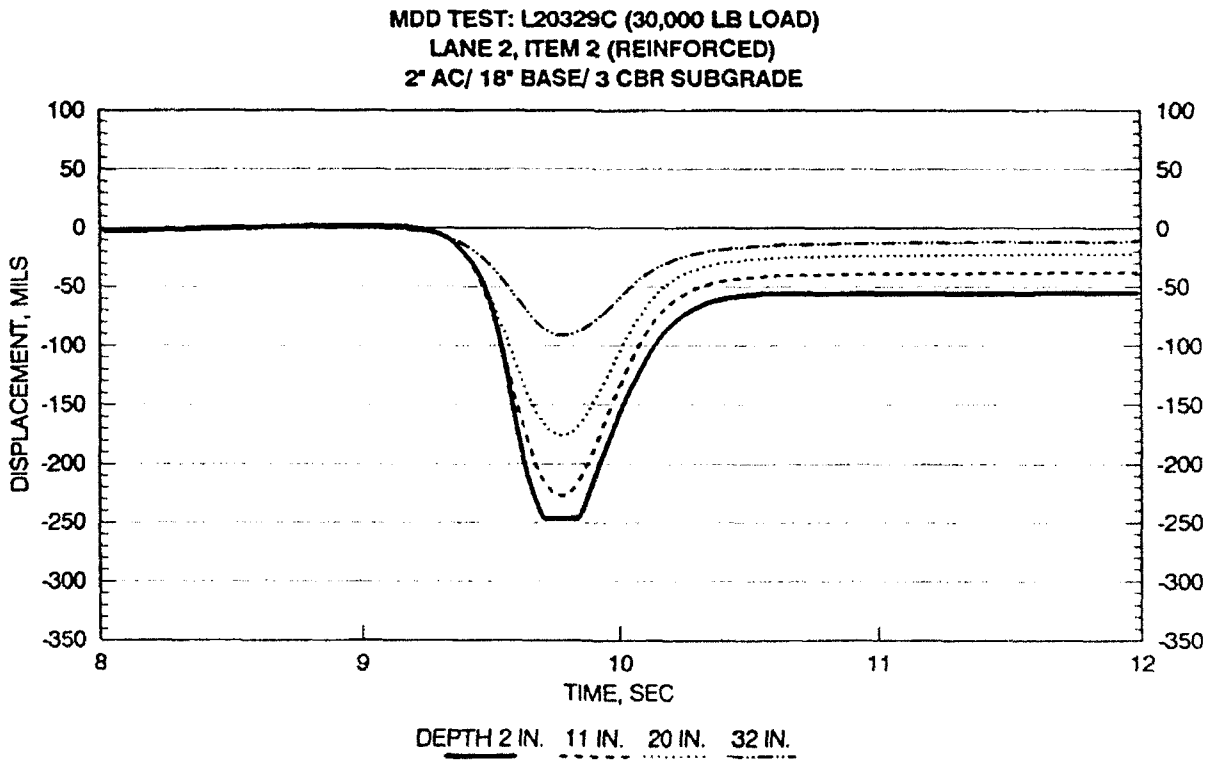

Figure 67. Displacements for pass 329, wheel Path C

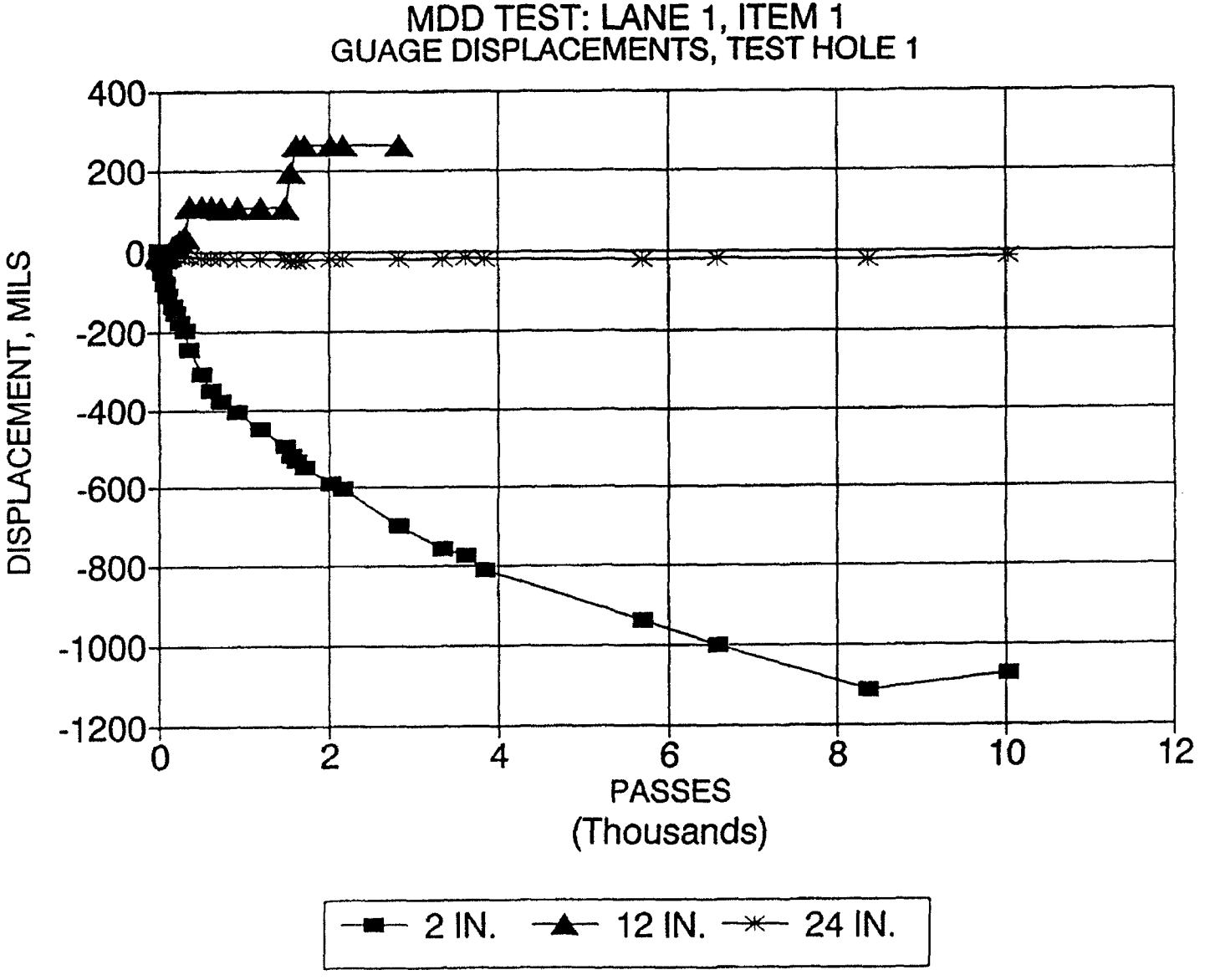

Figure 68. MDD permanent displacements LII1

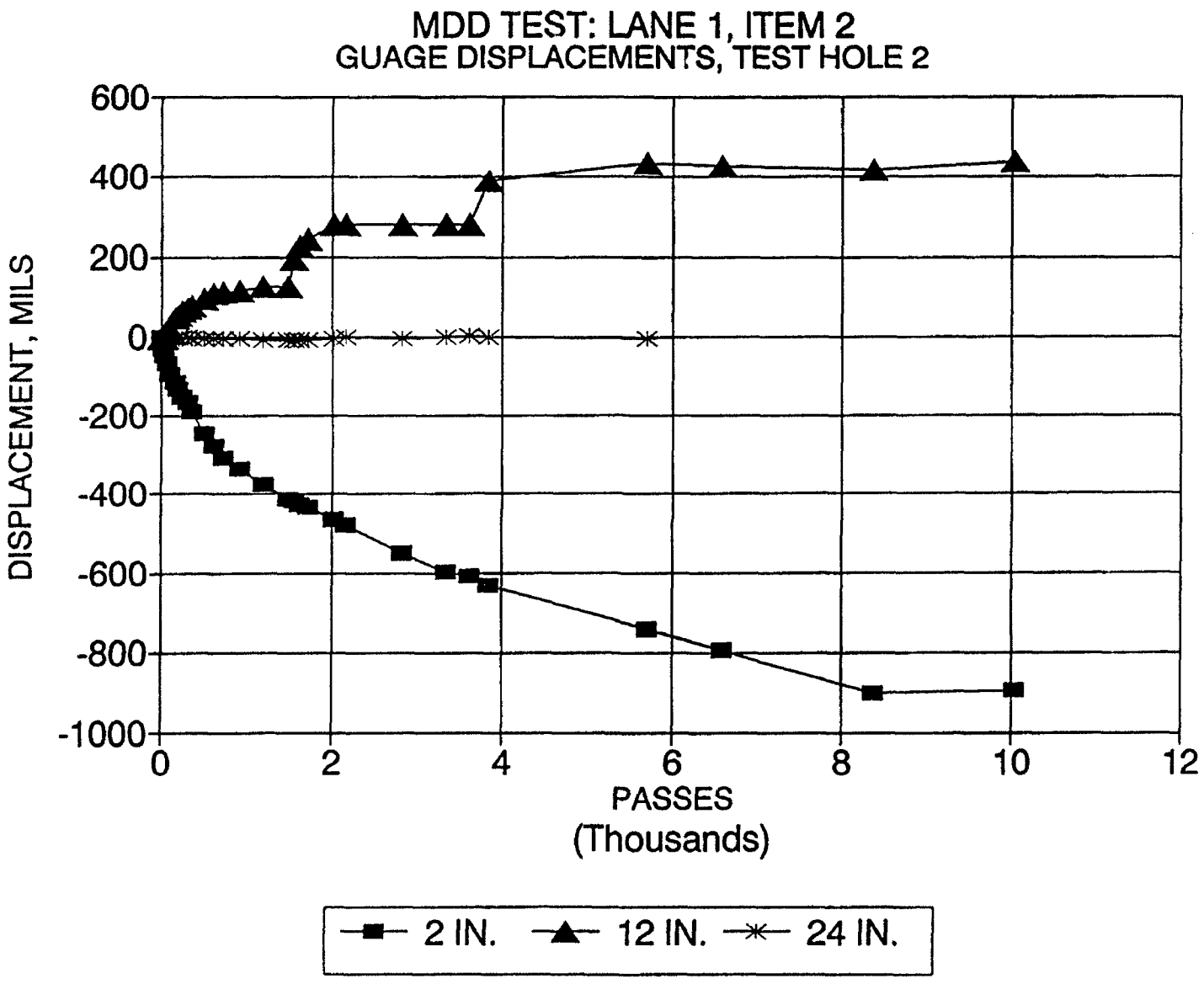

Figure 69. MDD permanent displacements L1I2

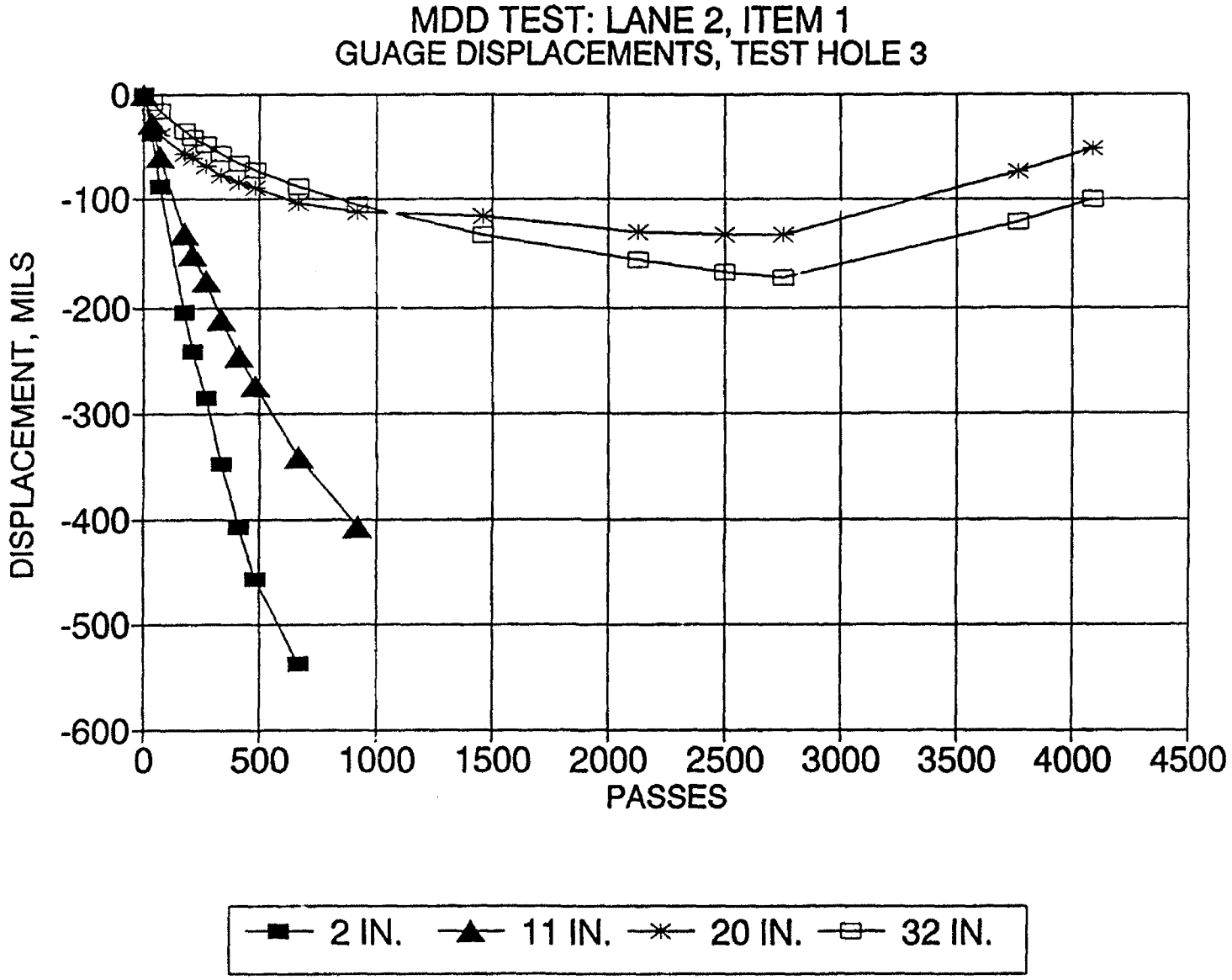

Figure 70. MDD permanent displacements L2I1

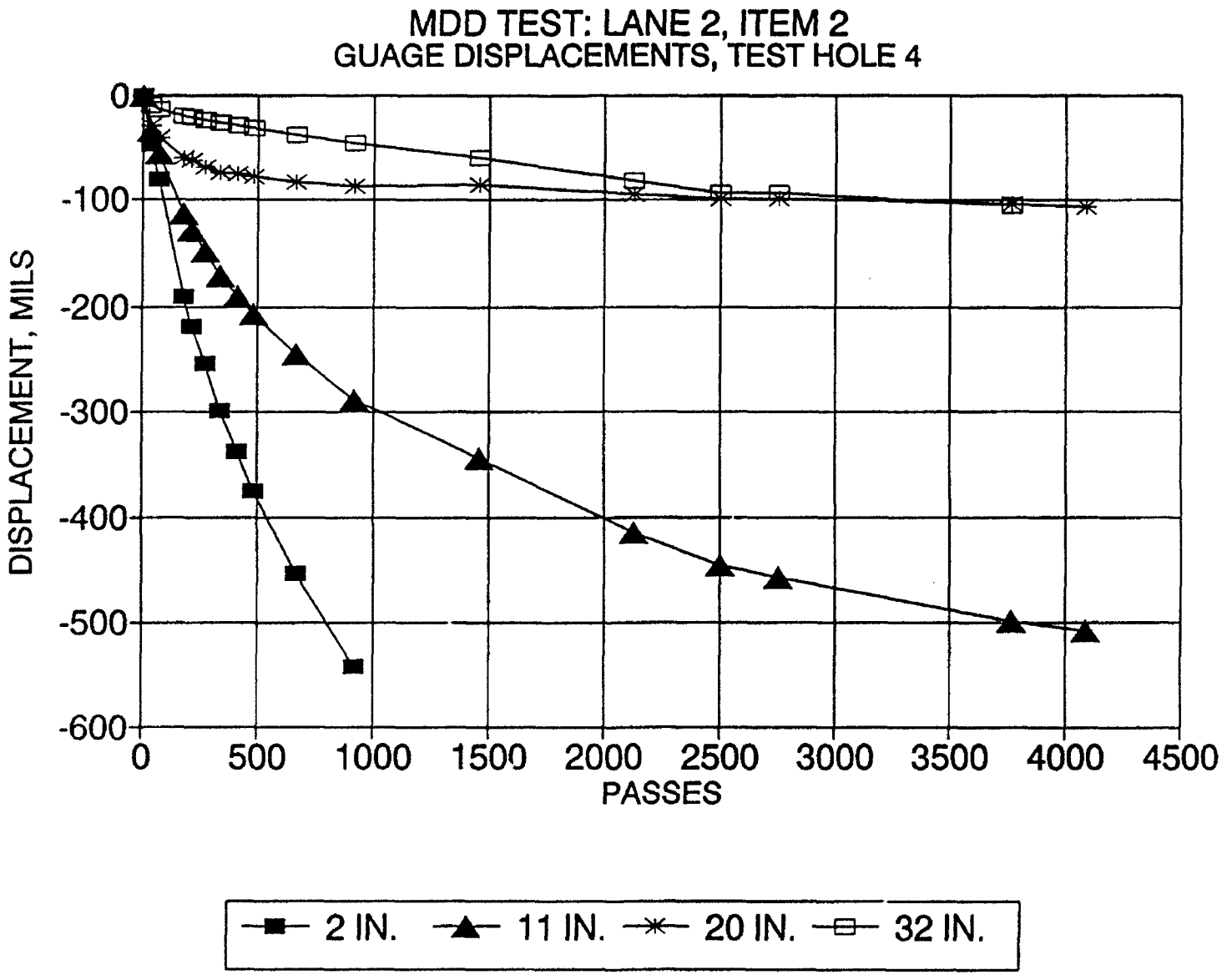

Figure 71. MDD permanent displacements L2I2

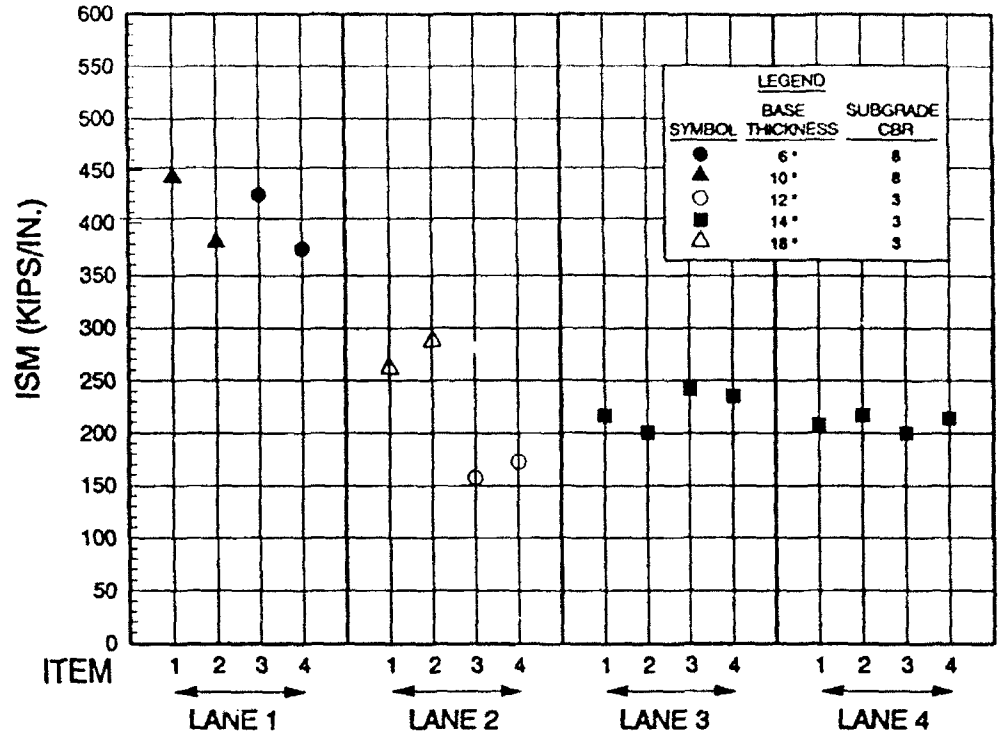

Figure 72. Impulse stiffness modulus for each test item

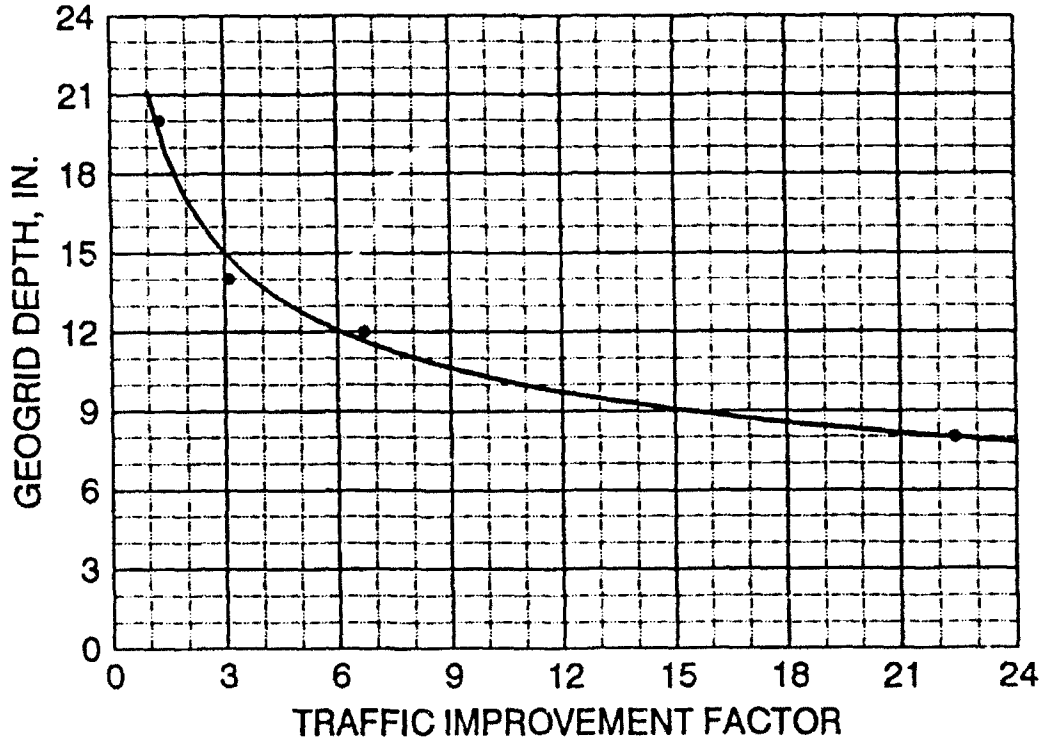

Figure 73. Geogrid placement depth versus traffic improvement factor

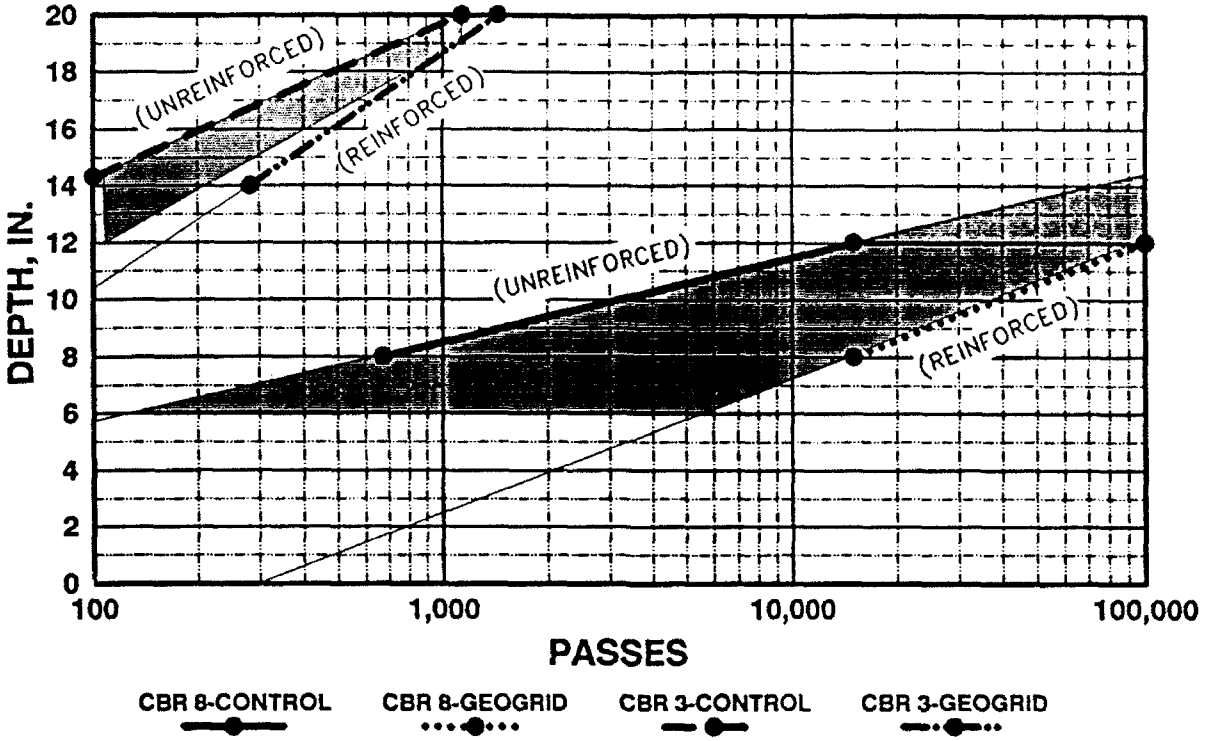

Figure 74. Plots of pavement thickness versus passes for a 1-in. Rut failure for Lane 1 (8 CBR subgrade) and Lane 2 (3 CBR subgrade) for a 30,000-lb single wheel

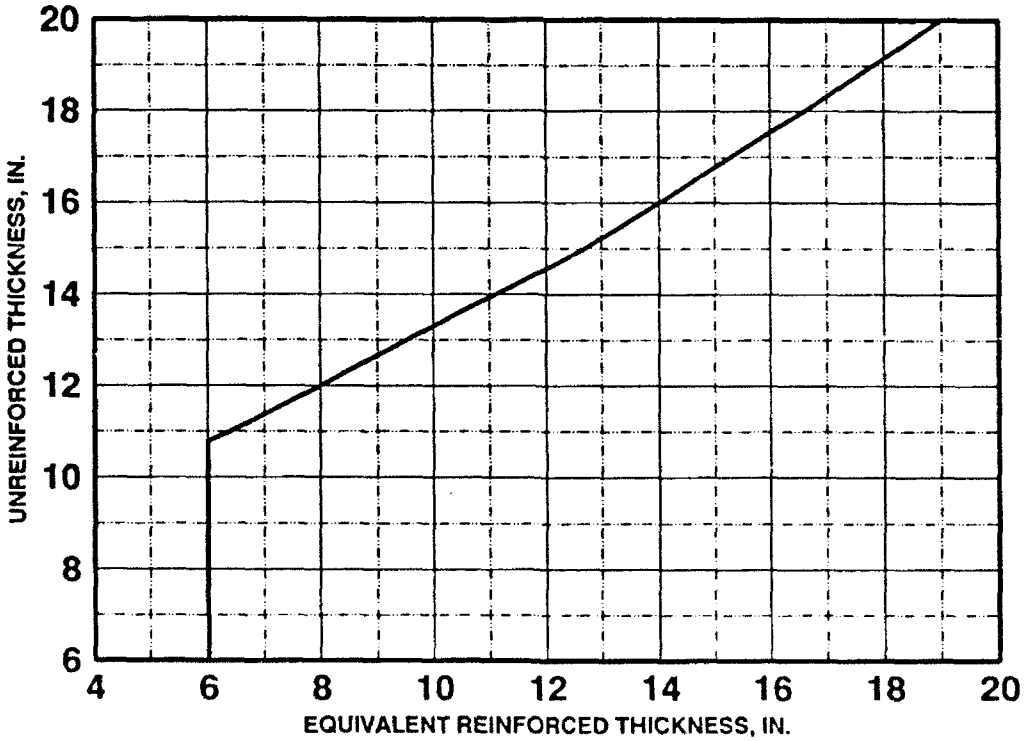

Figure 75. Design criteria for unreinforced thickness versus equivalent reinforced thickness (2-in. AC surface plus base)

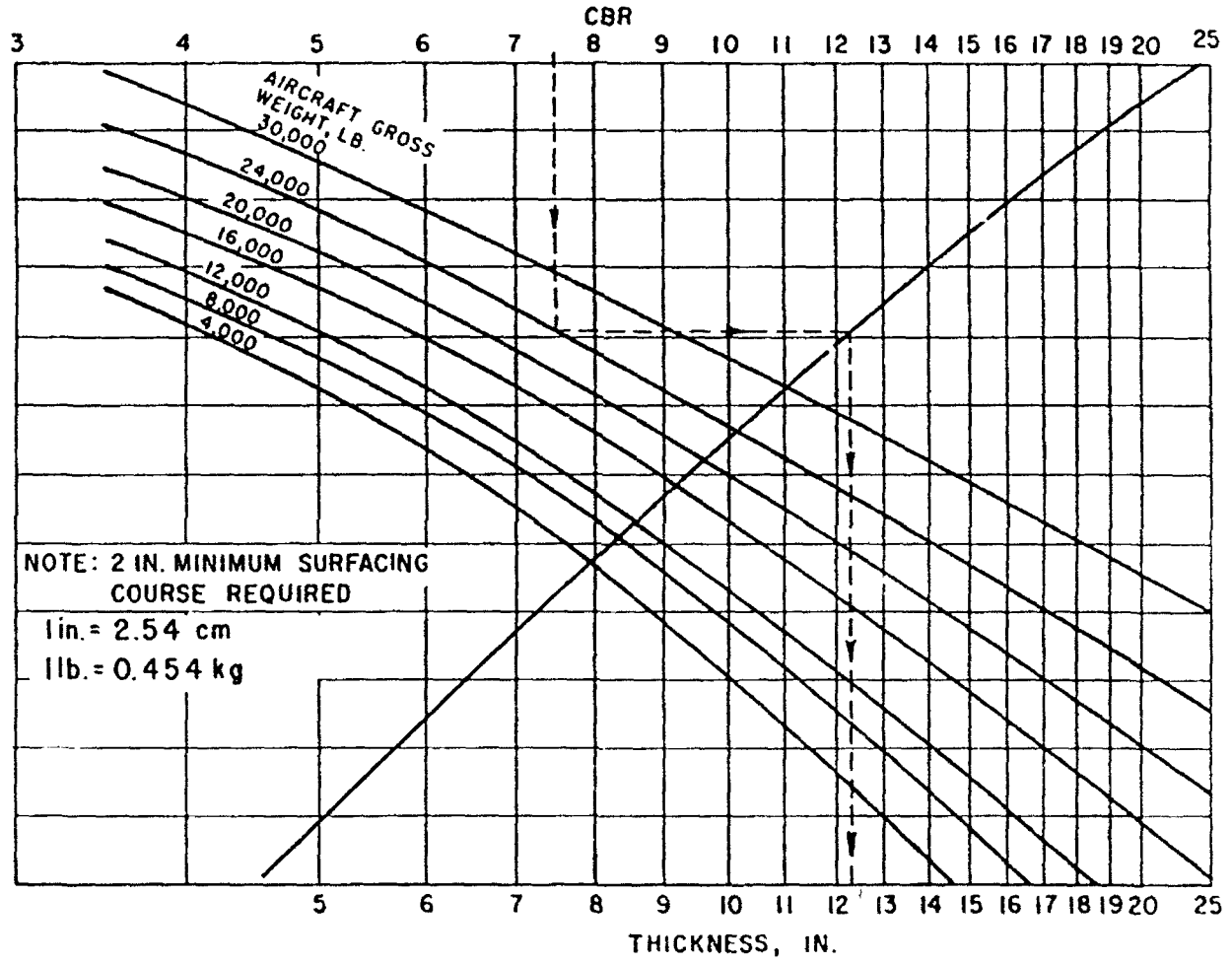

Figure 76. Design curves for flexible pavements, light aircraft[5]

APPENDIX A

DRAFT

GRID APERTURE STABILITY BY IN-PLANE ROTATION

Prepared by Dr. Thomas C Kinney
Geosynthetic Services of Alaska

Purpose:

1. This is an index test to measure the stability of a grid structure.

Significance:

The secant modulus seems to be significant in determining the performance characteristics when grid is placed in a paved airport runway between a CBR 3 to 8 clay subgrade and 6 to 18 inches of base course.

Apparatus:

See figure A1.

Method:

1. Lay grid on lower portions of clamps without stretching it. Put one node in the center.
2. Place upper portion of clamp on grid and bolt into place being careful not to move the grid.
3. Clamp ' st over center node.
4. Apply moment in approximately 5 cm-kg increments to 25 cm-kg or until the rotation will not drop below limits in 5 minutes.
5. Leave each load on until movement of the load is less than 0.01 cm in one minute. Record the times.
6. Unload in same increments as loaded.
7. Repeat steps 4 through 6 for a total of four load-unload cycles.
8. Repeat setups 1 through 7 on three different samples.

Analysis:

1. Plot all load cycles to detect any anomalies.
2. If there are any obvious anomalies or if the rotation at a given load from any one test is over 20 percent different from the other two then discard it and repeat that test with a new sample.
3. Average all of the data for the first and forth curves to get a single composite set of data for these two curves.
4. Determine a best fit quadratic curve through the composite initial and fourth loading curves.
5. Calculate the secant and tangent stability moduli at 5, 10, 15, 20, and 25 cm-kg torque increments for both the first and fourth fitted loading curves. Note: The stability modulus is the moment divided by the rotation in degrees expressed in units of cm-kg/deg.

Report:

1. Define the grid, polymer, construction process, aperture size and rib dimensions.
2. Show a table of the first and fourth loading secant and tangent aperture stability moduli. A plotted curve would be desirable also.

3. Show the longest length of time required for the final load in the first and fourth load sequences.

Accuracy:

Verified under limited conditions.

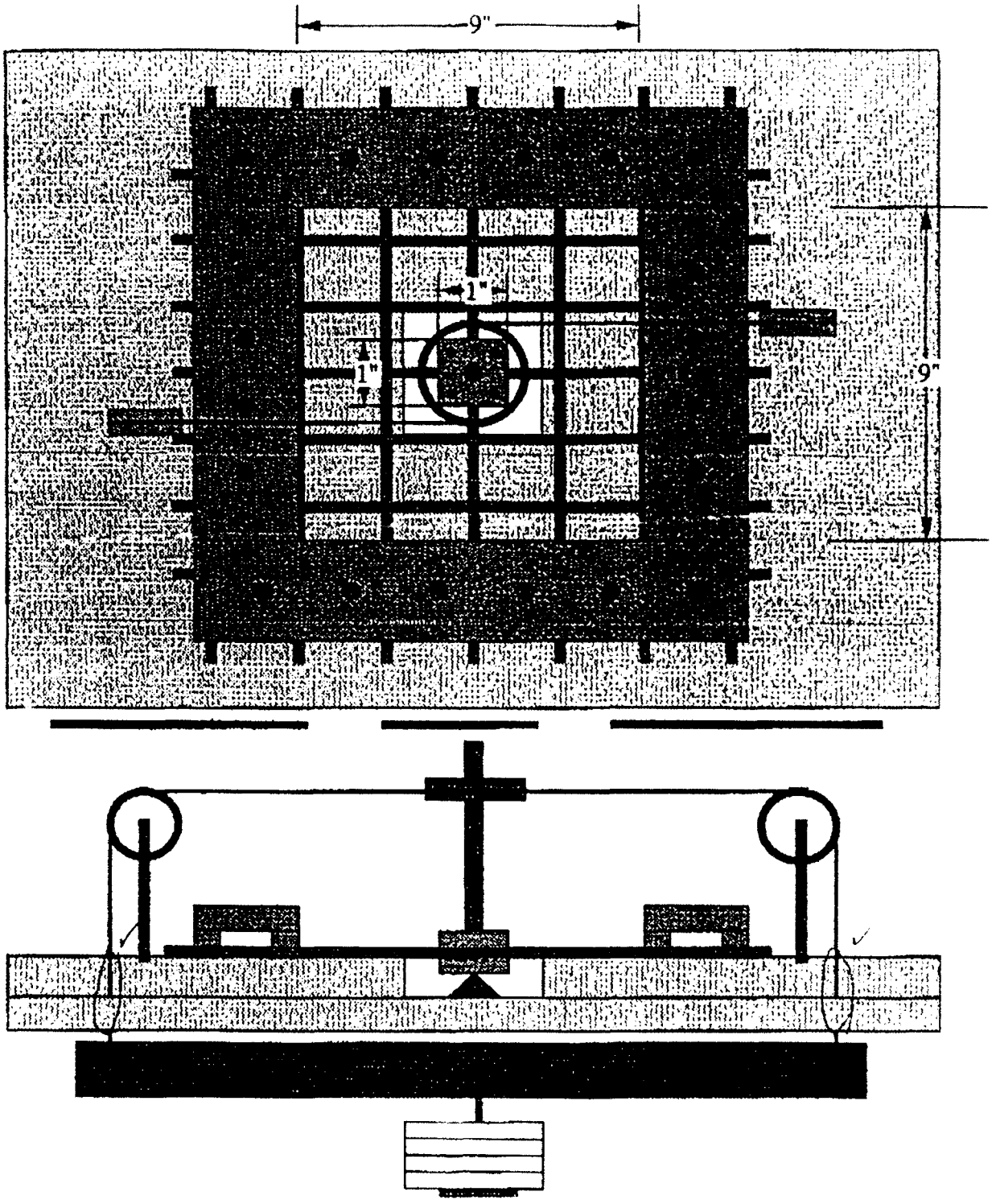

Figure A1. Schematic of test apparatus

In-Plane Rotation Index Tests
SS-2

Measurements					Reduced Data				
Load	Measured Rotation - Deg.				Moment	Relative Rotation - Deg.			
Kg	Test #1	Test #2	Test #3	Test #4	cm-Kg	Test #1	Test #2	Test #3	Test #4
0	76.0	72.0	71.0	71.0	0.00	0.00	0.00	0.00	0.00
2	75.0	71.1	70.1	70.1	9.53	1.00	0.90	0.90	0.90
4	73.7	70.0	69.0	69.0	19.05	2.30	2.00	2.00	2.00
6	72.0	68.5	67.8	67.5	28.58	4.00	3.50	3.20	3.50
7	71.0	67.0	66.8	66.7	33.34	5.00	5.00	4.20	4.30
9	68.0	66.0	65.2	65.0	42.86	8.00	6.00	5.80	6.00

Best Fit Quadratic Coefficients Ø = a*M^2 + b*M + c				
	Test #1			Test #4
a	0.0029			0.0014
b	0.0590			0.0823
c	0.0000			0.0000

Moment	Calculated Rotation			
cm-kg	Deg			
	Test #1			Test #4
0.00	0.00			0.00
5.00	0.37			0.45
10.00	0.88			0.96
15.00	1.54			1.54
20.00	2.34			2.19
25.00	3.29			2.91

Moment	Secant Modulus		Tangent Modulus	
cm-kg	cm-kg/deg		cm-kg/deg	
	Test #1	Test #4	Test #1	Test #4
0.00			16.95	12.15
5.00	13.61	11.22	11.36	10.43
10.00	11.36	10.43	8.55	9.13
15.00	9.76	9.74	6.85	8.12
20.00	8.55	9.13	5.71	7.32
25.00	7.60	8.60	4.90	6.65

Figure A2. Example test data

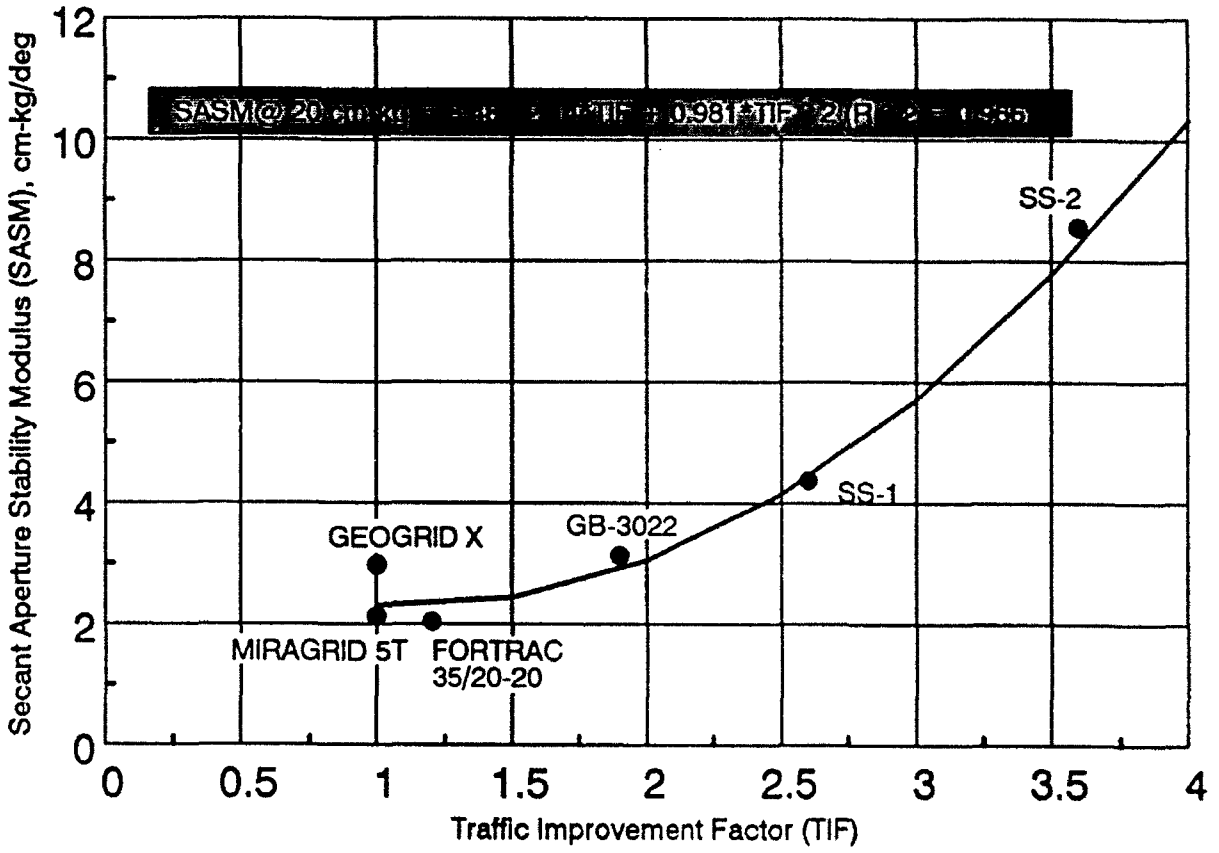

Figure A3. In-place rotation index test results

REPORT DOCUMENTATION PAGE

Form Approved
OMB No 0704-0188

1. AGENCY USE ONLY (Leave blank)	2. REPORT DATE	3. REPORT TYPE AND DATES COVERED
	May 1993	Final report

4. TITLE AND SUBTITLE

See reverse.

5. FUNDING NUMBERS

6. AUTHOR(S)

Steve L. Webster

7. PERFORMING ORGANIZATION NAME(S) AND ADDRESS(ES)

U.S. Army Engineer Waterways Experiment Station
Geotechnical Laboratory, 3909 Halls Ferry Road
Vicksburg, MS 39180-6199

8. PERFORMING ORGANIZATION REPORT NUMBER

Technical Report
GL-93-6

9. SPONSORING/MONITORING AGENCY NAME(S) AND ADDRESS(ES)

U.S. Department of Transportation, Federal Aviation Administration, 800 Independence Avenue, SW
Washington, DC 20591-0001

10. SPONSORING/MONITORING AGENCY REPORT NUMBER

DOT/FAA/RD-92/25

11. SUPPLEMENTARY NOTES

The document is available through the National Technical Information Service, 5285 Port Royal Road, Springfield, Virginia 22161.

12a. DISTRIBUTION/AVAILABILITY STATEMENT

Approved for public release; distribution unlimited.

12b. DISTRIBUTION CODE

13. ABSTRACT *(Maximum 200 words)*

A previous interim report presented the results of a literature review investigation geogrid reinforced base courses for flexible pavements for light aircraft and the design of a geogrid test section for field testing the validity of potential geogrid reinforcement results.

This report describes the construction of the field test section, the behavior of the test section under traffic testing using a 30,000 lb single tire load, the data collected, laboratory tests that were conducted on the various geogrid products used in the field test section, and development of design criteria for geogrid base reinforcement for flexible pavements for light aircraft.

Test results verified the validity of geogrid reinforced base courses for flexible pavements for light aircraft. A geogrid reinforcement product equivalent to the SS-2 geogrid used in the field tests can reduce the total pavement design thickness. The geogrid performance is a function of depth of placement. The thickness reductions range from approximately 40 percent for unreinforced pavement thicknesses of 11 in. to 5 percent for 30-in.-thick pavements.

(Continued)

14. SUBJECT TERMS			15. NUMBER OF PAGES
Base course	Geotextile	Reinforcement	100
Geogrid	Pavement	Subgrade	16. PRICE CODE

17. SECURITY CLASSIFICATION OF REPORT	18. SECURITY CLASSIFICATION OF THIS PAGE	19. SECURITY CLASSIFICATION OF ABSTRACT	20. LIMITATION OF ABSTRACT
Unclassified	Unclassified		

4. Continued.

Geogrid Reinforced Base Courses for Flexible Pavements for Light Aircraft: Test Section Construction, Behavior Under Traffic, Laboratory Tests, and Design Criteria

13. Continued.

The geogrid reinforcement performs best when placed between the base course and subgrade.

The improvement mechanisms for geogrid reinforcement include grid interlock with aggregate base material, subgrade confinement, and to some extent a tensioned membrane effect.

The geogrid property requirements for optimum performance are not totally known at this time. The performance of the various geogrid products tested ranged from no improvement up to 40 percent reduction in total pavement thickness requirement. A relatively rigid sheet-type product (SS-2) performed the best.